Universiteit
Leiden
The Netherlands

Warm IRAS sources. II - Optical spectroscopy of objects from the point source catalog

Grijp, M.H.K. de; Keel, W.C.; Miley, G.K.; Goudfrooij, P.; Lub, J.

Citation
Grijp, M. H. K. de, Keel, W. C., Miley, G. K., Goudfrooij, P., & Lub, J. (1992). Warm IRAS sources. II - Optical spectroscopy of objects from the point source catalog. *Astronomy And Astrophysics Supplement Series*, *96*, 389-428. Retrieved from https://hdl.handle.net/1887/7096

Version:	Not Applicable (or Unknown)
License:	Leiden University Non-exclusive license
Downloaded from:	https://hdl.handle.net/1887/7096

Note: To cite this publication please use the final published version (if applicable).

1992A&AS...96..389D

ASTRONOMY & ASTROPHYSICS
SUPPLEMENT SERIES

Astron. Astrophys. Suppl. Ser. **96**, 389-428 (1992)

Warm IRAS sources. II. Optical spectroscopy of objects from the point source catalog*

M.H.K. de Grijp[1], W.C. Keel[1,2], G.K. Miley[1], P. Goudfrooij[3] and J. Lub[1]

[1] Sterrewacht Leiden, Postbus 9513, 2300 RA Leiden, The Netherlands
[2] Dept. of Physics and Astronomy, University of Alabama, Box 870324, Tuscaloosa, Alabama 37587, U.S.A.
[3] Sterrenkundig Instituut, Universiteit van Amsterdam, Roetersstraat 15, 1018 WB Amsterdam, The Netherlands

Received October 21, 1991; accepted March 30, 1992

Abstract. — We present optical spectra for a sample of 563 high-latitude IRAS sources selected from the Point Source Catalog to have relatively warm 25 to 60 micron colours. We have shown this selection criterion to be an efficient indicator for finding Seyfert galaxies. Plots of the optical spectra are shown and the fluxes of the strongest emission lines in these spectra are tabulated. After excluding 128 sources which are clearly galactic foreground objects, we obtained spectroscopic information for 358 extragalactic objects. Emission-line ratios have been used to classify these objects, resulting in 80 Seyfert 1, 141 Seyfert 2 and 133 HII-type objects. In comparison with samples of active nuclei selected in other ways, about 50% of known Seyfert nuclei are included by our colour criteria. This fraction is larger for high luminosities, reaching 80% for quasar luminosities. For lower-luminosity objects, contamination by the host galaxies becomes important and the sample becomes seriously incomplete. It should be moderately complete and representative for core luminosities greater than $10^{23.5}$ W/Hz at 12μ. Finally, the infrared luminosity function for each type of object is derived; the shapes for Seyfert 1 and 2 nuclei are identical, with a type 2/type 1 space-density ratio of 3.0. Our census is consistent with an obscuration scheme for producing both types of object from a single parent population, though the origin of excess cool IR radiation from many Seyferts is still unclear. We note the appearance of an apparent type II supernova in IRAS 0225-103 observed in 1985 September. Its spectrum suggests that it was observed between 1 and 2 months after maximum, perhaps in a "plateau" phase.

Key words: active galaxies — Seyferts — redshifts — spectroscopy.

1. Introduction.

This is one in a series of papers designed to investigate the properties of warm IRAS sources. We have previously shown that galaxies with a relatively warm IRAS spectrum have a high chance of possessing Seyfert activity (de Grijp *et al.* 1985). With the aim of detecting hitherto unknown "IR Seyferts", we subsequently (de Grijp *et al.* 1987, hereafter Paper I) selected a list of 563 high-latitude ($\| b \| > 20°$ sources from the IRAS Point Source Catalog (PSC) having AGN-like colors ($-1.5 < \alpha_{25,60} < 0$), where $\alpha_{25,60}$ is the two-frequency spectral index between the 25μ and 60μ IRAS passbands. Note that this object list was selected with a somewhat wider range of $\alpha_{25,60}$ (-1.25 to -0.5) than originally used by de Grijp *et al.* (1985). Here we present the results of a spectroscopic investigation of 358 galaxies from this sample.

2. Observations and data reduction.

Observations were carried out both in the northern (La Palma) and southern (La Silla) hemispheres. Due to the size of the sample, the observations took several years to complete. An overview of the observations, instrumental configurations, and spectral ranges observed is given in Table 1.

Most of the northern-hemisphere observations were done with the Image Photon-Counting System detector (IPCS) and the Intermediate Dispersion Spectrograph (IDS) on the 2.5 m Isaac Newton Telescope (INT) at La Palma. A few of the faintest objects were observed with the 4.2 m William Herschel Telescope (WHT) in combination with the CCD-based Faint Object Spectrograph (FOS).

* Based in part on observations obtained at the European Southern Observatory, La Silla, Chile, and at the Observatorio del Roque de los Muchachos, which is operated by the Royal Greenwich Observatory on the island of La Palma.

© European Southern Observatory • Provided by the NASA Astrophysics Data System

1992A&AS...96..389D

Because of their blue sensitivity, the La Palma IPCS data are subject to contamination by the blue end of the second-order spectrum overlapping the red and of the first-order one. Although in principle this can be overcome by the use of a blocking filter, no filter with an appropriate wavelength cutoff was available. However, the relatively low reflection efficiency of the grating in second order combined with the higher dispersion resulted in a contamination of the spectrum that is less than about 5%.

The southern observations were carried out on the ESO 3.6 m telescope, using the Boller & Chivens spectrograph. Initially the Image Dissector Scanner (IDS) detector was used and the spectra were taken through a 4 arcsec square aperture. Later the IDS was replaced by an RCA CCD, with which spectra were taken along a slit of width 2 arcsec.

Typical exposure times were 10 minutes per object. For the brightest objects, neutral density filters were inserted in the optical path to prevent saturation. Two or three of the flux standard stars Feige 34, Feige 110, HZ 43, HZ 44, BD + 25°3941 (Oke 1974; Stone 1974) were observed every night to facilitate absolute flux calibration of the spectra. Further reduction was done using FIGARO, IHAP, IRAF, MIDAS and AIPS.

Wavelength calibration of the spectra was carried out using He-Ne-Ar comparison lamps, with possible shifts due to flexure monitored using telluric night-sky lines. Small linear shifts ($\leq$ 10 Å) were seen, probably due to telescope motions and thermal effects. After correction the resultant absolute accuracy of the wavelength calibration in the spectra is of the order of 1 Å, whereas the relative accuracy internal to a single spectrum is typically better than 0.6 Å. Therefore the calibration puts a limit to the accuracy of redshifts of 0.0002. In noisy spectra the additional uncertainty due to problems in emission line fitting is typically 0.0003.

The accuracy of the spectrophotometry is determined mainly by the weather conditions during the observations. For the slit spectra, an aperture correction for "missing" flux was made by measuring the light profile of the inner parts of the galaxies along the slit, and assuming circular symmetry. A considerable effort was devoted to checking the accuracy and consistency of fluxes obtained in this way. Several spectra were taken repeatedly on different instrumental setups and different seasons. Comparison generally showed agreement within 30%, except for a few cases known to be taken in bad weather. A further check was made by comparing the V-band flux in the spectrum with estimated magnitudes from the ESO/SRC J plates and the POSS E and O plates. The fluxes derived from the spectra agreed within 0.5 magnitude (1σ) with the photographic estimates.

Differential refraction introduces an additional colour correction to the spectrophotometry (e.g. Filippenko 1982). To minimize light loss caused by this effect, the slit should be positioned vertically, but in practice this was not always done (for instance when 2 objects are observed through the slit at the same time). We have modelled the effects of the atmosphere on the spectra that were affected, and for most cases the original spectral energy distributions could be reconstructed. In a few cases where objects were observed within 35° of the horizon, the effects were so severe that for the extreme ends of the spectra no trustworthy correction could be applied.

For each object in Table 2 the accuracy of the resultant absolute spectrophotometry can be estimated by referring to the quality of the relevant observation in Table 1. The absolute spectrophotometric accuracy is typically about 30%, but approaches 10% in good weather. Except for objects observed at very low elevation, the relative flux accuracy of the colours is typically about 10%.

3. Spectral classification.

As a first step, we discarded objects which inspection of the Palomar Sky Survey (POSS) or ESO-SRC survey plates shows to be obvious galactic foreground objects (bright SAO stars, planetary nebulae and other catalogued galactic objects). Other objects were designated "galactic" only after inspection of their spectra had clearly confirmed their local nature. In particular, faint stellar objects were observed as possible QSOs.

Nearly all extragalactic objects show emission lines; only a few redshifts are based on absorption features. No new BL Lac objects were discovered in this sample.

Objects were classified according to their ionization states estimated from the flux ratios between emission lines (Fig. 1). Before estimating the line fluxes, the relevant stellar "continuum" fluxes needed to be estimated and subtracted from the spectra. To do this optimally a correction was made for the underlying Hα and Hβ absorption features in the spectra of the stellar components. Our correction was derived empirically, using the known correlation between the strengths of these absorption features and the energy distribution of the stellar spectrum for galaxies with faint (LINER and borderline Seyfert) nuclei (Keel 1983). The effects of this correction were most severe for the Hβ emission line flux, which changed by up to 20%. Finally, a reddening correction was applied to the emission line ratios using the method of Baldwin *et al.* (1981).

The spectra have been used to classify the warm IRAS objects into "Seyfert 1", "Seyfert 2", "HII", "LINER" (Heckman 1980) and BL Lac classes. Emission line objects which had significantly broader (by 500 km/s) permitted lines than forbidden lines were classified as Seyfert 1 (Seyf1), regardless of the narrow line ratios. Following Baldwin *et al.* (1981) and Veilleux & Osterbrock (1987), the remaining narrow emission line objects having intensity ratios [O III] λ5007/Hβ > 3 and [N II] λ6582/Hα

© European Southern Observatory • Provided by the NASA Astrophysics Data System

1992A&AS...96..389D

> 0.5 were classified as Seyfert 2 (Seyf2). A few objects were found to fall in the "LINER" category ([N II]/Hα > 0.5 but [O III]/Hβ < 3). In a number of doubtful cases and transition objects other lines such as [O I] λ6300 were examined to determine the type of object. Emission-line objects whose line ratios lie outside the ranges appropriate for Seyfert 2 or LINER nuclei were categorized as H II- or starbust-type galaxies (HII). These objects have spectra which are similar to those of HII regions and are believed to be undergoing an intense burst of star formation (e.g. French 1980). The distinction between HII type objects on the one hand and Seyf2 and LINER objects on the other hand was confirmed by a multi-dimensional cluster analysis using the line ratios shown in Figure 1. In this Figure only sources are shown for which all 5 line ratios could be defined simultaneously. It reveals that although clusters are clearly different, using any two line ratios cannot separate them conclusively. However, we have more confidence in the manual procedure since the cluster analysis is sensitive to noisy (and sometimes spurious) emission lines, whereas by personal inspection the reliable lines can be better identified. Finally, only one object in this sample is catalogued as of BL-Lac type (object 464 = 3C371); no other featureless spectra showed up in this sample.

Some 77 objects have not yet been observed spectroscopically. Nearly all of these look like field galaxies on POSS and ESO-SRC plates. Nevertheless some galactic objects might be hidden among these objects. Therefore objects in this category have not been classified.

4. Results.

The results are tabulated in Table 2 and the spectra are plotted in Figure 2. For each object, the running number matches the one in the appropriate finding chart in Paper I. An emission-line classification is given where the available spectra are adequate. IRAS fluxes given are from co-added data and are thus more reliable than those from the Point-Source Catalog; note that as a result of revised fluxes some objects originally included in the sample of Paper I are found to have $\alpha_{25,60}$ outside the appropriate range, and they are included here only for completeness and consistency with Paper I. Clearly, some sources previously outside our criteria will have co-added fluxes consistent with our "warm" sample. For practical reasons these sources are ignored; this will be discussed more fully in Sect. 5.1. The quoted V magnitudes are estimated from the Sky Survey glass or film copies, with corrections for foreground extinction and galaxy inclination applied. For uniformity, Hβ fluxes or flux limits are listed, with limits indicating 3σ levels. Line ratios involving a non-detection of Hβ (column 12 - 14) are calculated using this upper limit (and are consequently denoted as a lower limit). As a result other line ratios can still be reconstructed, for example [N II] 6582/Hα can be calculated for objects without detected Hβ. Finally, measures of [O III] and [N II] refer only to the fluxes of the 5007 and 6582 Å line respectively.

The identification content of the warm IRAS sample is summarized in Table 3. Of the 358 classified objects in Table 2, only 101 were known before their appearance in the IRAS survey. The remaining 257 (half the sample) may be regarded as having been discovered via IRAS. IRAS colour selection is especially effective at finding type 2 Seyfert nuclei, which makes up 30% of the revised sample constructed with improved IRAS fluxes.

The identification content of this sample is quite comparable to that found in other studies of smaller samples of "warm" IRAS galaxies. We find that, of the extragalactic objects with spectroscopic information, 26% are type 1 Seyferts and 48% are type 2 Seyferts. These percentages compare well with those listed by de Grijp *et al.* (1985) (16 and 50% respectively), those from Osterbrock & De Robertis (1985) incorporting the work of Carter (1984) (13 and 42%), and the warm sample of Low *et al.* (1988) which is quite similar in scope to this survey within the northern hemisphere, which gives 21 and 39% for type 1 and 2 Seyferts. The concordance of these studies by different groups indicates that IR color-selected samples are quite rich in AGNs, and are one of the most fruitful ways of finding large numbers of active nuclei that have been missed in optical surveys.

In one case, a supernova appears to have been observed serendipitously in an IRAS warm galaxy. The 1985 September observations of IRAS 0225-103 included a stellar object located approximately 15 arcseconds SE of the nucleus, whose spectrum is shown in Fig. 3. This resembles certain type II supernovae, particularly those seen in a plateau phase of light-curve development. Many features of this spectrum are in common with those seen in SN 1987A between 60 and 80 days after outburst (Phillips *et al.* 1988), and there is an almost perfect match with the spectrum of SN 1988A in NGC 4579 as seen 20 days after maximum light (Ruiz-Lapuente *et al.* 1990). Since this galaxy shows spectroscopic evidence of a high rate of current star formation, a high rate of core-collapse supernovae is expected, and seeing such an outburst in one of the many starburst galaxies in our sample comes (in retrospect) as no surprise.

5. Sample completeness and infrared luminosity function.

Because our sample has been selected from the IRAS PSC in a uniform manner, it is interesting to use it to derive information about the infrared luminosity function of Seyfert and other emission line galaxies. This is of special importance since the 60μ emission is likely to be more isotropic than many other properties which have been used to define observed samples, and thus might

© European Southern Observatory • Provided by the NASA Astrophysics Data System

1992A&AS...96..389D

in principle produce an accurate picture of the relative numbers of type 1 and 2 objects even if an obscuration picture for Seyfert nuclei is correct. Before we do this, it is necessary to consider the completeness of the sample and to correct where possible for any systematic biases.

Several biases must be considered. First, the sample is flux-limited at both 25 and 60 microns. Second, an IR colour selection was applied. While this conveniently excluded many non-active galaxies, it also ignored potentially interesting AGNs. Third, not all sources were observed spectroscopically, so that some sources remain unclassified. We will show that this does not affect the representativeness of the sample. We then attempt to estimate the fraction of AGNs missed by our colour criteria, by comparison with samples of AGNs selected on various bases.

5.1. Flux completeness

The completeness of the IRAS PSC is a function of observing band, flux density and position on the sky. To derive completeness fractions for our sample, we have considered the departure of our observed source counts from that expected if the sources were distributed according to Euclidean cosmology, i.e. obey a number vs. flux density relation having a power law with an index $\alpha = 1.5$. This is only correct if evolutionary effects can be neglected. Although this is not strictly true, most of our objects are at small redshifts, so that we can make this assumption initially and later examine possible effects of evolution.

We define the flux density completeness fractions, f_{S60} and f_{S25} at 60 and 25 microns respectively as the ratio of the number of sources observed at a given flux density to the number of sources extrapolated from the strong source counts by a Euclidean power law of index -1.5.

The combined flux completeness correction $f(\mathrm{IR}) = f_{S60} \times f_{S25}$ as a function of 60 and 25 micron flux density is shown in Fig. 4. The completeness fraction for each object in our sample was estimated from this treatment and incorporated in our calculation of the 60 micron luminosity function, so that each detected object near the flux limits is considered to represent additional ones that were not detected.

Note that our sample was originally selected from the first version of the IRAS Point Source Catalog (IRAS PSC - Version 1), in which a systematic overestimation of faint fluxes occured. This affected both the 25 and 60 micron fluxes. Although we later obtained coadded data for all sources having dubious fluxes at 25 or 60 microns, the choice of sources is still based on the original list with PSC fluxes. For 132 sources, the better signal-to-noise and correction of the flux overestimation in the co-added data results in these sources having revised fluxes or colours that are no longer in agreement with the criteria which we used to define our original sample. The large number of such sources is consistent with errors applied to a steeply rising distribution, in this case the number of objects as a function of 25-60 micron spectral index. The distributions of objects in revised S_{60} and $\alpha_{25,60}$ are shown in Fig. 5, together with our final acceptance limits. Most of the "offending" sources have HII-type spectra. However, since they are no longer defined as "warm", they have been omitted from our revised sample. Likewise, the errors in the PSC fluxes will have resulted in (a much smaller number of) genuine warm sources being omitted from our original sample. However, since the flux densities used in Fig. 4 were co-added fluxes, the resultant completeness fractions should take this effect into account.

5.2. Spectroscopic completeness

Spectroscopic data are available for 86% of all warm extragalactic sources in our sample. Figure 6 shows this fraction as a function of V magnitude. Clearly, optically faint sources were not observed as extensively as bright ones. In deriving the IR luminosity function we compensate for this incompleteness by assuming that we observed a representative fraction $f(V)$ of the optically faint objects, weighing the contribution of the faint galaxies in inverse proportion to the fraction observed. Confidence in the validity of this procedure is provided by the fact that the distribution of the 25 to 60 micron colour of these faint galaxies is consistent with the rest of the sample.

5.3. Derivation of the luminosity function

The bivariate infrared-optical luminosity function for each class of extragalactic object in our warm sample was derived as follows.

In accordance with the results in Sect. 5.1, only "truly warm" sources were considered; sources with fluxes below 0.25 Jy at 25 micron or 0.45 Jy at 60 micron were also dropped from further consideration. Each source was then given a weight $W = 1/(\text{flux completeness}) = 1/f(\mathrm{IR})$ to offset the flux incompleteness of the sample. At the flux levels under consideration, these factors are still small.

The spectroscopic incompleteness reported in Sect. 5.2 was taken into account by applying a further weight depending on the optical magnitude: $W = 1/f(V) = 1/(\text{spectroscopic completeness})$.

Maximum distances out to which objects could still be observed while staying above the imposed flux limits were calculated by mumerically redshifting the IR-spectra. A Hubble constant $H_0 = 75$ km s^{-1} Mpc^{-1} and $q_0 = 0.5$ were assumed.

Each object "j" from Class i was taken as contributing to the space density at 60 micron luminosity L_{60} and optical absolute magnitude M_V.

© European Southern Observatory • Provided by the NASA Astrophysics Data System

1992A&AS...96..389D

$$\Phi_j(L_{60}, M_V)\mathrm{d}v = \frac{V_j}{V_{\max,j}} \times \frac{\mathrm{d}_v}{(f(\mathrm{IR}) \times f(V))}$$

The luminosity function derived in this way is shown in Fig. 7; Table 4 gives a detailed overview of the bivariate luminosity function for different types of object. For every bin values of $\Phi, V/V_{\max}$ and the number of objects involved are calculated.

5.4. Evolutionary effects ?

As can be seen in Fig. 8, $< V/V_{\max} >$ deviates from the expected value of 0.5. At low luminosities an excess of nearby sources is evident, while at the high luminosity end sources tend to be predominantly close to their maximum distances.

The discrepancy at low-luminosity can be explained by the Local Supercluster, as sources with 60 micron luminosities below $10^{10.6}$ can be detected only to distances of 150 Mpc (comparable to the extent of the Local Supercluster). This excess is real, but indicates spatial rather than temporal structure.

At the high luminosity end $< V/V_{\max} >$ may show weak evidence of evolution. The standard deviation of the numbers are large; by lumping together all sources with $L_{60} > 10^{10.6} L_\odot$, a $V/V_{\max}$ of 0.58 ± 0.028 (2.8σ from a flat distribution) is derived. This in itself is insufficient to warrant the conclusion that any effect is present. It is interesting to note that on the basis of the deeper IRAS Faint Source Survey, Lonsdale *et al.* (1990) come to a similar conclusion. Sources so luminous at 60μ that they are detected over distances great enough to search for evolution are so rare that much deeper IR surveys than this (for example from the IRAS deep fields, Keel *et al.* 1988) will be required to address this issue.

5.5. Luminosity dependence of identification fraction

Table 5 shows the identification content of the sample as a function of 60 micron luminosity. Clearly, HII-type galaxies are less luminous on average than the AGNs. In particular we do not detect the "ultraluminous" sources with steep IRAS spectra such as Arp 220. While many of these objects at $\log (L_{60}/L_\odot) > 12$ show evidence of having active nuclei (Kleinmann *et al.* 1988), these objects mostly have cooler 25-60 micron spectra, even though they may still have unusually warm 60-100 micron colors (Heckman *et al.* 1987; Armus *et al.* 1988). Several studies have shown that these objects are as numerous as AGNs at the highest luminosities; objects of this kind will not be strongly represented in samples selected as we have done. Thus any population of AGNs in these most luminous sources, such as postulated by Sanders *et al.* (1988), must either be so heavily dust-shrouded as to have a significant 25μ optical depth, have associated star formation so luminous as to "cool" the integrated IR spectral shape, or have some additional source of far-IR reradiation linked to the nucleus, perhaps in extensive dust distributions such as were postulated by Valentijn (1990).

5.6. Completeness and representative nature of AGNs in warm infrared sample

As pointed out by de Grijp *et al.* (1985) and Véron (1985), although use of the IRAS colour criterion is an efficient tool for detecting AGNs, not all AGNs have warm infrared sources. In particular, Fig. 9 presents the AGN-content of 60μ IRAS sources as a function of $\alpha_{25,60}$. It shows that at $\alpha_{25,60} < -1.5$ the AGN-fraction is small, but significant due to the overwhelming number of these cold sources in the IRAS Point Source Catalog. The results of IRAS measurements on various optically-defined samples of Seyfert galaxies (Table 6) indicate that 30% of all optically selected AGNs do not pass the "warm" colour criterion.

Comparison with samples derived in other ways is of interest to assess the contribution of "warm", predominantly luminous, AGN to the whole population of IR-bright galaxies, and in testing models that require AGNs to predominate among the most luminous objects (Sanders *et al.* 1988). We can also test for an expected selection effect: since most Seyfert nuclei are hosted by disk galaxies that will have a significant level of cooler infrared emission associated with their disks, we should find mostly nuclei that outshine the disks at 60 microns. This contrast selection will result in a *de facto* luminosity selection if the host galaxy disks span a more limited luminosity range.

Ideally we would compare the objects selected from IRAS colours to some list containing all AGN to specified flux limits. Only approximations to such a list are available, so we have compared the content of our sample to several others selected in various ways. There will be a certain amount of luminosity segregation built into any such list, since low-luminosity AGNs are difficult to detect and classify spectroscopically without data of unusually high quality. Thus our definition of "Seyfert" has an implicit (and ill-defined) lower luminosity bound, depending on the contrast against the observed section of the host galaxy.

Spinoglio & Malkan (1989) have introduced the notion of a "pivot point" in the spectra of AGN, such that near 12μ the spectrum is minimally affected by reddening or possible nonthermal emission. Thus they define a "complete" sample of AGNs based on optical spectroscopy of a sample of galaxies complete to a stated flux limit at 12μ. Of 390 galaxies in their whole sample, 27 are type 1

© European Southern Observatory • Provided by the NASA Astrophysics Data System

1992A&AS...96..389D

Seyferts and 32 are type 2. Of these, our sample contains 15 and 14 respectively, for a completeness fraction close to 50% for each type if the 12μ sample is really complete. Since physical situations can exist in which some classes of AGN might be under-represented in such a sample, it is useful to compare our colour-selected sample with additional samples selected in different ways.

The optically-selected CfA sample of Seyfert galaxies was analyzed by Edelson (1987) and Edelson *et al.* (1987). These objects are selected spectroscopically from an optically complete galaxy sample, and thus are biased only in the sense that the emission lines must have adequate contrast against the surrounding galaxy light within the spectrograph aperture (Edelson 1990). Edelson found that only 7 of 40 CFA Seyferts (17%) had $(-1.25 < \alpha_{25,60} < -0.5)$. However, using the less restrictive spectral range used to define our present sample, we find that as many as 20/37 (54%) of the CFA Seyferts have warm IRAS spectra. (We omitted three Seyferts with IRAS neighbouring sources which could contaminate the infrared fluxes from our consideration.) We find no dependence of the IRAS spectral index distribution on 12μ (predominantly core) luminosity within the CfA sample.

A large sample of X-ray selected and IRAS-detected AGN has been presented by Kirhakos & Steiner (1990). This sample should be free of the biases against heavily-reddened systems that operate in, for instance, UV-excess selection. Of the 11 objects in their list with 12μ detections, 4 are in common with our sample, and one more has colours (apparently not from the first version of the PSC) such that it would be included. Thus, 5 out of 11 (44%) of these jointly selected AGNs are found by the "warm" colour range we have adopted.

These three samples of Seyfert nuclei, selected on the basis of mid-IR flux, optical spectroscopy, and X-ray detection, all have about 50% of their AGNs in the IR colour range included in our sample. We can also compare our detections to the IR properties of Markarian Seyferts, which are selected from near-UV excess and are thus biased against reddened and dusty objects and in favor of the strong nonstellar continua of type 1 Seyfert nuclei. Table 6 shows the relevant figures for the colour distribution of Markarian Seyferts (Miley *et al.* 1985; Meurs 1982). In these samples, the "warm" colour criterion excludes about 30% of all AGNs; the difference from the 50% above may reflect variation of properties related to the selection criteria for Markarian objects (such as prominance of the nucleus), since the other values are all closely similar.

We may also examine the colours of luminous QSOs with regard to our selection criteria, since these objects should suffer the least contamination of IR flux by a surrounding galaxy. We have taken the data for the Palomar-Green sample of UV-excess QSOs (Schmidt & Green 1983) as presented by Sanders *et al.* (1989). Of the 34 PG objects with detections at both 25 and 60μ, 26 fall within our selection range of α_{25-60} between 0 and -1.5. Of the remaining eight, only two fall more than 2σ outside this range; evidently for these objects IR colour selection is a very effective recognition tool. Given the low detection rate for these relatively faint objects, such a conclusion must be qualified in light of the many limits on α, and the many objects without detections by IRAS at either wavelength. A Kaplan-Meier estimate of the mean of the distribution incorporating upper limits to $\alpha_{25,60}$ is only slightly different from that incorporating only detections (mean $\alpha = 0.65 \pm 0.09$ using upper limits as opposed to -0.41 ± 0.04 for detections only).

Comparison of this result with those for the samples of nearby Seyferts discussed above suggests a luminosity dependence of the scatter in IR spectral shapes, in the sense that more luminous objects show smaller scatter and in particular are less likely to show a "cool excess" such as might be produced by surrounding star formation of a normal spiral-galaxy disk. This conclusion is quantified in Fig. 10, in which $\alpha_{25,60}$ is shown as a function of luminosity for the Palomar-Green, CFA, and 12μ samples. We follow Spinoglio & Malkan in using the luminosity at 12μ as an approximate, uniform indicator of core luminosity. We have incorporated K-corrections to the luminosities, but not made corrections for IR spectral curvature here. Above a monochromatic luminosity $L(12\mu) = 10^{24.2}$ W Hz^{-1}, nearly 90% of the AGNs have colours in our selection range. However, below $10^{23.2}$ W Hz^{-1}, less than 30% fall in this range of $\alpha_{25,60}$. We tentatively interpret this distinction as resulting from contamination of the spectral slope by cool emission from the disks of the host galaxies. Thus, selection of AGNs by infrared colours is very efficient at high luminosities and is at present a poor means of finding low-luminosities objects.

6. Conclusions.

We have presented a large body of spectroscopic data on 358 objects selected from the IRAS PSC on the basis of unusually "warm" infrared colours. Our main conclusions are

(1) Selection of objects by relatively "warm" 25-60μ colours is a very efficient way of finding Seyfert galaxies.

(2) This selection seems to find about half of the Seyfert nuclei revealed by other kinds of surveys, with this fraction approaching unity at the highest core luminosities. Its efficiency (in terms of relative numbers of Seyferts in a sample of given size) is unmatched except by X-ray surveys.

(3) The luminosity functions of Seyfert 1 and Seyfert 2 nuclei in this sample (which should be unbiased by anisotropic emission processes) are identical except for a scale factor of 3.0. This is consistent with an obscuration picture for the difference between the two classes; we will

© European Southern Observatory • Provided by the NASA Astrophysics Data System

1992A&AS...96..389D

present more detailed consistency tests in a later paper, in an analysis of the detailed spectroscopic properties.

Acknowledgements.

The work presented here would not have been possible without the painstaking efforts of the staff of the observatories at La Palma and La Silla for which we are most grateful. We also wish to thank R.S. le Poole and P. Katgert for their help with the observations, E. Tolstoy and H. Versteege for assisting with various stages of the reduction and analysis and J.P. Vader for kindly making available some of her spectra. During the early stages of this project MdG was partially supported by a grant from the European Space Agency. During a considerable portion of the research GM was an ESA staff member of the Space Telescope Science Institute (STScI). MdG and GM acknowledge travel support from the STScI and GM from a NATO grant. We acknowledge useful discussions with M. Malkan and R. Edelson and thank E. Meurs for his comments on the manuscript.

References

Armus L., Heckman T.M., Miley G.K., 1988, ApJ 316, L45
Baldwin J.A., Phillips M.M., Terlevich R., 1981, PASP 93, 5
Carter D., 1984, Astron. Express 1, 61
de Grijp M.H.K., Miley G.K., Lub J., de Jong T., 1985, Nat 314, 240
de Grijp M.H.K., Miley G.K., Lub J., 1987, A & AS 70, 95 (Paper I)
Edelson R., 1987, ApJ 313, 651
Edelson R., 1990, private communication
Edelson R., Malkan M., Rieke G., 1987, ApJ 321, 233
Filippenko A.V., 1982, PASP 94, 715
French H.B., 1980, ApJ 240, 41
Heckman T.M., 1980, A & A 87, 152
Heckman T.M., Armus L., Miley G.K., 1987, AJ 93, 276
Joint IRAS Science Working Group, 1985, IRAS Point Source Catalog (Washington DC: US Government Printing Office)
Keel W.C., 1983, ApJ, 269, 466
Keel W.C., de Grijp M.H.K., Miley G.K., 1988, A & A 203, 250
Kirhakos S.D., Steiner J.E., 1990, AJ 99, 1722
Kleinmann S.G., Hamilton D., Keel W.C., *et al.*, 1988, ApJ 328, 161
Lonsdale C.J., Hacking P.B., Conrow T.P., Rowan-Robinson M., 1990, ApJ 358, 60
Low F.J., Huchra J.P., Kleinmann S.G., Cutri R.M., 1988, ApJ 327, L41
Meurs E.J.A., 1982, The Seyfert Galaxy Population, Ph.D. thesis Leiden University
Miley G.K., Neugebauer G., Soifer B.T., 1985, ApJ 293, L11
Oke J.B., 1974, ApJS 27, 21
Osterbrock D.E., de Robertis M.M., 1985, PASP 97, 1129
Palumbo G.G.C., Tanzella-Nitti G., Vettolani G., 1983, Catalogue of radial velocities, New York: Gordon and Breach
Phillips M.M., Heathcote S.R., Hamuy M., Navarrete M., 1988, AJ 95, 1087
Ruiz-Lapuente P., Kidger M., Lopez R., Canal R., 1990, AJ 100, 782
Sandage A., 1973, ApJ 183, 711
Sandage A., Tammann G.A., 1976, ApJ 210, 7
Sanders D.B., Soifer B.T., Elias J.H. *et al.*, 1988, ApJ 325, 74
Sanders D.B., Phinney E.S., Neugebauer G., Soifer B.T., Matthews K., 1989, ApJ 347, 29
Schmidt M., Green R.F., 1983, ApJ 269, 352
Spinoglio L., Malkan M., 1989, ApJ 342, 83
Stone R.P.S., 1974, ApJ 193, 135
Stone R.P.S., 1977, ApJ 218, 767
Valentijn E., 1990, Nat 346, 153
Veilleux S., Osterbrock D.E., 1987, ApJS 63, 295
Véron P., 1985, in Structure and Evolution of Active Galactic Nuclei
Véron-Cetty M.P., Véron P., 1989, ESO Scientific Report No. 7: A Catalogue of Quasars and Active Nuclei (Munich: European Southern Observatory)

© European Southern Observatory • Provided by the NASA Astrophysics Data System

1992A&AS...96..389D

TABLE 2. *Observed data of the IR-defined sample.*

num	object	type	z	S12 (Jy)	S25 (Jy)	S60 (Jy)	S100 (Jy)	V (mag)	sp.indx. (V,60)	Hbeta (1E-15)	[OIII]/Hbeta	Halfa/Hbeta	[NII]/Hbeta	date (t.1)
1	IRAS0001-309			1.19	0.72	0.82	1.40	16.5	-1.425					
2	IRAS0002-084	HII	0.0301	0.22	0.42	1.40	1.57	15.9	-1.423	<1.22		>5.23	>2.47	20
3	IRAS0006+215	HII	0.0774	<0.17	0.28	0.78	0.58	16.9	-1.503	20.8	3.88	4.03	0.35	6
4	IRAS0016-073	Seyf2	0.0178	0.22	0.61	1.68	1.36	14.1	-1.116	<4.14	0.97	>6.23	>3.40	21
5	IRAS0019-625	HII	0.0321	<0.25	0.28	0.94	1.05	15.1	-1.180	21.9	2.45	4.76	0.76	18
6	IRAS0019-794	Seyf2	0.0728	0.33	1.22	3.18	2.63	14.8	-1.392	3.36	11.56	6.41	3.05	9
7	IRAS0026-102E	HII	0.0496	0.16	0.51	1.07	0.97	15.8	-1.351	18.3	1.20	3.61	1.86	20
8	IRAS0026-732	local	0.0000	<0.25	2.16	5.52	4.36							
9	IRAS0032-003	Seyf2	0.0420	0.09	0.31	0.89	1.02	15.5	-1.246	1.35	7.55	3.85	3.37	23,27
10	IRAS0032-617SW	HII	0.0286	0.12	0.16	1.16	2.03	14.8	-1.168	9.65	0.42	5.22	2.35	18
11	IRAS0033-819E	Seyf2	0.1271	0.07	0.23	0.58	0.91	16.1	-1.286	4.94	6.01		0.00	18
12	IRAS0033-736			<0.25	0.47	1.14	1.56	17.5	-1.545					
13	IRAS0034-338	HII	0.0205	0.43	2.52	6.71	4.53	13.8	-1.349	48.1	2.85	2.85	0.60	7
14	IRAS0038+235W	HII	0.0852	0.07	0.14	0.77	0.91	17.1	-1.537	1.31	0.53	3.37	<0.63	22
15	IRAS0043+419	local	0.0000	<0.25	0.44	1.46	<7.10							
16	IRAS0046+316	Seyf2	0.0149	0.31	0.79	1.44	1.83	13.4	-0.938	25.9	13.88	4.78	3.39	4
17	IRAS0046-127	HII	0.0288	0.11	0.23	1.36	1.97	14.4	-1.126	19.2	0.56	4.47	1.14	7
18	IRAS0050+124	Seyf1	0.0610	0.52	1.25	2.17	2.53	13.5	-1.057	220.	0.13	3.40	<0.50	5,23
19	IRAS0052-709	Seyf2	0.0688	0.29	0.85	1.11	<1.00	15.7	-1.341	9.60	8.00	6.06	4.59	18
20	IRAS0059-199W	Seyf2	0.0560	<0.25	0.29	0.72	1.01	15.8	-1.263	3.19	6.59	4.26	3.11	23
21	IRAS0102-643	HII	0.0198	<0.25	0.80	2.81	2.93	13.5	-1.102	111.	2.28	4.20	1.11	19
22	IRAS0105+331	HII	0.0155	0.07	0.17	0.67	1.06	13.5	-0.808	5.12	0.19	4.65	1.79	20
23	IRAS0107-038	Seyf2	0.0546	<0.27	0.66	1.05	<1.00	14.5	-1.097	29.7	14.18	4.00	2.34	18
24	IRAS0109-383	Seyf2	0.0110	1.09	1.76	1.84	2.04	11.0	-0.540					
25	IRAS0111+849	Seyf2	0.0564	<0.25	0.72	1.30	1.74	15.6	-1.341	<2.53	>4.10	>3.83	>4.00	6,22
26	IRAS0113+328	Seyf2	0.0154	1.74	0.88	2.47	2.56	13.7	-1.120	33.6	10.21	3.32	2.83	20
27	IRAS0124+189	Seyf1	0.0167	0.17	0.50	1.17	1.86	13.4	-0.896	44.9	1.92	3.76	1.39	5
28	IRAS0134-094W	Seyf2	0.0698	0.17	0.28	0.82	1.16	15.8	-1.289	4.34	2.90	3.48	1.44	21
29	IRAS0135+350	local	0.0000	0.97	0.42	0.57	1.62							
30	IRAS0135-131	Seyf2	0.0404	<0.46	0.47	0.97	1.22	14.3	-1.045	13.3	12.91	6.71	4.49	7
31	IRAS0137-225	Seyf1	0.0861	0.11	0.34	0.57	0.33	15.5	-1.162	39.8	0.58	4.70	0.63	18
32	IRAS0140-539	local	0.0000	0.82	0.34	0.85	<1.03							
33	IRAS0141+020	Seyf2	0.0172	<0.29	0.80	1.27	1.26	12.6	-0.766	81.2	11.42	3.90	2.97	18
34	IRAS0142-420	HII	0.0208	<0.11	0.37	1.42	1.71	13.8	-1.020	22.4	0.10	4.02	1.91	18
35	IRAS0145+413S	HII	0.0338	<0.09	0.18	0.62	0.55	15.3	-1.145	1.04	1.30	9.08	3.95	21
36	IRAS0146-615NW	HII	0.0421	<0.08	0.18	0.89	1.62	14.8	-1.120	4.90	0.65	5.38	1.95	19
37	IRAS0147-076	Seyf2	0.0177	0.33	0.82	1.16	0.41	14.0	-1.024	10.2	5.21	7.62	3.76	18
38	IRAS0147+359	Seyf2	0.0808	<0.25	0.32	0.61	<1.00	15.3	-1.130	<5.77	>4.21	>4.15	>2.80	6
39	IRAS0157+001	Seyf1	0.1628	<0.25	0.63	2.34	2.29	15.1	-1.380	64.3	1.02			18
40	IRAS0202-605	HII	0.0875	<0.06	0.16	0.54	0.33	17.1	-1.459	8.10	2.83	3.78	1.01	19
41	IRAS0204-554	Seyf2	0.0198	0.09	0.19	0.93	2.30	12.9	-0.757	<5.09	>8.23	>5.95	>6.41	19
42	IRAS0207-104	HII	0.0127	0.58	2.21	12.17	18.13	12.6	-1.236	<13.0	>1.01	>6.70	>4.36	21
43	IRAS0209-499	Seyf2	0.0475	<0.25	0.17	0.58	1.43	14.0	-0.863	<9.31	>4.57	>1.79	>1.17	9
44	IRAS0210-505	HII	0.0212	<0.25	0.17	0.89	1.78	13.6	-0.881	7.53	1.18	7.08	2.16	19
45	IRAS0214+336	local	0.0000	1.07	0.47	0.86	0.85							
46	IRAS0225-103E	HII	0.0068	0.11	0.36	1.50	1.91	13.2	-0.908	141.	4.80	3.18	0.19	20,28
47	IRAS0225+310	Seyf1	0.0158	0.66	1.31	2.76	4.92	13.1	-1.032	104.	0.72	4.23	0.38	21
48	IRAS0226-390	HII	0.0478	<0.25	0.27	0.68	<2.17	15.3	-1.160	66.2	4.79	2.94	0.45	9
49	IRAS0227+284	HII	0.0369	<0.08	0.11	0.66	1.36	15.8	-1.247					
50	IRAS0227-741	local	0.0000	<0.25	0.25	0.40	<1.00							19
51	IRAS0229+025	HII	0.0272	0.09	0.20	0.62	1.11	15.5	-1.178	1.83	0.66	2.55	0.53	22
52	IRAS0229-368	Seyf2	0.0168	<0.25	0.41	1.42	2.40	12.2	-0.706	20.5	13.59	6.04	5.82	19
53	IRAS0230+002	Seyf2	0.0221	<0.25	0.87	2.76	2.72	13.7	-1.147	<6.93	>3.54	>3.55	>2.86	21
54	IRAS0232-090	Seyf1	0.0431	<0.27	0.55	1.44	2.00	13.8	-1.019	222.	1.00	4.59	0.65	18
55	IRAS0236-310	Seyf1	0.0620	0.15	0.26	0.72	1.32	14.2	-0.955	37.8	0.31	7.14	1.47	19
56	IRAS0238-084	liner	0.0044	<0.21	0.50	0.94	1.22	10.3	-0.253	47.1	1.91	4.55	4.63	18
57	IRAS0240-002	Seyf2	0.0026	38.30	86.83	185.60	238.70	8.9	-1.087	304.	15.94	4.29	6.70	20,23
58	IRAS0240-601E	HII	0.0388	<0.25	0.34	0.90	1.22	14.1	-0.986	13.9	0.81	3.33	2.28	9
59	IRAS0241-140	local	0.0000	0.66	0.48	1.35	1.77							
60	IRAS0242-187	local	0.0000	1.88	0.65	1.63	5.01							
61	IRAS0246+263			0.14	0.36	1.22	2.58	15.1	-1.237					
62	IRAS0249-335			0.14	0.21	1.01	2.71	12.4	-0.671					
63	IRAS0253+021	HII	0.0276	<0.25	0.81	2.77	1.79	15.9	-1.565	<1.86		>3.60	>1.36	23
64	IRAS0253-166	Seyf2	0.0315	<0.25	0.29	0.72	1.44	14.4	-1.002	30.8	3.57	3.57	2.07	7
65	IRAS0255-167	Seyf1	0.0680	0.11	0.29	0.92	0.91	15.4	-1.235					
66	IRAS0258-173			0.22	0.17	0.66	1.85	12.8	-0.659					
67	IRAS0258-116	Seyf2	0.0296	<0.29	0.49	0.56	0.77	13.8	-0.821	11.8	15.52	3.10	2.50	21
68	IRAS0301-012	Seyf1	0.0132	0.31	0.54	0.78	<1.00	13.5	-0.830	<1.73	>8.42	>5.59	>1.64	20
69	IRAS0302-472	HII	0.0305	0.09	0.25	0.90	1.81	13.9	-0.944	20.0	1.29	4.39	2.52	19
70	IRAS0302-729	liner	0.0431	0.07	0.25	0.83	1.33	14.8	-1.099	<3.88	>1.45	>7.02	>5.41	18
71	IRAS0303-835			<0.25	0.29	1.04	1.43	14.0	-0.990					
72	IRAS0305-231	Seyf2	0.0355	0.28	0.81	1.54	1.86	13.7	-1.020	13.3	8.38	4.55	3.59	18
73	IRAS0306-328	HII	0.0516	<0.25	0.26	1.11	1.60	14.8	-1.168	<10.1	>0.43	>3.77	>1.75	7
74	IRAS0310+308	local	0.0000	1.92	0.54	0.55	<1.73							
75	IRAS0310-029	Seyf2	0.0272	<0.41	0.42	1.10	<1.01	13.7	-0.949	<5.42	>4.32	>3.02	>4.20	21
76	IRAS0310-515NW	Seyf2	0.0778	0.11	0.21	0.52	0.83	14.8	-0.997	9.33	10.26	4.71	2.20	19
77	IRAS0311+245			0.19	0.35	1.17	0.98	17.1	-1.614					
78	IRAS0312+013	Seyf2	0.0233	<0.25	0.28	0.85	1.99	14.3	-1.004	9.86	6.23	3.98	2.81	23
79	IRAS0316+871			<0.06	0.19	0.44	1.06	16.6	-1.323					
80	IRAS0320-518	Seyf2	0.0578	<0.25	0.51	0.59	<0.85	14.8	-1.033	6.10	11.38	4.57	4.08	19
81	IRAS0321+309	local	0.0000	<0.25	0.82	0.87	<9.12							
82	IRAS0322+305	local	0.0000	0.90	2.82	3.95	9.60							
83	IRAS0322-032	Seyf2	0.0087	0.34	1.08	2.33	2.76	12.2	-0.805	13.6	8.98	4.24	2.54	23
84	IRAS0323-580	Seyf2	0.0437	<0.12	0.17	0.66	0.48	15.3	-1.150	0.84	7.21	8.27	4.74	19
85	IRAS0323-609	Seyf2	0.0185	0.25	0.63	1.51	2.07	12.7	-0.810	<17.4	>3.00	>2.81	>2.19	9
86	IRAS0325+308	local	0.0000	0.43	1.76	4.29	7.21							
87	IRAS0325+305	local	0.0000	0.52	0.50	0.73	5.77							
88	IRAS0326-123			0.20	0.32	1.49	4.30	13.0	-0.879					
89	IRAS0327+303	local	0.0000	<0.38	0.87	1.34	<8.15							
90	IRAS0327-434W	Seyf2	0.0584	<0.25	0.37	1.26	1.95	15.1	-1.242	4.82	2.63	3.14	3.15	19
91	IRAS0328+306	local	0.0000	<0.40	0.56	0.64	<13.49							23
92	IRAS0330-623	HII	0.0280	0.06	0.36	0.78	1.02	14.9	-1.113	25.1	0.77	5.12	1.60	19
93	IRAS0331-260	local	0.0000	<0.36	0.41	1.44	8.11							
94	IRAS0333-564S	Seyf2	0.0785	<0.27	0.54	1.36	1.42	14.9	-1.232	<8.78	>8.46	>5.37	>4.39	19
95	IRAS0334-210	HII	0.0058	0.45	1.93	7.12	5.71	12.2	-1.040	<11.3			>0.46	18
96	IRAS0335+010S	Seyf2	0.0396	<0.25	0.46	0.67	<1.00	14.5	-0.998	6.13	12.41	4.46	2.57	21
97	IRAS0335+295	local	0.0000	1.19	1.45	2.00	2.10							
98	IRAS0336-167	Seyf2	0.0369	<0.39	0.54	1.05	<3.41	15.4	-1.271	2.90	6.20	5.91	3.67	20
99	IRAS0338-712	HII	0.0475	<0.25	0.22	1.23	2.08	14.9	-1.211	<2.29	>1.14	>3.80	>0.78	19
100	IRAS0342+017	local	0.0000	1.42	0.50	0.67	2.88							

© European Southern Observatory • Provided by the NASA Astrophysics Data System

1992A&AS...96..389D

TABLE 2. *(continued)*

num	object	type	z	S12 (Jy)	S25 (Jy)	S60 (Jy)	S100 (Jy)	V (mag)	sp.indx. (V,60)	Hbeta (1E-15)	[OIII] / Hbeta	Halfa / Hbeta	[NII] / Hbeta	date (t.1)
101	IRAS0343+237	local	0.0000	1.31	2.17	4.58	<9.41							
102	IRAS0346+253			<0.10	0.11	0.58	2.37	15.5	-1.167					
103	IRAS0349-033			0.09	0.16	0.99	3.11	17.1	-1.575					
104	IRAS0350+193	local	0.0000	0.08	0.79	0.64	2.47							20,21
105	IRAS0351-174S	HII	0.0282	<0.30	0.46	1.48	2.31	14.8	-1.227	<2.31		>4.26	>1.95	23
106	IRAS0355-630			<0.27	0.53	0.94	1.08	16.9	-1.543					
107	IRAS0355+013	local	0.0000	1.83	0.58	0.94	<1.98							
108	IRAS0357-615	Seyf2	0.0474	<0.25	0.45	1.53	2.65	14.2	-1.112	12.2	7.36	4.73	4.21	19
109	IRAS0408+165	local	0.0000	0.52	0.46	1.58	6.00							
110	IRAS0410-286		0.119?	<0.25	0.57	1.77	1.85	16.9	-1.668	3.49	1.97			12
111	IRAS0411-551			<0.25	0.30	1.80	3.44	14.4	-1.195					
112	IRAS0411-128	local	0.0000	1.43	9.09	16.10	9.76							
113	IRAS0412-512			0.13	0.18	1.05	1.50	15.0	-1.188					
114	IRAS0412-080	Seyf1	0.0379	<0.26	0.54	0.66	<1.00	13.9	-0.873	276.	2.30	5.14	0.59	10
115	IRAS0418+203	local	0.0000	0.39	1.79	3.32	1.92							23
116	IRAS0419+194	local	0.0000	14.94	44.12	98.26	96.84							
117	IRAS0419+153	local	0.0000	0.41	2.02	7.40	<3.76							21
118	IRAS0420-014	Seyf1	0.9150	0.07	0.16	0.47	<1.02	17.6	-1.515					
119	IRAS0421+040		0.0460	0.10	0.27	0.70	1.26	15.2	-1.141					
120	IRAS0421+130	local	0.0000	0.54	0.86	1.40	<1.83							10
121	IRAS0422-147	HII	0.0175	<0.25	0.37	1.18	2.53	14.8	-1.177	<4.55		>4.38		10
122	IRAS0422-254	Seyf2	0.0436	<0.27	0.32	1.11	1.32	15.4	-1.275	<7.75	4.01	3.58	3.50	12
123	IRAS0424-637			<0.27	0.29	0.57	<1.00	14.1	-0.892					
124	IRAS0425-072	HII	0.0986	<0.38	0.30	0.76	0.86	16.1	-1.331	35.1	3.37	<0.11	<0.08	11
125	IRAS0425+012	local	0.0000	0.35	1.06	2.61	3.49							
126	IRAS0425-046		0.016:	<0.25	1.43	3.94	3.32	14.6	-1.389					10,21
127	IRAS0427+181	local	0.0000	<0.25	1.51	3.48	4.14							21
128	IRAS0427-637	liner?	0.0575	<0.25	0.33	0.74	<1.00	14.9	-1.089	<8.78		>2.20	>1.74	12
129	IRAS0428-097	HII	0.0469	<0.25	0.37	0.60	0.75	15.4	-1.155	<6.23		>1.82	>2.62	11,23
130	IRAS0428+180	local	0.0000	10.05	106.20	372.90	456.00							
131	IRAS0429+174	local	0.0000	1.27	1.65	3.03	5.16							23
132	IRAS0430+052	Seyf1	0.0327	0.33	0.71	1.31	2.64	14.1	-1.056	376.	0.81	5.45	1.10	10
133	IRAS0432-474			<0.34	0.30	0.77	<1.00	17.6	-1.619					12
134	IRAS0432-143A	local	0.0000	1.20	3.67	7.03	<10.24							11
135	IRAS0432-143B	local	0.0000	0.46	0.38	0.49	<6.01							11
136	IRAS0432-542			0.09	0.18	0.80	0.89	15.7	-1.258					
137	IRAS0433+021	HII	0.0116	0.27	0.99	3.61	3.81	14.3	-1.310	<7.33	>1.32	>7.39	>1.28	10
138	IRAS0433+142			0.11	0.26	1.52	2.38	13.9	-1.058					
139	IRAS0433-104	Seyf1	0.0344	0.33	0.79	2.75	4.07	13.5	-1.105	267.	0.60	3.75	1.17	10
140	IRAS0435-691			0.05	0.12	0.48	0.52	16.7	-1.345					
141	IRAS0438-086	Seyf2	0.0149	0.45	1.67	2.95	2.14	13.8	-1.165	<2.90	>2.15	>5.06	>3.29	10,20
142	IRAS0438-216			<0.09	0.15	0.95	1.83	15.7	-1.297					
143	IRAS0439-597NW	Seyf2	0.0577	<0.27	0.20	0.47	<1.03	14.8	-0.987	<5.18	>2.77	>2.80	>2.57	11
144	IRAS0439-272		0.0835	<0.30	0.31	0.71	1.63	16.5	-1.390					12
145	IRAS0440-497	HII	0.0269	<0.25	0.33	1.18	2.06	14.1	-1.034	<11.7	>1.70	>4.63	>2.65	12
146	IRAS0442-579			<0.16	0.14	0.68	1.15	14.8	-1.052					
147	IRAS0443+129	local	0.0000	0.75	0.36	1.97	7.32							
148	IRAS0444-052	Seyf1	0.0442	<0.39	0.29	0.84	<1.30	14.6	-1.069	39.1	0.58	4.42	1.45	11
149	IRAS0445-056	local	0.0000	0.27	0.48	0.60	<2.73							11
150	IRAS0445-587			0.09	0.14	0.67	1.51	14.2	-0.932					
151	IRAS0447-635			0.25	0.11	0.74	1.99	13.3	-0.778					
152	IRAS0449-360			<0.09	0.21	0.35	0.32	15.0	-0.949					
153	IRAS0449-646	Seyf1	0.0600	0.20	0.28	0.36	0.57	15.4	-1.034	14.4	2.34	5.20	1.89	12
154	IRAS0450-032	Seyf2	0.0158	<0.25	0.43	0.91	1.13	13.6	-0.884	<10.5	>7.47	>6.32	>5.21	11
155	IRAS0450-299	Seyf1	0.2860	<0.34	0.19	0.67	<1.00	15.7	-1.223					10
156	IRAS0450+039	Seyf2?	0.0297	0.27	0.58	0.66	<1.00	13.9	-0.880	23.0	11.77	5.48	1.53	11
157	IRAS0457-756	Seyf2	0.0181	0.39	0.44	0.70	1.55	13.5	-0.805	<7.49	>7.56	>4.53	>5.99	12
158	IRAS0458+074			<0.25	0.47	1.60	3.47	14.3	-1.148					
159	IRAS0459-089	local	0.0000	0.40	1.36	2.52	17.25							
160	IRAS0459-229	HII	0.0408	<0.27	0.26	0.80	1.60	14.0	-0.938	35.5	1.11	6.73	2.45	10
161	IRAS0501-398	local	0.0000	<0.38	0.31	0.65	<1.00							12
162	IRAS0501-107	local	0.0000	1.28	0.38	0.71	1.93							
163	IRAS0501-067	local	0.0000	0.57	0.80	2.93	11.98							
164	IRAS0503-764			0.06	0.11	0.58	1.02	14.5	-0.958					
165	IRAS0507-006	local	0.0000	1.61	0.42	0.51	<1.00							
166	IRAS0509-024	local	0.0000	0.25	1.20	1.79	<1.22							2
167	IRAS0509-009	local	0.0000	1.22	0.29	0.59	1.12							
168	IRAS0509-344			0.07	0.19	0.68	0.82	12.7	-0.650					
169	IRAS0510-072	local	0.0000	<0.25	0.32	0.63	<1.02							10
170	IRAS0510-129	local	0.0000	0.60	0.30	0.42	<5.39							
171	IRAS0513-002	Seyf1	0.0312	<0.40	0.47	0.66	1.30	13.6	-0.820	495.	0.10	3.56	0.27	10
172	IRAS0514+791	local	0.0000	1.15	0.24	0.28	<1.00							
173	IRAS0517-719			<0.25	0.59	1.16	2.24	16.9	-1.575					
174	IRAS0517-327	Seyf1	0.0126	<0.25	0.59	1.49	2.02	12.5	-0.782	208.	1.64	3.63	0.73	11
175	IRAS0521+762			<0.09	0.19	0.56	0.56	16.4	-1.337					
176	IRAS0521-122	Seyf1	0.0490	0.10	0.28	0.43	1.02	14.4	-0.887	160.	1.20	5.24	0.59	2
177	IRAS0522-087	local	0.0000	0.67	2.06	3.01	3.43							
178	IRAS0523-070	local	0.0000	<0.25	0.70	0.80	<1.04							10
179	IRAS0523-460	Seyf2	0.0439	0.24	1.01	2.80	2.97	14.2	-1.239	18.9	5.25	5.58	3.60	12
180	IRAS0524-192	HII	0.0280	0.10	0.11	0.47	1.02	13.0	-0.625					3
181	IRAS0530-056	local	0.0000	4.26	19.40	55.33	82.40							23
182	IRAS0531-065	local	0.0000	1.04	3.36	5.49	18.29							12
183	IRAS0531-063	local	0.0000	0.32	0.75	2.18	<14.28							3
184	IRAS0531-124	HII	0.0287	<0.09	0.17	0.82	1.04	15.3	-1.202	4.90	0.21	5.44	2.18	20
185	IRAS0533-739			0.16	0.13	0.84	1.34	15.2	-1.179					
186	IRAS0534-320			<0.09	0.17	0.75	0.75	16.7	-1.454					
187	IRAS0536-608			<0.25	0.30	1.04	1.13	13.8	-0.959					
188	IRAS0537-441	Seyf1	0.8940	<0.27	0.18	0.49	<1.00	16.5	-1.320					
189	IRAS0546-510	local	0.0000	3.48	9.10	19.61	10.87							
190	IRAS0555-654			0.08	0.36	0.41	0.50	17.7	-1.511					
191	IRAS0557-813	HII?	0.0126	<0.25	0.53	1.16	1.15	13.9	-0.989	15.1	4.56	3.00	1.36	11
192	IRAS0558-421			0.13	0.16	1.13	2.82	13.0	-0.813					
193	IRAS0558-756	local	0.0000	<0.26	0.24	0.72	<1.23							11
194	IRAS0559-579	Seyf2	0.0383	<0.25	0.23	0.77	1.01	14.0	-0.936	<10.1	>6.24	>3.62	>2.88	12
195	IRAS0602+675			0.09	0.31	1.10	1.01	14.7	-1.137					
196	IRAS0609+710	Seyf2	0.0130	0.70	2.86	3.88	3.35	12.5	-0.980	72.1	14.84	5.89	5.70	23
197	IRAS0611-326	Seyf2	0.0500	<0.25	0.28	0.83	1.13	14.1	-0.973	8.48	5.01	4.02	2.88	2
198	IRAS0611-728			0.11	0.13	0.44	0.56	15.4	-1.078					
199	IRAS0612-330			0.08	0.20	0.75	1.17	13.9	-0.898					
200	IRAS0614-498	HII	0.0373	<0.25	0.16	0.61	<1.05	15.1	-1.087	<5.66	>0.87	>3.86	>3.77	12

© European Southern Observatory • Provided by the NASA Astrophysics Data System

1992A&AS...96..389D

TABLE 2. *(continued)*

num	object	type	z	S12 (Jy)	S25 (Jy)	S60 (Jy)	S100 (Jy)	V (mag)	sp.indx. (V,60)	Hbeta (1E-15)	[OIII]/Hbeta	Halfa/Hbeta	[NII]/Hbeta	date (t.l)
201	IRAS0625+637	Seyf2	0.0402	<0.25	0.50	1.76	2.46	14.8	-1.263	18.7	3.96	2.70	1.52	20
202	IRAS0627+689E	Seyf2	0.0650	<0.37	0.29	0.85	<1.15	16.0	-1.329	1.78	6.62	5.05	3.01	23
203	IRAS0628+637	Seyf1	0.0123	<0.25	0.35	1.46	3.21	12.9	-0.852	104.	0.56	3.75	0.32	23
204	IRAS0629-664A	Seyf2	0.0466	<0.08	0.18	0.71	1.06	15.3	-1.167	9.33	10.20	2.99	1.54	12
205	IRAS0629-664B	HII?	0.0484	<0.25	0.31	0.54	0.67	15.4	-1.123					
206	IRAS0631-640	Seyf2	0.0485	<0.26	0.25	0.57	0.99	14.9	-1.040	<5.10	>8.17	>4.15	>2.70	12
207	IRAS0635-698			0.07	0.22	0.66	0.83	16.7	-1.422					
208	IRAS0641+636W	HII	0.0189	<0.25	0.27	0.60	<1.05	15.0	-1.066	30.1	3.15	3.25	0.74	23
209	IRAS0645+744	Seyf1	0.0184	<0.31	0.68	1.12	0.82	13.3	-0.873	330.	2.12	7.58	0.72	23
210	IRAS0647-672			<0.06	0.06	0.65	1.46	14.5	-0.982					
211	IRAS0650+504	Seyf1	0.0200	0.14	0.25	1.77	2.66	14.1	-1.133					
212	IRAS0652-663			0.14	0.17	0.28	0.34	16.7	-1.231					
213	IRAS0656-654	Seyf1	0.0295	<0.25	0.19	0.78	1.13	14.2	-0.976	76.4	0.36	2.92	0.70	12
214	IRAS0703+591			0.08	0.19	1.30	2.50	14.6	-1.163					
215	IRAS0710+457	Seyf1	0.0559	<0.35	0.57	0.87	<1.27	13.8	-0.909	386.	0.07	2.36	0.07	23
216	IRAS0712+879NW	HII	0.0875	<0.28	0.19	0.83	<4.04	16.7	-1.468	2.73	0.78	10.04	6.71	23
217	IRAS0714+410		0.0230	0.12	0.26	1.39	1.93	13.9	-1.035					
218	IRAS0731+621	HII	0.1207	<0.25	0.48	1.44	1.24	17.2	-1.681	8.61	1.22			23
219	IRAS0731+329			0.20	0.35	1.48	3.42	12.1	-0.701					
220	IRAS0732+588	Seyf1	0.0390	<0.29	0.53	0.88	1.41	13.9	-0.941					
221	IRAS0732-870	HII	0.0165	<0.25	0.17	0.65	<4.24	14.7	-1.038	28.2	2.57	4.02	1.05	11
222	IRAS0732+697			<0.25	0.43	1.64	0.90	17.3	-1.720					
223	IRAS0734+497			0.28	0.18	1.34	2.21	15.3	-1.305					
224	IRAS0737+652	Seyf2	0.0380	<0.25	0.54	1.12	1.23	13.5	-0.903					
225	IRAS0738+499	Seyf1	0.0220	0.27	0.78	1.50	2.19	12.5	-0.774					
226	IRAS0741+293	Seyf2	0.0160	0.28	0.34	0.63	1.95	10.8	-0.263					
227	IRAS0743+610	Seyf1	0.0300	<0.25	0.28	0.85	2.23	12.6	-0.687					
228	IRAS0748+280			<0.14	0.13	0.62	1.21	15.5	-1.174					
229	IRAS0748-733			0.12	0.19	0.62	2.72	15.0	-1.071					
230	IRAS0750+246			0.10	0.15	0.83	1.19	15.6	-1.253					
231	IRAS0751+534	HII	0.0248	0.13	0.20	1.37	3.24	13.4	-0.943					26
232	IRAS0755+509			<0.25	0.38	0.75	<1.00	15.1	-1.128					
233	IRAS0757+267	Seyf1	0.0255	<0.25	0.44	0.99	<1.51	13.2	-0.822	<10.0	>18.79	>11.07	>12.96	26
234	IRAS0759+260			0.22	0.26	0.51	0.50	14.7	-0.987					
235	IRAS0759+651		0.1500	0.24	0.62	1.75	1.87	14.2	-1.134					
236	IRAS0804+391	Seyf2	0.0230	<0.25	0.45	1.38	1.51	13.2	-0.894					
237	IRAS0807+187	HII	0.0160	<0.31	0.73	2.79	3.08	13.9	-1.172	<4.99		>4.68	>2.69	10
238	IRAS0807+581	Seyf2	0.0280	0.15	0.21	1.34	2.36	13.6	-0.973					26
239	IRAS0811+462			0.10	0.28	1.24	1.81	13.6	-0.951					
240	IRAS0813+261		0.0420	<0.09	0.41	1.21	1.14	15.5	-1.307					
241	IRAS0818+532	local	0.0000	0.50	3.62	7.48	4.89							
242	IRAS0821+174		0.0370	0.15	0.28	0.61	1.16	14.0	-0.879					
243	IRAS0821+364			0.10	0.21	0.67	1.62	15.0	-1.085					
244	IRAS0825-776	Seyf2	0.0175	<0.28	0.45	1.32	4.65	13.7	-0.986	11.2	2.81	4.64	2.37	11
245	IRAS0827-027	Seyf2	0.0404	<0.25	0.42	1.52	1.82	14.0	-1.075	8.77	14.00	6.90	8.99	10
246	IRAS0832+664	HII	0.0180	<0.28	0.49	1.58	1.16	15.1	-1.295					
247	IRAS0844+180	local	0.0000	2.12	41.49	89.31	49.44							
248	IRAS0851+179	Seyf1	0.0640	0.17	0.22	0.82	1.11	14.8	-1.107					
249	IRAS0856+559		0.0080	0.11	0.12	0.51	1.75	12.4	-0.535					
250	IRAS0910+411	Seyf2	0.4420	0.17	0.39	0.55	<0.39	17.8	-1.587					
251	IRAS0911+679	HII	0.0308	<0.09	0.23	1.01	1.62	14.4	-1.071	14.8	0.17	3.86	2.07	14
252	IRAS0916+264	local	0.0000	2.05	0.59	1.02	<1.00							
253	IRAS0918-078	Seyf2	0.0198	0.14	0.48	0.74	1.06	13.7	-0.866	5.82	15.36	8.61	4.43	3
254	IRAS0930-841	Seyf2	0.0628	<0.25	0.36	0.48	2.14	15.6	-1.145	<5.62	>4.79	>11.56	>6.28	11
255	IRAS0930+682	Seyf2	0.0703	0.10	0.26	0.45	<1.15	15.7	-1.149	5.27	8.85	4.90	4.97	14
256	IRAS0943-131	Seyf2	0.1310	<0.28	0.42	0.52	<1.00	16.3	-1.290	15.4	10.59			10
257	IRAS0943+032N	HII	0.0202	0.48	0.59	5.19	11.32	13.8	-1.284	<4.10	>0.85	>5.55		10
258	IRAS0945+594	HII	0.0072	0.09	0.23	0.89	1.20	13.4	-0.837	12.3	0.74	6.16	1.72	15
259	IRAS0945+507E	Seyf1	0.0563	0.13	0.25	0.69	0.71	15.1	-1.126	46.3	0.78	5.40	1.49	15
260	IRAS0949-013	Seyf1	0.0194	0.70	1.20	1.41	1.07	13.3	-0.922	425.	1.10	5.22	1.16	10
261	IRAS0952+136SE	HII	0.0192	<0.25	0.39	0.80	<1.41	14.2	-0.969	63.6	2.45	5.38	1.54	10
262	IRAS1020+331N	HII	0.1256	<0.11	0.15	0.58	0.55	17.7	-1.579	3.31	0.90			16
263	IRAS1021+675	Seyf2	0.0386	<0.35	0.43	0.77	<1.43	14.3	-0.994	12.7	9.24	6.10	3.15	14
264	IRAS1022-183	local	0.0000	4.52	35.53	53.00	28.85							
265	IRAS1022-828			0.20	0.33	0.58	1.32	15.0	-1.065					
266	IRAS1028+290	HII	0.0041	<0.25	0.67	2.21	3.40	12.0	-0.766	80.9	0.41	4.73	1.46	13
267	IRAS1030+602	Seyf2	0.0505	<0.26	0.47	0.95	<1.10	14.1	-0.996	43.3	9.69	3.27	2.77	14
268	IRAS1033+636	HII	0.0377	<0.09	0.19	0.74	0.86	15.9	-1.296	4.23	1.33	8.55	2.70	14
269	IRAS1037+598			0.09	0.23	0.78	0.92	17.5	-1.620					
270	IRAS1040+706	Seyf2	0.0328	<0.25	0.26	0.95	2.82	14.2	-1.004	4.54	12.61	7.20	9.22	14
271	IRAS1045+503	HII	0.0229	0.20	0.33	0.58	1.32	14.0	-0.871	9.81	<0.30	4.76	2.32	15
272	IRAS1045-248	Seyf2	0.0137	<0.25	0.71	2.38	3.94	11.9	-0.751	68.5	14.38	5.04	5.06	12
273	IRAS1046-316			<0.14	0.26	1.05	1.48	16.1	-1.403					
274	IRAS1047-281	Seyf1	0.1929	<0.78	0.36	0.98	<1.65	15.5	-1.264	<6.23	>5.92			12
275	IRAS1051-273	Seyf2	0.1599	<0.25	0.35	0.91	<1.00	16.1	-1.381	3.47	17.44			2
276	IRAS1056-333	HII	0.0595	<0.25	0.70	2.12	<1.34	16.6	-1.650	5.82	3.35	4.90	0.55	12
277	IRAS1059-344	local	0.0000	0.70	2.46	3.88	4.85							3
278	IRAS1103+728	Seyf1	0.0086	0.45	0.92	1.74	2.17	11.9	-0.689	280.	0.44	6.21	0.21	5
279	IRAS1105-115	Seyf2	0.0548	<0.25	0.42	0.72	<1.38	14.9	-1.099	27.5	7.09	3.70	1.79	2
280	IRAS1119+045	HII	0.0378	0.88	0.49	0.84	2.15	15.2	-1.176	5.88	0.33	7.02	3.17	2
281	IRAS1121-281	Seyf2	0.0135	<0.44	0.31	0.59	<1.00	13.0	-0.682	<7.75	>6.61	>3.85	>2.42	2
282	IRAS1124-289	Seyf2	0.0234	0.11	0.34	0.60	0.94	13.4	-0.767	10.6	10.74	5.04	4.85	3
283	IRAS1129+532	Seyf2	0.0254	0.16	0.26	0.68	1.74	13.2	-0.747	<15.5	>11.47	>5.41	>8.32	15
284	IRAS1131+216	HII	0.0214	0.17	0.22	1.00	2.38	12.9	-0.762	70.2	0.29	3.42	0.66	13
285	IRAS1133+572	Seyf2	0.0507	0.16	0.52	1.55	2.17	14.7	-1.210	10.1	6.64	3.53	5.35	15
286	IRAS1136-374	Seyf1	0.0107	0.80	2.45	3.33	4.93	12.0	-0.841	829.	0.92	3.72	0.79	12
287	IRAS1151-395	local	0.0000	1.98	0.67	1.00	3.94							
288	IRAS1152+229	local	0.0000	0.15	0.27	1.34	1.97							
289	IRAS1159+046	liner	0.0210	<0.17	0.18	0.66	1.28	13.9	-0.884	<9.39		>3.32	>2.64	11
290	IRAS1210+060	HII	0.0814	<0.20	0.23	0.49	0.81	16.2	-1.260	<12.4		>3.65	>1.15	11
291	IRAS1215+064	HII	0.0184	0.22	0.86	2.72	3.11	13.4	-1.082	16.9	<0.62	10.01	6.24	8
292	IRAS1215+300	Seyf1	0.0123	0.41	1.38	4.01	4.07	12.7	-1.024	270.	1.68	5.04	1.14	13
293	IRAS1223+129	Seyf2	0.0084	1.00	3.57	10.73	17.27	11.5	-0.996	47.9	11.78	5.73	2.47	11
294	IRAS1223-388	HII	0.0120	0.09	0.26	1.13	2.66	13.2	-0.850					
295	IRAS1226+023	Seyf1	0.1580	0.52	0.93	2.22	2.91	13.1	-0.985					3
296	IRAS1227-355	local	0.0000	<0.25	0.60	0.78	<1.00							
297	IRAS1231+828	local	0.0000	0.77	7.16	8.44	4.30							
298	IRAS1231+779SE	HII	0.0277	0.08	0.12	0.89	1.97	14.2	-0.998	<10.1		>4.72	>2.17	14
299	IRAS1232-396	Seyf2	0.0132	0.46	1.42	4.52	5.40	12.2	-0.950	105.	7.89	3.76	1.74	12
300	IRAS1233-395	local	0.0000	<0.43	3.40	7.23	3.67							

© European Southern Observatory • Provided by the NASA Astrophysics Data System

1992A&AS...96..389D

TABLE 2. *(continued)*

num	object	type	z	S12 (Jy)	S25 (Jy)	S60 (Jy)	S100 (Jy)	V (mag)	sp.indx. (V,60)	Hbeta (1E-15)	[OIII]/Hbeta	Halfa/Hbeta	[NII]/Hbeta	date (t.1)
301	IRAS1237-050	Seyf1	0.0078	0.34	0.92	2.81	6.00	11.3	-0.687	407.	0.33	3.34	0.66	8
302	IRAS1238-364	Seyf2	0.0125	0.66	2.32	7.08	10.77	12.3	-1.058	41.5	7.58	6.14	3.79	11
303	IRAS1244+268	HII	0.0027	<0.25	0.35	0.48	<1.00	12.6	-0.561	51.1	2.69	4.13	0.37	13,28
304	IRAS1244-024	HII	0.0052	<0.12	0.52	1.38	2.00	11.7	-0.609	250.	1.33	3.33	0.90	26
305	IRAS1245-424	local	0.0000	<0.25	1.02	2.70	1.43							
306	IRAS1246+421	Seyf2	0.0270	<0.28	0.48	1.70	2.32	13.6	-1.018	<6.01	>15.36	>2.64	>3.27	13,29
307	IRAS1246-111	Seyf2	0.0481	<0.25	0.76	1.44	1.55	14.9	-1.231	33.0	12.38	5.09	3.60	1
308	IRAS1247+437S	HII	0.0622	<0.26	0.40	1.05	0.94	15.4	-1.267	26.0	2.93	4.48	1.89	15
309	IRAS1249-131	Seyf1	0.0136	0.23	0.31	1.08	2.04	13.0	-0.815	450.	0.81	2.73	0.73	3
310	IRAS1250-413	Seyf2	0.0162	<0.25	0.30	0.98	1.73	12.4	-0.667	<10.9	>7.46	>4.51	>3.40	11
311	IRAS1254-301	Seyf2	0.0546	0.10	0.31	1.05	1.46	15.6	-1.304	<4.89	>5.54	>4.81	>3.49	11
312	IRAS1258-306			0.09	0.37	0.92	2.38	12.8	-0.741					
313	IRAS1304-234	Seyf2	0.0093	0.37	1.25	2.34	3.34	12.5	-0.871	8.24	21.50	11.94	12.08	3
314	IRAS1305-241	Seyf2	0.0141	<0.25	0.71	1.41	1.75	13.9	-1.036	<3.99	>2.92	>4.83	>2.41	2
315	IRAS1314+451E	Seyf2	0.0905	<0.25	0.49	0.72	<1.40	15.8	-1.258	16.2	5.00	3.47	1.82	15
316	IRAS1317-232			<0.14	0.38	0.80	0.88	15.0	-1.134					
317	IRAS1319-164	Seyf2	0.0164	0.89	2.81	5.60	5.61	12.5	-1.049	78.1	19.35	8.14	8.10	2
318	IRAS1321+058		0.1900	0.26	0.41	1.20	0.81	18.0	-1.794					
319	IRAS1322-381			<0.12	0.34	1.23	2.03	15.0	-1.217					
320	IRAS1324+268W	HII	0.0234	0.14	0.24	0.71	0.71	14.1	-0.938	27.7	0.72	3.65	1.15	4
321	IRAS1329-393			0.13	0.26	0.94	0.89	15.3	-1.217					
322	IRAS1330-337	Seyf2	0.0128	<0.25	0.39	0.65	<1.00	13.6	-0.813	17.7	8.49	5.58	1.30	7
323	IRAS1332-344	HII	0.0492	<0.14	<0.12	0.52	0.85	15.4	-1.127	11.5	0.39	3.57	1.65	11
324	IRAS1332-340	Seyf1	0.0075	0.40	0.81	1.12	<1.00	12.7	-0.749	106.	0.71	7.25	1.30	2,11
325	IRAS1337-313	HII	0.0009	2.59	12.21	30.91	29.04	9.9	-0.907	824.	5.49	3.59	0.48	8
326	IRAS1343-121	local	0.0000	2.36	0.57	0.89	1.99							
327	IRAS1344+351	HII	0.0539	<0.25	0.49	1.02	0.87	15.7	-1.325	21.7	2.51	4.15	0.62	5
328	IRAS1345+125W	Seyf2	0.1202	<0.25	0.66	2.01	2.14	16.3	-1.581	<6.88	>4.95	>5.53	>4.02	28
329	IRAS1351+337	Seyf2	0.0076	0.34	0.93	1.44	2.59	12.2	-0.709	<5.01	>8.95	>5.14	>3.99	4
330	IRAS1351-375	Seyf1	0.0520	<0.39	0.40	0.50	<1.00	14.5	-0.938	32.4	<2.64	10.99	<3.17	11
331	IRAS1351+640	Seyf1	0.0878	<0.26	0.54	0.72	0.79	14.0	-0.924	197.	0.70	2.54	0.15	14
332	IRAS1351+695	Seyf1	0.0294	<0.25	0.26	1.08	2.28	14.3	-1.056	443.	0.19	3.43	0.54	14
333	IRAS1353+186E	Seyf2	0.0498	0.57	1.61	2.18	1.87	13.8	-1.105	62.5	9.01	4.23	1.69	11
334	IRAS1357+562	HII	0.0338	<0.07	0.21	0.83	1.28	15.2	-1.175	8.91	<0.30	4.29	2.00	14
335	IRAS1402-316		0.0923	<0.11	<0.11	0.54	0.47	16.5	-1.337					3,28
336	IRAS1402+436S	Seyf1	0.3233	<0.45	0.26	0.61	1.28	15.2	-1.104	10.8	2.39	57.69	2.36	29
337	IRAS1404+012			0.13	0.34	0.89	0.55	18.4	-1.809					
338	IRAS1404+286W	Seyf1	0.0769	<0.40	0.38	0.74	<1.00	14.9	-1.093	30.2	0.63	7.95	0.39	4
339	IRAS1407+266	HII	0.0597	0.07	0.07	0.89	1.13	15.5	-1.246					29,6
340	IRAS1408+137	Seyf2	0.0158	<0.26	1.04	3.64	2.85	13.9	-1.238	<7.08	>3.91	>8.08	>7.25	11,16
341	IRAS1410-029	Seyf2	0.0070	1.30	3.66	8.67	9.40	10.9	-0.839					
342	IRAS1411+078	liner	0.0235	<0.12	0.21	1.36	2.14	12.8	-0.813	<16.1		>3.25	>3.53	13
343	IRAS1414+463	local	0.0000	1.15	0.36	0.47	<1.00							
344	IRAS1415+253	Seyf1	0.0169	0.36	0.76	1.04	1.73	12.1	-0.627	750.	0.48	4.95	0.70	
345	IRAS1417-841			0.08	0.24	0.68	0.87	16.2	-1.333					
346	IRAS1426+274	HII	0.0143	<0.12	0.24	0.86	0.80	13.6	-0.884	31.3	1.54	4.90	1.35	13
347	IRAS1426+573	Seyf2	0.0428	0.11	0.19	0.51	0.95	14.8	-0.995	7.09	7.80	3.54	1.92	5
348	IRAS1428-030	HII	0.0428	0.13	0.17	0.77	1.60	17.0	-1.508	<2.11		>4.36	>1.13	1
349	IRAS1431-326	Seyf2	0.0254	<0.27	0.32	0.94	<1.00	14.4	-1.054	<5.07	>4.19	>6.58	>7.50	1
350	IRAS1434+590	Seyf1	0.0305	0.40	1.23	2.24	2.19	13.6	-1.083	281.	0.43	4.73	0.06	4
351	IRAS1435+386	HII	0.0115	<0.25	0.37	1.27	2.61	12.5	-0.751	17.3	0.30	4.06	2.09	13
352	IRAS1439+537	Seyf2	0.0378	<0.25	0.54	1.34	1.85	13.9	-1.022	140.	11.08	4.54	1.46	26
353	IRAS1442+590	HII	0.0388	0.12	0.11	0.75	1.66	14.8	-1.080	9.80	<0.25	4.11	1.68	14
354	IRAS1443+272	Seyf2	0.0294	<0.25	0.34	0.78	1.24	14.7	-1.063	19.4	7.60	5.44	2.08	13
355	IRAS1445-828	Seyf2	0.1144	<0.25	0.39	1.09	1.29	16.0	-1.399	5.54	8.72			8
356	IRAS1447+425	Seyf2	0.1783	<0.31	0.30	0.49	<1.00	17.0	-1.417	<1.31	>31.48	>16.86	>13.43	5,29
357	IRAS1454+491	Seyf2	0.2459	0.05	0.21	0.55	0.53	18.2	-1.670					15
358	IRAS1455-285	Seyf1	0.0481	0.31	0.38	0.67	0.78	15.3	-1.143	12.8	5.01	4.15	2.73	11
359	IRAS1501+106	Seyf1	0.0362	<0.39	0.45	0.49	<1.00	13.7	-0.771	693.	0.48	3.39	0.40	10
360	IRAS1506+661	HII	0.0286	0.15	0.16	1.80	3.51	13.9	-1.088	13.4	0.52	6.46	1.89	14
361	IRAS1506+283	HII	0.0268	<0.25	0.27	0.84	<1.17	15.3	-1.207	10.5	1.26	4.42	1.54	5
362	IRAS1506+092SE	Seyf2	0.0450	<0.25	0.29	0.71	1.12	14.4	-0.995	<11.2	>8.85	>6.49	>0.72	11
363	IRAS1509-211	Seyf1	0.0444	<0.41	0.64	1.61	1.75	14.1	-1.099	141.	1.12	6.74	1.11	1
364	IRAS1512-324	local	0.0000	0.81	0.31	0.44	<7.12							
365	IRAS1514+601	HII	0.0447	<0.07	0.15	0.74	1.06	15.3	-1.172	15.2	1.94	5.70	2.46	6,15
366	IRAS1517+522NW	Seyf2	0.1371	<0.25	0.33	0.83	1.48	16.2	-1.367	<2.68	>10.03			
367	IRAS1518+085	Seyf2	0.0306	0.18	0.25	0.82	1.55	13.9	-0.914	12.2	5.60	7.90	3.31	13
368	IRAS1518+657SW	Seyf2	0.0444	0.15	0.35	0.88	1.19	13.9	-0.947	<5.31	>16.53	>7.04	>3.58	30
369	IRAS1519+393	Seyf1	0.0292	0.10	0.15	0.46	0.78	14.1	-0.847	13.8	3.78	6.52	0.87	13
370	IRAS1521+087	Seyf2	0.0364	<0.25	0.34	0.78	<1.03	14.8	-1.088	<6.06	>2.17	>4.12	>6.68	11,16
371	IRAS1521-110			<0.11	0.26	0.79	1.21	16.2	-1.362					
372	IRAS1524+007	Seyf2	0.0508	<0.25	0.47	0.91	1.26	15.0	-1.165	3.64	10.00	5.59	3.27	3
373	IRAS1529+242S	Seyf2	0.0961	0.10	0.34	1.07	1.06	15.7	-1.335	4.12	16.48	7.33	3.73	13
374	IRAS1529+471			<0.07	0.18	0.89	0.99	13.8	-0.916					
375	IRAS1530+302	Seyf2	0.0650	0.09	0.26	0.33	0.44	15.1	-0.956	<5.61	>9.21	>2.19	>2.73	6
376	IRAS1531+580S	HII	0.0391	0.13	0.24	1.10	1.39	15.2	-1.232	28.0	1.60	3.96	1.11	15
377	IRAS1536+736	Seyf2	0.0248	<0.29	0.61	1.31	2.01	13.3	-0.897	7.60	6.14	4.00	3.56	6
378	IRAS1537+251SW	HII	0.0228	<0.25	0.61	2.27	2.88	14.4	-1.243	14.0	4.19	3.97	1.40	15
379	IRAS1541+286	Seyf2	0.0320	<0.25	0.38	1.24	1.47	14.3	-1.097	11.0	10.60	5.46	4.92	15
380	IRAS1543+272	Seyf1	0.0310	<0.05	0.12	0.69	0.85	14.6	-1.016	<6.05	>1.49	>3.41	>1.56	15,29
381	IRAS1544+060	liner	0.0413	<0.25	0.32	1.07	1.46	13.9	-0.982	<13.4	>0.73	>2.37	>2.53	7,16
382	IRAS1547-037	local	0.0000	0.55	1.89	5.43	3.36							
383	IRAS1548-037	Seyf2	0.0303	<0.28	0.75	1.18	<4.14	14.2	-1.061	5.98	23.11	10.19	5.82	3
384	IRAS1550-200	local	0.0000	0.56	0.39	0.65	<1.27							
385	IRAS1555-141	local	0.0000	<0.25	0.90	2.89	<1.36							11
386	IRAS1555-204	HII	0.0150	<0.11	<0.17	0.94	2.13	14.9	-1.149	<2.15	>2.54	>6.72		11,29
387	IRAS1555-228	local	0.0000	0.87	3.18	6.45	4.71							
388	IRAS1556+269	HII	0.0136	<0.25	0.83	3.04	2.94	13.3	-1.074	23.6	0.43	7.93	4.21	13
389	IRAS1557-225	local	0.0000	<0.43	1.46	3.97	<9.80							29
390	IRAS1557+351	Seyf1	0.0316	<0.25	0.27	0.64	1.34	14.0	-0.897	48.2	0.41	3.73	0.23	6
391	IRAS1559+832	HII	0.0216	1.26	0.44	0.76	1.18	14.7	-1.067	<2.71		>9.45	>3.72	14
392	IRAS1559+021	Seyf2	0.1034	<0.30	0.28	0.57	<1.00	15.9	-1.232	4.50	18.13	6.49	3.40	16
393	IRAS1600+264N	Seyf1	0.0724	0.20	0.18	0.56	1.40	15.3	-1.119	36.2	0.45	3.26	0.45	15
394	IRAS1602-182	local	0.0000	<0.33	0.73	1.61	<1.52							
395	IRAS1602+408	local	0.0000	<0.25	0.74	1.91	1.58							15
396	IRAS1603+632	HII	0.0558	<0.08	0.15	1.03	1.37	15.5	-1.281	17.1	1.07	5.30	1.70	14
397	IRAS1606-167	local	0.0000	0.67	0.64	0.90	<6.85							18
398	IRAS1606+124	Seyf1	0.0323	<0.25	0.36	0.82	1.02	13.7	-0.891	101.	0.60	5.35	1.07	16
399	IRAS1608-185	local	0.0000	9.47	13.88	18.95	15.77							
400	IRAS1611-195	local	0.0000	0.61	1.32	2.20	<6.73							

© European Southern Observatory • Provided by the NASA Astrophysics Data System

1992A&AS...96..389D

TABLE 2. *(continued)*

num	object	type	z	S12 (Jy)	S25 (Jy)	S60 (Jy)	S100 (Jy)	V (mag)	sp.indx. (V,60)	Hbeta (1E-15)	[OIII]/Hbeta	Halfa/Hbeta	[NII]/Hbeta	date (t.1)
401	IRAS1612-192	local	0.0000	0.75	1.87	6.32	<46.20							
402	IRAS1612-078	liner?	0.0326	0.16	0.15	1.09	1.87	14.7	-1.141	6.56	2.03	7.80	5.01	18
403	IRAS1615+141	HII	0.0333	<0.33	0.26	1.01	1.72	14.9	-1.156	13.1	0.44	5.05	1.94	13
404	IRAS1616-147	local	0.0000	6.91	1.78	1.93	5.99							
405	IRAS1616-197	local	0.0000	0.28	0.86	1.03	<11.26							18
406	IRAS1618-001	local	0.0000	<0.25	0.77	1.02	<1.00							18
407	IRAS1619-196	local	0.0000	2.38	5.96	11.19	<16.57							
408	IRAS1626+518	Seyf1	0.0547	0.13	0.29	0.38	0.32	14.9	-0.954	23.8	4.85	6.22	0.94	14
409	IRAS1628+394W	Seyf2	0.0297	<0.41	0.18	0.69	<1.00	13.6	-0.828	14.5	4.77	4.04	3.28	15
410	IRAS1632+425	local	0.0000	0.96	0.25	0.26	<1.00							
411	IRAS1633-104	local	0.0000	<0.26	0.31	1.40	<10.86							
412	IRAS1634-103A	local	0.0000	0.48	4.96	16.49	<21.11							18
413	IRAS1634-103B	local	0.0000	0.90	6.06	19.58	17.70							
414	IRAS1634+074	local	0.0000	1.14	0.26	0.57	0.89							
415	IRAS1634+441	HII	0.0350	<0.25	0.21	0.84	1.68	14.0	-0.945	67.5	0.42	4.13	1.71	15
416	IRAS1634+145	local	0.0000	<0.25	0.43	1.04	1.44							
417	IRAS1636+856	Seyf1	0.0631	0.08	0.20	0.43	0.61	15.5	-1.093	84.9	0.22	2.98	0.11	5
418	IRAS1638-062W	Seyf2?	0.0279	0.20	0.27	0.88	0.73	14.7	-1.102	7.85	3.56	8.04	5.88	26,29
419	IRAS1638-093			<0.25	0.35	0.69	3.83	17.0	-1.497					
420	IRAS1641+399	Seyf1	0.5940	<0.32	0.27	0.60	0.85	15.9	-1.254					
421	IRAS1641+156NW	HII	0.0662	<0.13	0.19	1.01	1.11	15.9	-1.350	7.14	0.62	6.28	3.38	16
422	IRAS1642+238	local	0.0000	2.07	25.89	34.63	14.62							
423	IRAS1643-113	local	0.0000	0.33	0.79	1.13	<10.15							
424	IRAS1643-097	local	0.0000	<0.25	0.20	1.51	<9.20							
425	IRAS1644-095	local	0.0000	0.57	3.32	7.73	7.40							
426	IRAS1645+391NW	HII	0.0291	<0.07	0.26	1.20	1.62	14.5	-1.119	29.0	0.13	3.32	1.51	14
427	IRAS1645-099	local	0.0000	<0.25	0.35	0.56	<8.26							
428	IRAS1647-090	local	0.0000	<0.25	0.30	0.93	9.73							
429	IRAS1649+220N	Seyf2	0.0546	<0.25	0.45	0.99	0.94	15.6	-1.290	6.76	3.37	5.19	6.53	16
430	IRAS1657+290	HII	0.0322	0.18	0.13	1.07	2.42	13.1	-0.833	30.7	0.93	7.81	4.14	15
431	IRAS1658-041	local	0.0000	13.73	4.18	5.03	6.10							
432	IRAS1700+518	Seyf1	0.2920	0.11	0.23	0.42	0.44	15.2	-1.037					4
433	IRAS1702+457S	Seyf2	0.0604	<0.25	0.42	1.10	1.60	15.1	-1.221	13.6	3.04	5.40	3.06	15
434	IRAS1704+673N	HII	0.1349	<0.25	0.30	1.28	<1.12	17.2	-1.656	1.12	3.29	12.04	5.43	14,29
435	IRAS1705+148	local	0.0000	1.67	0.42	0.65	<1.06							
436	IRAS1707+636	local	0.0000	0.09	0.13	0.86	2.03	13.3	-0.826					14,29
437	IRAS1710-032	local	0.0000	<0.25	1.30	2.77	<1.63							
438	IRAS1712+395	Seyf2	0.0362	0.14	0.17	0.71	1.29	14.7	-1.039	<2.68	>2.04	>3.21	>1.63	22
439	IRAS1715+133	local	0.0000	1.09	0.32	0.28	1.50							
440	IRAS1716+152	local	0.0000	1.51	0.39	0.28	<1.07							
441	IRAS1716+302NE	HII	0.0140	0.07	0.25	0.92	1.00	14.2	-1.003	56.3	2.80	4.22	0.86	15
442	IRAS1721+365SW	Seyf1	0.0400	0.14	0.14	0.34	0.81	14.1	-0.781	71.4	1.30	3.61	0.31	6
443	IRAS1722+230	local	0.0000	0.37	0.29	0.57	<1.00							
444	IRAS1727+575E	HII	0.0282	<0.25	0.15	0.96	1.67	14.0	-0.983	48.3	1.08	3.56	0.86	14
445	IRAS1729+596	Seyf2	0.0281	0.07	0.11	0.70	1.70	14.0	-0.906	<4.78	>4.53	>3.31	>3.23	15
446	IRAS1732+389			0.11	0.19	0.39	0.58	16.7	-1.307					
447	IRAS1733+208	Seyf2	0.0240	<0.25	0.39	0.70	1.57	13.4	-0.796	26.5	9.74	3.99	1.67	13
448	IRAS1734+177	local	0.0000	<0.25	0.99	1.50	<1.00							6
449	IRAS1734+493W	Seyf2	0.0748	<0.25	0.30	0.79	1.06	15.8	-1.289	2.99	9.09	7.15	3.79	4
450	IRAS1737+562S	Seyf2	0.0646	<0.25	0.38	1.01	1.51	15.2	-1.214	<4.97	>9.67	>4.60	>6.15	15
451	IRAS1740+518	local	0.0000	1.58	0.38	0.46	1.00							
452	IRAS1740+214	local	0.0000	<0.25	0.34	0.96	<1.31							
453	IRAS1743+579S	HII	0.0386	0.06	0.14	0.77	0.77	15.6	-1.231	4.70	1.87	6.01	3.89	14
454	IRAS1746+676	local	0.0000	0.74	0.17	0.22	0.35							
455	IRAS1749+269	Seyf1	0.1453	<0.26	0.22	0.44	<1.01	15.1	-1.024	90.0	0.09	4.11	0.31	26
456	IRAS1750+508	Seyf1	0.2997	<0.25	0.33	0.47	<1.00	15.4	-1.104	170.	0.43	4.54	0.58	27
457	IRAS1752+189	Seyf2	0.0395	0.09	0.18	0.69	1.06	14.2	-0.936	<3.84	>0.78	>3.99	>2.76	6,15
458	IRAS1752+280	local	0.0000	<0.25	1.65	2.19	0.87							
459	IRAS1758+666	local	0.0000	7.51	113.50	133.40	62.79							
460	IRAS1759+423	Seyf2	0.0526	<0.07	0.15	0.63	0.69	14.5	-0.983	<20.7	>4.61	>1.88	>3.84	13
461	IRAS1800+666			0.23	1.08	2.59	2.87	18.2	-1.993					
462	IRAS1801+414NE	HII	0.0426	<0.06	0.09	0.62	1.11	15.6	-1.193	<0.73	>1.47	>5.39	>3.47	15,22
463	IRAS1803+468		0.0240	0.16	0.14	0.92	2.54	13.4	-0.842					13,22
464	IRAS1807+698	BL-Lac	0.0510	0.10	0.19	0.31	0.37	13.3	-0.599					14
465	IRAS1813+368	local	0.0000	0.62	0.26	0.41	<1.00							
466	IRAS1818+526	local	0.0000	0.65	0.23	0.57	1.51							
467	IRAS1821+643	Seyf1	0.2970	0.26	0.44	1.26	2.26	14.1	-1.053					14
468	IRAS1825+717	HII	0.0832	<0.05	0.11	0.85	1.06	16.7	-1.479	<1.47	>0.72	>8.15	>4.72	14
469	IRAS1825+412SW	HII	0.0833	<0.25	0.37	1.10	<4.00	16.1	-1.421	23.3	3.05	4.74	0.68	16
470	IRAS1829+412N	Seyf1	0.0922	0.06	0.19	0.39	0.68	15.4	-1.051	69.4	1.11	3.34	0.50	16
471	IRAS1832-594	Seyf2	0.0192	0.60	1.39	3.17	4.09	13.2	-1.071	50.0	4.52	9.91	6.20	1
472	IRAS1834-674			0.18	0.26	1.39	4.07	12.3	-0.715					
473	IRAS1840-624	Seyf1	0.0136	0.38	0.86	2.00	2.62	12.8	-0.893	279.	0.69	4.59	0.89	3
474	IRAS1840+773E	HII	0.0875	<0.08	0.26	0.82	0.94	17.4	-1.609	2.35	1.78	14.31	4.70	23,30
475	IRAS1846+721	Seyf2	0.0461	<0.25	0.26	0.95	0.97	14.0	-0.973	25.3	5.23	5.90	2.31	14
476	IRAS1850-782	Seyf1	0.0610	<0.25	0.25	1.10	1.93	16.1	-1.421					18
477	IRAS1855+716S	HII	0.0923	<0.07	0.15	0.75	0.71	16.3	-1.377	37.6	2.58	3.35	0.47	14
478	IRAS1900-672	HII	0.0155	<0.25	0.31	1.15	1.47	14.4	-1.083	18.1	1.40	5.11	1.54	18
479	IRAS1908-539NW	HII	0.0230	0.18	0.36	1.45	4.10	13.6	-0.994	2.98	<0.38	4.28	1.84	18
480	IRAS1908-609	liner	0.0143	0.34	0.29	1.16	4.04	12.0	-0.623	<5.57		>1.54	>1.31	18
481	IRAS1910+846	Seyf1	0.3544	<0.25	0.15	0.57	<2.45	16.2	-1.300	47.0	0.15	6.57	0.41	16,29
482	IRAS1911-498	Seyf2	0.0492	<0.09	0.31	0.89	0.89	16.0	-1.349	<1.35	>2.46	>6.34	>6.73	19
483	IRAS1913-397	local	0.0000	0.37	2.89	5.55	3.10							
484	IRAS1916-587	Seyf1	0.0360	0.31	0.38	0.61	<4.55	13.3	-0.751	609.	0.27	4.73	0.58	19
485	IRAS1918-578	Seyf2	0.0587	<0.06	0.16	0.87	1.79	15.2	-1.193	<0.95	>2.29	>4.18	>3.52	18
486	IRAS1918-558	HII	0.0120	0.09	0.18	0.54	1.71	12.9	-0.648	2.98	<0.18	3.55	1.34	18
487	IRAS1918-545	local	0.0000	0.54	0.48	0.53	<1.00							
488	IRAS1924-416E	HII	0.0094	<0.44	0.44	1.64	1.11	13.0	-0.894	271.	5.74	3.19	0.07	19
489	IRAS1925-727	Seyf2	0.0615	0.33	1.44	5.18	6.03	14.5	-1.429	<9.11	>2.15	>8.63	>8.07	19
490	IRAS1926-425E	HII	0.0596	0.09	0.11	1.10	2.02	16.4	-1.479	<1.80		>6.29	>3.80	19
491	IRAS1926-436E	HII	0.0597	0.36	0.53	0.71	1.04	15.8	-1.262	<1.44		>8.89	>6.00	19
492	IRAS1944-464	HII	0.0196	<0.25	0.31	1.23	1.85	13.9	-1.017	17.0	0.32	4.88	2.25	18
493	IRAS1953-646	HII	0.0122	<0.08	0.26	0.48	0.68	14.2	-0.860	31.0	1.54	3.43	1.65	
494	IRAS1957+763	local	0.0000	2.19	0.61	0.71	1.31							
495	IRAS1958-183	Seyf1	0.0370	0.36	0.69	0.92	1.21	14.7	-1.102					7,8
496	IRAS2002-204NW	HII	0.0687	0.20	0.22	0.40	0.60	16.9	-1.349	<1.83		>6.22	>4.15	19
497	IRAS2004-612	Seyf1	0.0097	0.28	0.40	1.05	2.47	12.7	-0.743	141.	0.18	5.52	<0.77	7
498	IRAS2008-291N	HII	0.0230	<0.09	0.19	0.94	1.59	14.0	-0.968	8.16	0.84	5.72	2.89	19
499	IRAS2013-089	local	0.0000	1.15	0.52	1.26	2.44							
500	IRAS2016-416	local	0.0000	<0.28	1.19	1.42	<1.65							

© European Southern Observatory • Provided by the NASA Astrophysics Data System

1992A&AS...96..389D

TABLE 2. *(continued)*

num	object	type	z	S12 (Jy)	S25 (Jy)	S60 (Jy)	S100 (Jy)	V (mag)	sp.indx. (V,60)	Hbeta (1E-15)	[OIII] Hbeta	Halfa Hbeta	[NII] Hbeta	date (t.1)
501	IRAS2016-527	Seyf2	0.0163	<0.25	0.36	0.90	1.28	12.8	-0.738	19.3	14.48	5.37	2.87	7
502	IRAS2020-565NW	Seyf2	0.0596	0.09	0.22	0.76	0.94	15.1	-1.131	11.3	13.41	4.71	3.27	19
503	IRAS2024-024	local	0.0000	0.37	0.91	1.12	1.68							7
504	IRAS2025-818	Seyf2	0.0344	0.32	0.67	1.16	<1.21	15.8	-1.372	<10.1	>3.57	>4.49	>5.11	7,8
505	IRAS2031-607	local	0.0000	0.96	0.27	0.52	<1.18							
506	IRAS2032-503E	Seyf2?	0.0087	<0.25	0.26	0.68	1.00	12.5	-0.605	48.8	2.77	3.69	0.63	18
507	IRAS2037-669	local	0.0000	0.41	0.31	0.67	<1.11							
508	IRAS2038-383	liner	0.0204	0.11	0.27	1.31	1.64	12.9	-0.829	<26.6			>1.02	19
509	IRAS2041-109	Seyf1	0.0340	0.34	0.74	1.43	1.43	12.6	-0.795	1350.	0.40	3.96	0.72	7
510	IRAS2045+002E	Seyf2	0.0122	<0.35	0.42	1.14	<1.13	12.8	-0.782	<4.33	>5.97	>3.66	>3.79	4
511	IRAS2045-529	HII	0.0469	<0.06	0.19	0.96	1.22	15.5	-1.270	5.27	0.34	5.10	2.68	18
512	IRAS2048-572	Seyf2	0.0113	1.17	3.87	5.89	4.26	11.7	-0.909	62.9	8.97	5.90	3.36	19
513	IRAS2055-521	Seyf2	0.0513	<0.25	0.35	1.20	1.44	14.0	-1.026	17.5	8.62	4.89	3.91	18
514	IRAS2058+774	local	0.0000	1.21	3.24	11.56	17.60							
515	IRAS2100+781	local	0.0000	6.25	11.16	35.97	75.37							15
516	IRAS2101-115	local	0.0000	6.37	56.70	90.64	46.99							
517	IRAS2116-206	HII	0.0390	0.10	0.57	1.81	2.31	14.3	-1.169	15.6	0.56	6.65	3.09	19
518	IRAS2117-492W	HII	0.0541	0.10	0.13	0.73	1.22	15.7	-1.241	5.72	0.28	4.27	1.65	19
519	IRAS2121-850	local	0.0000	2.40	0.70	0.92	2.09							
520	IRAS2121-179	Seyf1	0.1123	<0.29	0.41	1.14	1.26	14.5	-1.100	69.0	0.26	3.46	0.51	7,27
521	IRAS2129+099	Seyf1	0.0621	0.14	0.31	0.54	0.43	13.8	-0.821	298.	0.35	3.69	0.72	19
522	IRAS2134+125	local	0.0000	<0.25	1.13	3.64	3.04							
523	IRAS2135-289	local	0.0000	0.11	0.26	0.61	0.51							19
524	IRAS2136-270	Seyf2	0.0308	<0.25	0.30	1.22	1.74	14.1	-1.051	10.1	1.90	4.90	3.54	19
525	IRAS2143-045	Seyf2	0.1034	<0.25	0.57	0.96	<1.13	15.7	-1.312	<5.62	>8.90	>5.85	>5.73	7,27,30
526	IRAS2145-475	local	0.0000	0.81	0.22	0.25	<1.00							
527	IRAS2154-348	HII	0.0088	<0.25	0.40	1.75	4.82	12.2	-0.746	13.6	0.15	3.54	2.03	19
528	IRAS2201+033	Seyf2	0.0611	<0.66	0.74	1.13	1.24	15.4	-1.275	23.5	9.29	3.81	1.82	5
529	IRAS2205-519W	Seyf2	0.0648	0.11	0.39	0.62	0.62	16.1	-1.288	11.1	6.80	5.60	1.34	18
530	IRAS2206-474	Seyf1	0.0050	0.63	0.74	2.56	8.63	10.7	-0.539	186.	0.72	8.12	1.49	18
531	IRAS2211-393	Seyf1	0.0394	<0.40	0.45	0.77	<1.04	14.1	-0.954	57.1	0.36	6.83	0.87	18
532	IRAS2217-490	HII	0.0306	<0.11	0.17	0.71	1.51	14.0	-0.909	9.50	0.75	5.28	3.24	18
533	IRAS2219-321	local	0.0000	<0.14	0.15	0.89	1.25							19
534	IRAS2220-074	local	0.0000	1.30	0.42	0.61	1.17							
535	IRAS2226-659	HII	0.0106	0.24	0.48	1.74	3.67	12.5	-0.811	18.0	<0.13	4.56	1.48	19
536	IRAS2230-649	HII	0.0114	<0.11	0.13	0.56	1.34	13.2	-0.708	<4.84		>4.41	>1.64	19
537	IRAS2234-128E	Seyf1	0.0242	0.15	0.43	0.52	0.91	13.8	-0.813	81.2	3.79	6.96	1.19	19
538	IRAS2237+077E	Seyf1	0.0246	0.15	0.32	0.84	1.29	13.7	-0.883	53.1	2.71	6.18	1.60	19
539	IRAS2239+200SW	Seyf2?	0.0233	<0.25	0.78	2.49	2.66	14.0	-1.168	58.7	3.61	4.44	1.43	19
540	IRAS2240+294	Seyf1	0.0240	0.09	0.20	0.76	1.79	13.6	-0.858	230.	0.70	3.56	0.12	20
541	IRAS2240-186W	HII	0.0380	<0.46	0.31	0.88	1.74	15.2	-1.191	5.72	0.26	5.05	1.95	22
542	IRAS2241-608	Seyf1	0.1130	0.14	0.32	0.45	0.52	15.4	-1.085	72.5	1.34			19
543	IRAS2245-669	HII	0.0377	<0.25	0.52	1.47	2.29	14.2	-1.113	49.3	0.83	3.94	2.39	19
544	IRAS2246-195	Seyf2	0.0318	<0.39	0.88	2.45	3.66	13.7	-1.110	<16.1	>7.91	>3.84	>3.92	7
545	IRAS2254-298	local	0.0000	18.27	4.85	8.84	10.78							
546	IRAS2259-366	local	0.0000	0.84	0.22	0.54	<1.00							
547	IRAS2301+223	Seyf1	0.0385	<0.39	0.37	1.51	<2.73	14.0	-1.074	32.2	1.14	6.34	1.80	18
548	IRAS2302+120	Seyf2	0.0074	0.75	3.33	11.93	24.26	12.0	-1.110	<0.98	>2.34	>3.56	>5.82	21,27
549	IRAS2302-000	Seyf2	0.0253	<0.25	0.49	1.06	1.62	13.1	-0.813	21.6	6.17	4.85	5.36	6
550	IRAS2306+050	Seyf2	0.1730	<0.32	0.46	1.16	<1.06	17.3	-1.649	<1.77	>9.24	>13.76	>7.34	5,27
551	IRAS2309-733	HII	0.0570	<0.06	0.19	0.84	0.94	16.0	-1.342	9.92	2.17	5.03	2.38	19
552	IRAS2311-578E	HII	0.0348	0.10	0.13	0.71	1.14	15.0	-1.099	6.52	<0.33	7.43	3.34	19
553	IRAS2312+238	local	0.0000	1.37	0.28	1.06	1.74							
554	IRAS2314-443SE	HII	0.0480	<0.25	0.30	1.22	1.23	16.1	-1.429	10.3	1.91	4.04	0.82	18
555	IRAS2325+085	Seyf2	0.0286	0.78	1.79	5.14	7.63	13.0	-1.140	63.7	11.27	5.19	3.33	7
556	IRAS2339-044	HII	0.0188	0.14	0.39	2.00	3.40	13.8	-1.087	8.96	<0.19	4.79	2.34	20
557	IRAS2344+153	Seyf2	0.0260	<0.25	1.23	4.14	3.39	14.0	-1.287	<2.64	>1.26	>3.54	>3.92	22,27
558	IRAS2346+019	HII	0.0304	0.32	0.57	1.66	2.69	14.6	-1.201	11.1	0.46	7.60	4.00	7
559	IRAS2353+299	Seyf2	0.0307	<0.45	0.39	0.70	<1.00	14.5	-0.998	33.0	10.53	5.95	3.18	4
560	IRAS2354+192	HII	0.0265	<0.27	0.38	0.93	0.68	15.9	-1.331	<0.71		>5.43	>4.42	20,27
561	IRAS2357+397W	HII	0.0828	0.10	0.30	0.44	0.26	17.2	-1.433	6.15	4.19	2.87	0.43	22
562	IRAS2358+182	HII	0.0553	<0.14	0.33	0.87	0.61	15.6	-1.257	45.3	3.26	2.63	0.18	5
563	IRAS2358-012	HII	0.0854	0.09	0.52	0.67	0.98	17.6	-1.603					7,23

© European Southern Observatory • Provided by the NASA Astrophysics Data System

1992A&AS...96..389D

Explanation of Table 2:

1) Running catalogue number from Paper I.

2) IRAS name as given in Paper 1; in some cases 2 objects are close to the IRAS position. In those cases the true counterpart to the IRAS source was determined spectroscopically. Its position relative to the confusing object is indicated by one or two extra characters. (e.g. NW = North Western member of a pair).

3) The optical spectroscopic classification as described in Sect. 2.

4) The measured redshift. Accuracy is about 0.0003; no correction was made for solar motion. For those objects having an entry in column 4, but no entry in column 15, the redshift was taken from Palumbo *et al.* (1983) or from Veron-Cetty & Veron (1985).

5-8) The IRAS flux densities. Note that these are co-added fluxes. They are more accurate than the flux densities given in the PSC. When a source was not detected in some wavelength band, a 3σ upper limit is given.

9) The optical visual magnitude, corrected to the face-on value and corrected for galactic foreground absorption (Sandage & Tamman 1976; Sandage, 1973). The accuracy is $\sigma = 0.5$ magnitudes.

10) The ratio of optical to infrared flux. This "colour" is given in the form of a power-law spectral index. Objects which emit equal powers per frequency decade in the optical and infrared have an index of -1. The more negative the index, the more the IR dominates the optical emission.

11) The flux in the Hβ (λ4861) emission line in units of 10^{-15} ergs cm^{-2} sec^{-1}, corrected for the underlying dip in stellar continuum according to Keel (1983). When no emission was detected, a 3σ upper limit is given.

12) The flux ratio of the [O III] λ 5007 line to the flux given in column 11. Upper limits are 3σ.

13) The flux ratio of the Hα λ 6563 line to the flux given in column 11. The flux is corrected for continuum dips according to Keel (1983).

14) The flux ratio of the [N II] λ 6583 line to the flux in column 11.

15) The date(s) on which an object was observed, coded as entry to column 1 of Table 1.

© European Southern Observatory • Provided by the NASA Astrophysics Data System

1992A&AS...96..389D

TABLE 1. *Overview of the observing campaign.*

num	obs.	tel.	instrum.	wavelength range (A)	slit dim. (")	resol. FWHM (A)	date	photom. quality	seeing (")	remarks
1	ESO	3.6m	B&C+IDS	3800-7200	4x4	11.	7/8 Mar 84	good	4.0	
2				3800-7200	4x4	11.	8/9 Mar 84	good	2.0	
3				3800-7200	4x4	11.	9/10 Mar 84	good	1.5	
4	RGO	2.5m	IDS+IPCS	3400-7500	1.0	4.5	4/5 Jul 84	fair	1.2	(1)
5				3400-7500	1.5	6.7	5/6 Jul 84	fair	1.5	(1)
6				3400-7500	1.5	6.7	6/7 Jul 84	fair	1.3	(1)
7	ESO	3.6m	B&C+IDS	3800-7200	4x4	11.	1/2 Aug 84	good	2.5	
8				3800-7200	4x4	11.	2/3 Aug 84	fair	2.5:	
9				3800-7200	4x4	11.	3/4 Aug 84	fair	2.5:	
10	ESO	3.6m	B&C+IDS	3800-7200	4x4	11.	19/20 Feb 85	good	2.0:	
11				3800-7200	4x4	11.	20/21 Feb 85	good	2.0:	
12				3800-7200	4x4	11.	21/22 Feb 85	good	2.0:	
13	RGO	2.5m	IDS+IPCS	3600-7300	1.0	11.	10/11 May 85	bad	2.2	(2)
14				3600-7300	1.0	11.	11/12 May 85	bad	1.6--0.9	(2)
15				3600-7300	1.0	11.	12/13 May 85	good	1.2	
16				3600-7300	1.0	11.	13/14 May 85	good	1.3	
17	RGO	2.5m	FOS	5000-10000	1.1	20.	13/14 May 85	good	1.3	(3)
18	ESO	3.6m	B&C+CCD	4000-7300	2.0	12.	21/22 Aug 85	good	1.8	
19				4000-7300	2.0	12.	22/23 Aug 85	fair	2.0	(4)
20	RGO	2.5m	IDS+IPCS	3300-7300	1.0	4.5	19/20 Sep 85	bad	1.2	(2)
21				3300-7300	1.0	4.5	20/21 Sep 85	very bad	1.0	(2)
22				3300-7300	1.0	4.5	21/22 Sep 85	fair	1.0	(5)
23				3300-7300	1.0	4.5	22/23 Sep 85	bad	1.0	(2)
24	RGO	2.5m	FOS	5000-10000	1.5	22.	13/14 Mar 86	good	1.0	
25			IDS+IPCS	3300-7300	1.5	4.5	14/15 Mar 86	fair	1.2	
26	RGO	2.5m	FOS	5000-10000	1.5	20.	16/17 Jun 88	good	1.2	
27	RGO	4.0m	FOS	4800-9800	1.5	20.	17/18 Jul 88	good	1.5	
28				4800-9800	1.5	20.	18/19 Jul 88	good	1.5	
29				4800-9800	1.5	20.	19/20 Jul 88	good	1.5	
30	RGO	4.0m	FOS	4800-9800	1.5	20.	24/25 Jul 88	good	1.4	

Remarks:
(1): sahara dust
(2): cloudy
(3): this setup during last part of night
(4): cirrus at end of night
(5): thin clouds

TABLE 3a. *Identification content of the sample (all sources).*

	Number of Objects	Fractional Ident.
total	563	100%
non-local	435	77
non-local with spectra	357	64
Seyfert 1	80	14
Seyfert 2	141	25
LINER	5	1
HII	130	23
Featureless	1	0.4

TABLE 3b. *Identification content of the revised sample (truly warm sources only).*

	Number of Objects	Fractional Ident.
total	431	100%
non-local	313	73
non-local with spectra	269	62
Seyfert 1	70	16
Seyfert 2	130	30
LINER	1	0.2
HII	67	16
Featureless	1	0.2

TABLE 4a. *Bivariate luminosity function. All sources.*

log(L60) \ M(V)	-19..-20	-20..-21	-21..-22	-22..-23	-23..-24	-24..-25	-25..-26	total
<9.4	8.30E-5 0.55 5	3.01E-5 0.54 5	0	0	0	0	0	1.13E-4 0.55 10
9.4..9.8	8.04E-6 0.59 5	2.30E-5 0.41 12	2.95E-6 0.36 2	6.29E-7 0.12 1	0	0	0	3.46E-5 0.44 20
9.8..10.2	4.54E-6 0.49 8	6.21E-6 0.37 17	6.88E-6 0.54 17	5.71E-7 0.61 2	0	0	0	1.82E-5 0.47 44
10.2..10.6	1.82E-7 0.36 2	3.33E-6 0.53 22	4.25E-6 0.49 36	5.24E-7 0.44 5	0	0	0	8.29E-6 0.50 65
10.6..11.0	6.31E-8 0.17 1	3.88E-7 0.58 11	9.78E-7 0.58 27	5.20E-7 0.57 14	4.42E-8 0.76 1	0	0	1.99E-6 0.58 54
11.0..11.4	1.34E-8 0.57 1	6.13E-8 0.68 3	1.23E-7 0.59 10	5.81E-8 0.51 7	9.99E-9 0.31 2	0	0	2.66E-7 0.57 23
11.4..11.8	0	3.41E-9 0.39 1	1.30E-8 0.77 2	1.38E-9 0.41 5	3.20E-9 0.50 1	0	0	3.33E-8 0.59 9
11.8..12.2	0	0	3.04E-9 0.37 2	3.65E-10 0.77 1	1.88E-9 0.46 2	1.32E-9 0.95 2	4.80E-10 0.19 1	7.08E-9 0.59 8
>12.2	0	0	0	0	0	1.58E-10 0.93 1	3.07E-10 0.54 1	6.98E-10 0.94 2
total	9.59E-5 0.51 22	9.73E-5 0.49 71	1.52E-5 0.55 96	2.32E-6 0.52 35	5.93E-8 0.50 6	1.49E-9 0.94 3	7.87E-10 0.37 2	2.11E-4 0.53 235

© European Southern Observatory • Provided by the NASA Astrophysics Data System

1992A&AS...96..389D

TABLE 4b. *Bivariate luminosity function. Seyfert 1.*

M(V) log(L60)	-19..-20	-20..-21	-21..-22	-22..-23	-23..-24	-24..-25	-25..-26	total
<9.4	4.02E-6 0.26 1	4.79E-6 0.47 2	0	0	0	0	0	1.89E-5 0.31 3
9.4..9.8	0	5.62E-6 0.40 4	2.06E-6 0.15 1	0	0	0	0	7.68E-6 0.34 5
9.8..10.2	0	1.49E-6 0.21 4	1.56E-6 0.54 6	5.71E-7 0.61 2	0	0	0	3.62E-6 0.45 12
10.2..10.6	0	1.47E-7 0.09 4	6.74E-7 0.50 9	4.82E-7 0.47 4	0	0	0	1.30E-6 0.46 14
10.6..11.0	0	0	2.45E-7 0.76 5	1.59E-7 0.50 5	4.42E-8 0.76 1	0	0	4.49E-7 0.66 11
11.0..11.4	0	0	0	2.10E-8 0.82 2	9.99E-9 0.31 2	0	0	3.10E-8 0.61 4
11.4..11.8	0	0	0	0	3.20E-9 0.51 1	0	0	3.20E-9 0.50 1
11.8..12.2	0	0	0	0	1.88E-9 0.46 2	1.32E-10 0.95 2	4.80E-10 0.19 1	3.67E-9 0.64 5
>12.2	0	0	0	0	0	1.58E-10 0.93 1	3.07E-10 0.54 1	4.65E-10 0.75 2
total	4.02E-6 0.26 1	2.22E-5 0.29 11	4.53E-6 0.57 21	1.23E-6 0.57 13	5.93E-8 0.50 6	1.47E-9 0.94 3	7.87E-10 0.37 2	3.20E-5 0.53 57

TABLE 4c. *Bivariate luminosity function. Seyfert 2.*

M(V) log(L60)	-19..-20	-20..-21	-21..-22	-22..-23	-23..-24	-24..-25	-25..-26	total
<9.4	0	2.67E-6 0.18 1	0	0	0	0	0	2.67E-6 0.18 1
9.4..9.8	2.92E-6 0.45 2	1.28E-5 0.39 6	8.90E-7 0.58 1	6.29E-7 0.12 1	0	0	0	1.72E-5 0.40 10
9.8..10.2	5.08E-7 0.21 1	3.08E-6 0.37 9	5.33E-6 0.54 11	0	0	0	0	8.92E-6 0.46 21
10.2..10.6	4.87E-8 0.25 1	1.85E-6 0.52 10	2.81E-6 0.40 22	4.19E-8 0.33 1	0	0	0	4.75E-6 0.43 34
10.6..11.0	0	2.99E-7 0.70 7	5.68E-7 0.54 17	2.88E-7 0.61 8	0	0	0	1.15E-6 0.59 32
11.0..11.4	0	0	1.03E-7 0.56 8	3.71E-8 0.36 5	0	0	0	1.40E-7 0.49 13
11.4..11.8	0	0	1.30E-8 0.77 2	1.38E-8 0.41 5		0	0	2.67E-8 0.62 7
11.8..12.2	0	0	3.04E-9 0.37 2	3.65E-10 0.77 1		0	0	3.40E-9 0.53 3
>12.2	0	0	0	0	0	0	0	0
total	3.48E-6 0.34 4	1.51E-5 0.50 33	9.71E-6 0.52 63	1.01E-6 0.48 21		0	0	2.93E-5 0.50 121

© European Southern Observatory • Provided by the NASA Astrophysics Data System

1992A&AS...96..389D

TABLE 4d. *Bivariate luminosity function. HII galaxies.*

M(V) / log(L60)	-19..-20	-20..-21	-21..-22	-22..-23	-23..-24	-24..-25	-25..-26	total
<9.4	7.92E-5 0.46 4	2.26E-5 0.94 1	0	0	0	0	0	1.02E-4 0.69 5
9.4..9.8	5.12F-6 0.66 3	4.61E-6 0.47 2	0	0	0	0	0	9.73E-6 0.59 5
9.8..10.2	4.03E-6 0.53 7	1.64E-6 0.51 4	0	0	0	0	0	5.67E-6 0.52 11
10.2..10.6	1.33E-7 0.47 1	1.33E-6 0.57 11	7.71E-7 0.85 5	0	0	0	0	2.23E-6 0.64 17
10.6..11.0	6.31E-8 0.17 1	8.97E-8 0.33 4	1.64E-7 0.51 5	7.22E-8 0.70 1	0	0	0	3.89E-7 0.42 11
11.0..11.4	1.34E-8 0.57 1	6.13E-8 0.68 3	2.04E-8 0.70 2	0		0	0	9.50E-8 0.66 6
11.4..11.8	0	3.41E-9 0.39 1	0	0	0	0	0	3.41E-9 0.39 1
11.8..12.2	0	0	0	0	0	0	0	0
>12.2	0	0	0	0	0	0	0	0
total	8.84E-5 0.55 17	3.04E-5 0.56 26	9.56E-7 0.68 12	7.22E-8 0.70 1	0	0	0	1.20E-4 0.58 56

TABLE 5. *Object type as function of 60μ luminosity.*

log(L60)	total	Seyf1	Seyf2	HII
<9.4	10	3	1	5
9.4-9.8	20	5	10	5
9.8-10.2	44	21	12	11
10.2-10.6	65	14	34	17
10.6-11.0	54	11	32	11
11.0-11.4	23	4	13	6
11.4-11.8	9	1	7	1
11.8-12.2	8	5	3	0
>12.2	2	2	0	0

© European Southern Observatory • Provided by the NASA Astrophysics Data System

1992A&AS...96..389D

TABLE 6. *IR colours of variously defined Seyferts.*

	total	warm	warm fraction	type
12μ sample (Spinoglio and Malkan 1988):	27	15	0.56	S1
	32	14	0.44	S2
CfA Seyferts (Edelson et al. 1987)	37	20	0.54	all
Kirhakos and Steiner (1990) X-ray/IRAS	11	5	0.44	all
Markarian Seyferts (Meurs, 1982):	45	33	0.73	S1
	18	13	0.72	S2
Miley et al. (1985):	50	median $\alpha_{(25,60)}$ = -1.0		S1
	66	median $\alpha_{(25,60)}$ = -1.2		S2
PG QSOs (Sanders et al. 1989)	34	26	0.76	QSO

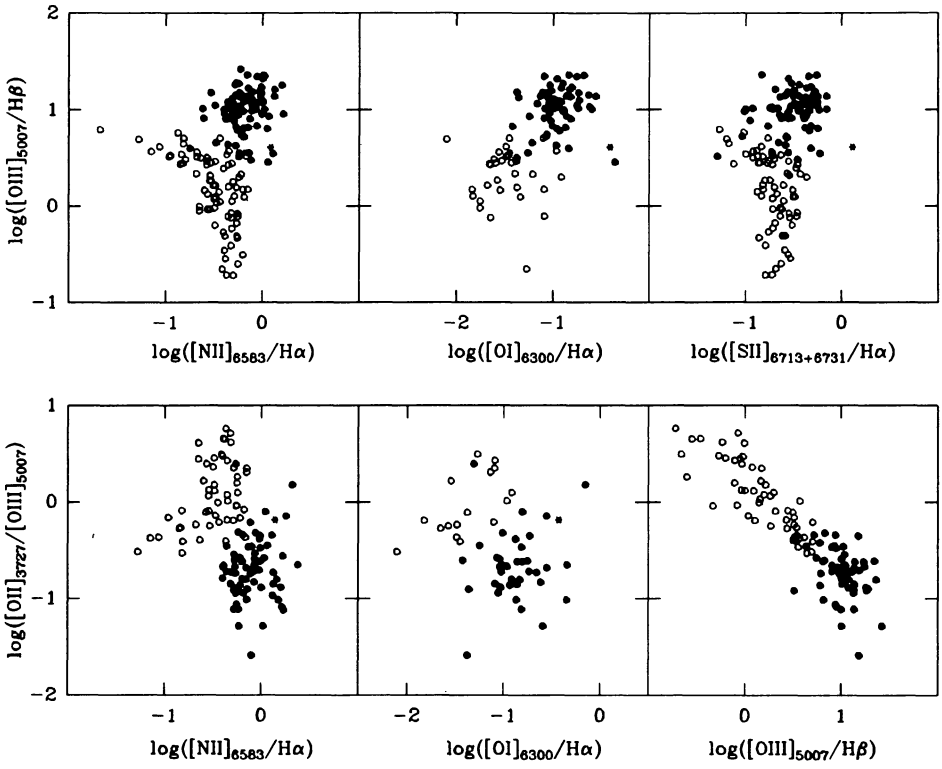

FIGURE 1. Emission line ratios for the narrow emission line objects. HII-galaxies are denoted by open circles, Seyfert 2s by filled circles and LINERS by asterisks. The ratios displayed have been corrected for reddening and underlying stellar continuum features (see text).

© European Southern Observatory • Provided by the NASA Astrophysics Data System

1992A&AS...96..389D

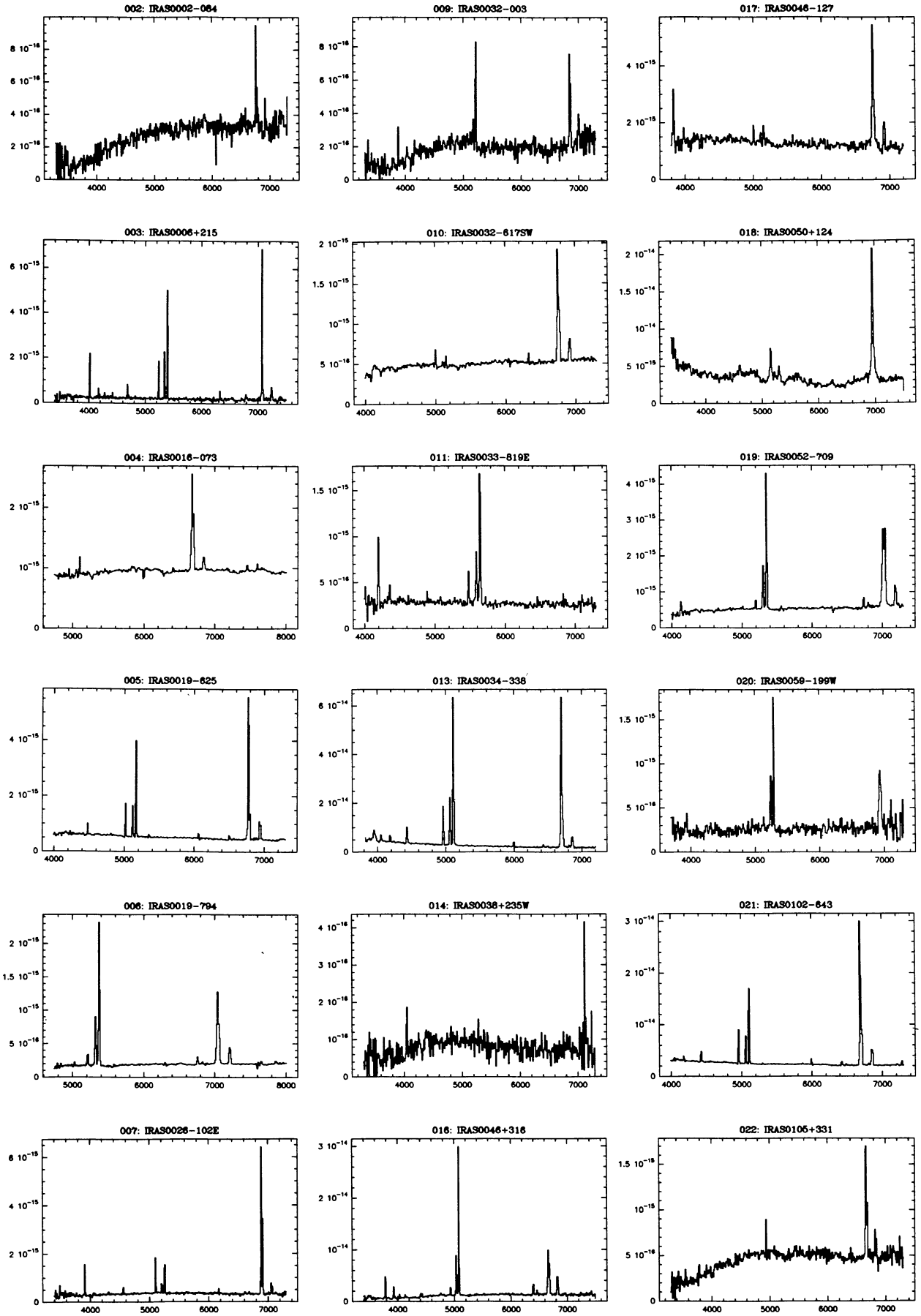

FIGURE 2. The observed spectra of extragalactic objects. Wavelengths are in Angstroms, flux units are ergs cm^{-2} s^{-1} $Å^{-1}$.

© European Southern Observatory • Provided by the NASA Astrophysics Data System

1992A&AS...96..389D

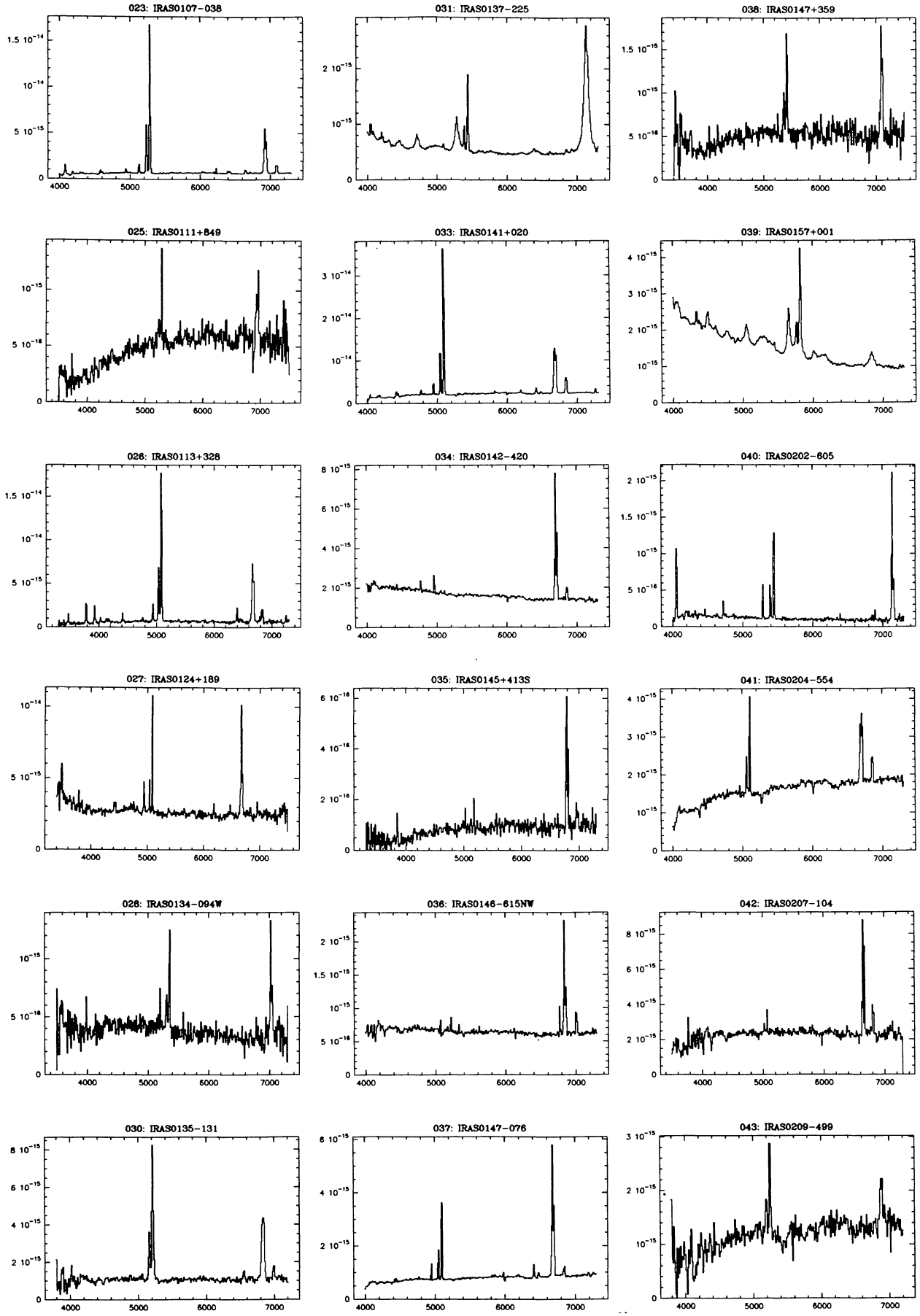

FIGURE 2. *(continued)*

© European Southern Observatory • Provided by the NASA Astrophysics Data System

1992A&AS...96..389D

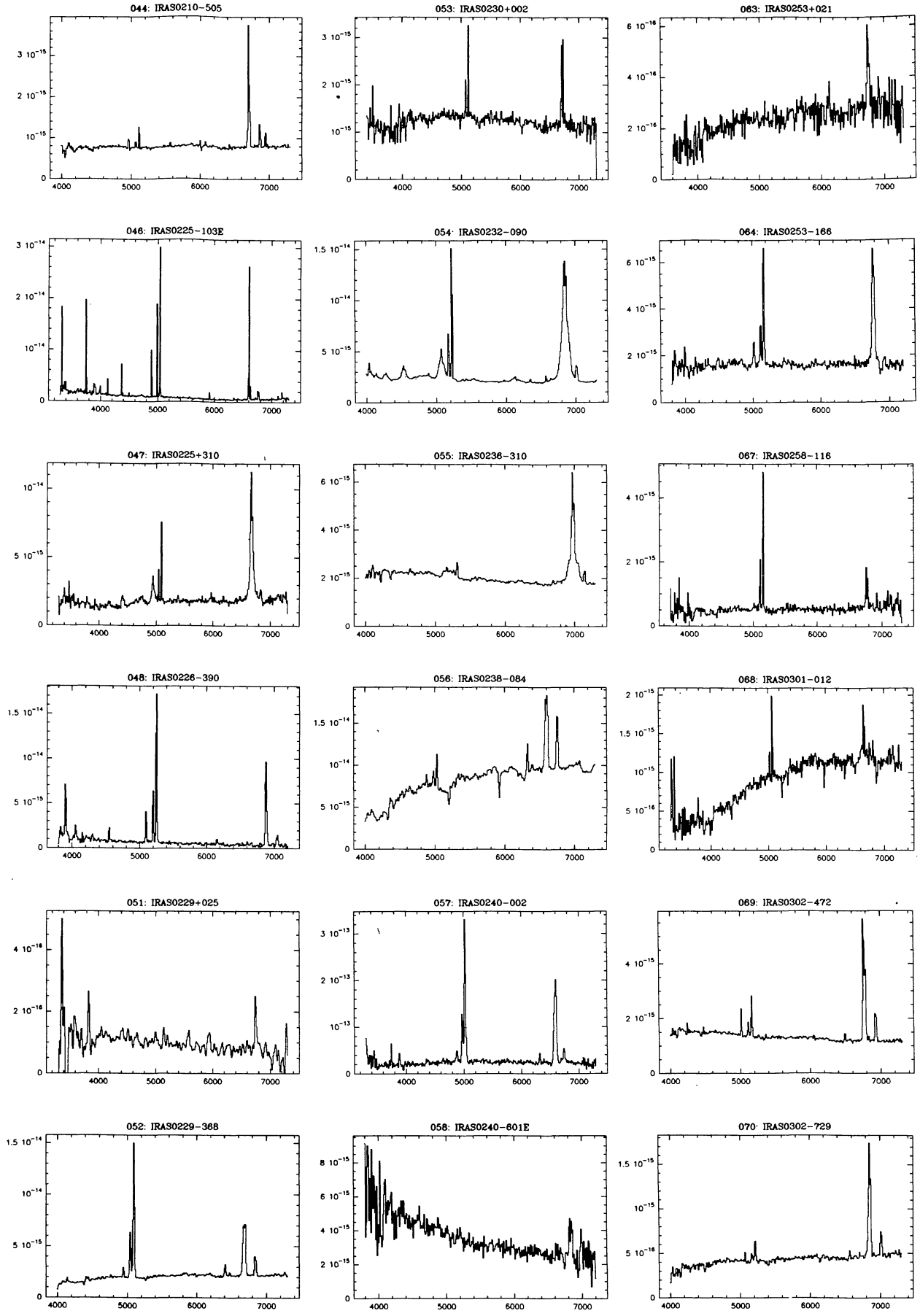

FIGURE 2. *(continued)*

© European Southern Observatory • Provided by the NASA Astrophysics Data System

1992A&AS...96..389D

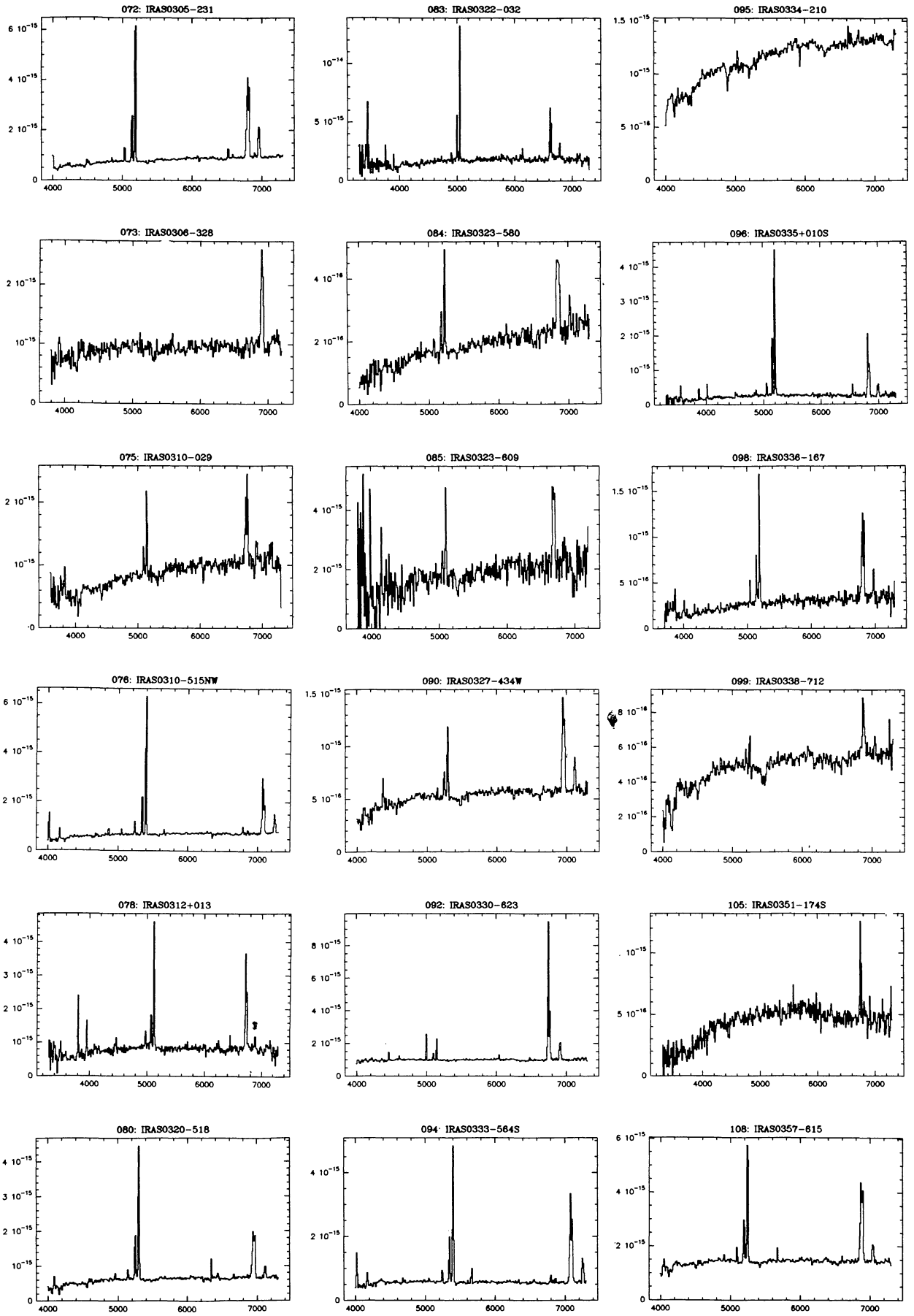

FIGURE 2. *(continued)*

© European Southern Observatory • Provided by the NASA Astrophysics Data System

1992A&AS...96..389D

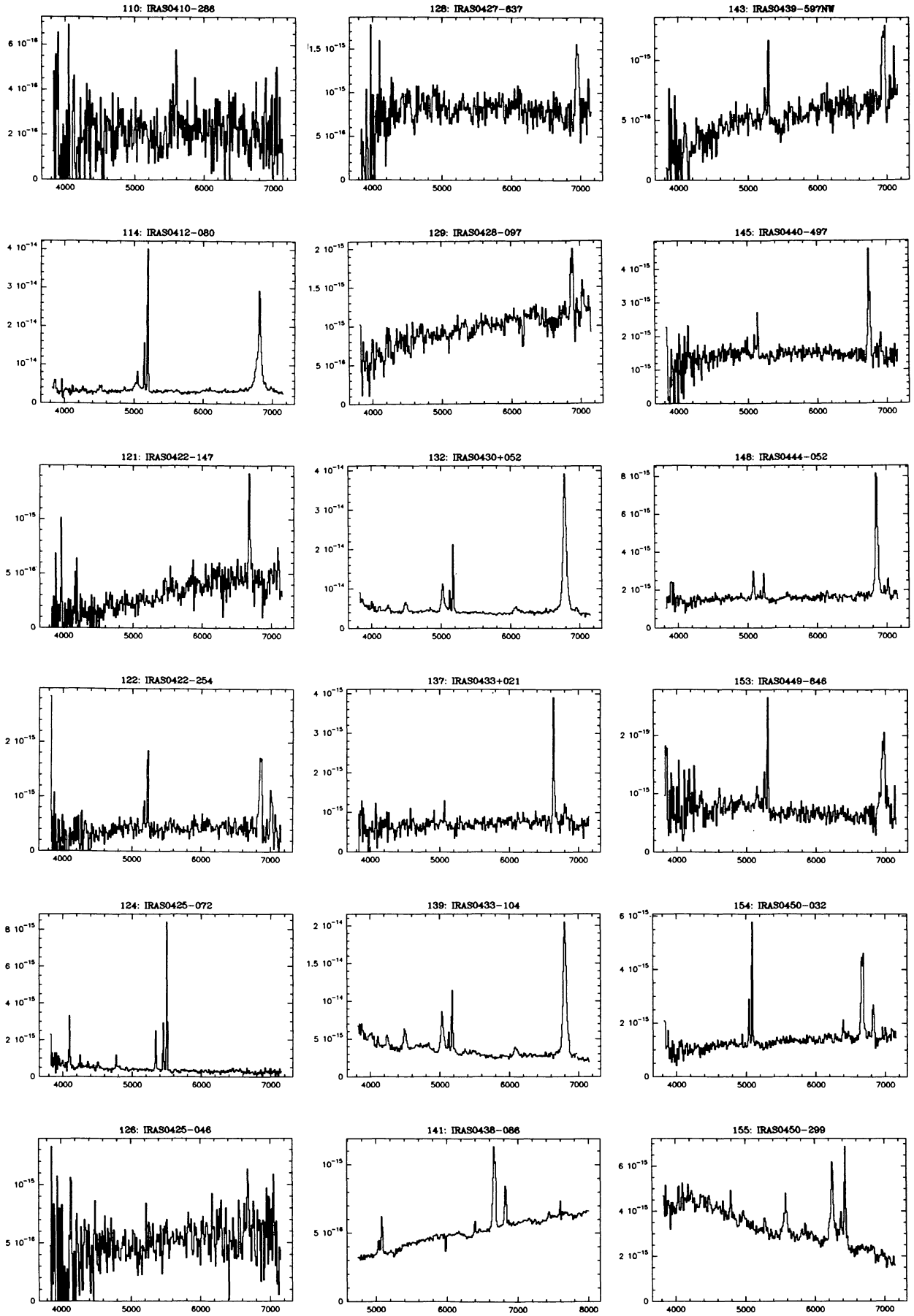

FIGURE 2. *(continued)*

© European Southern Observatory • Provided by the NASA Astrophysics Data System

1992A&AS...96..389D

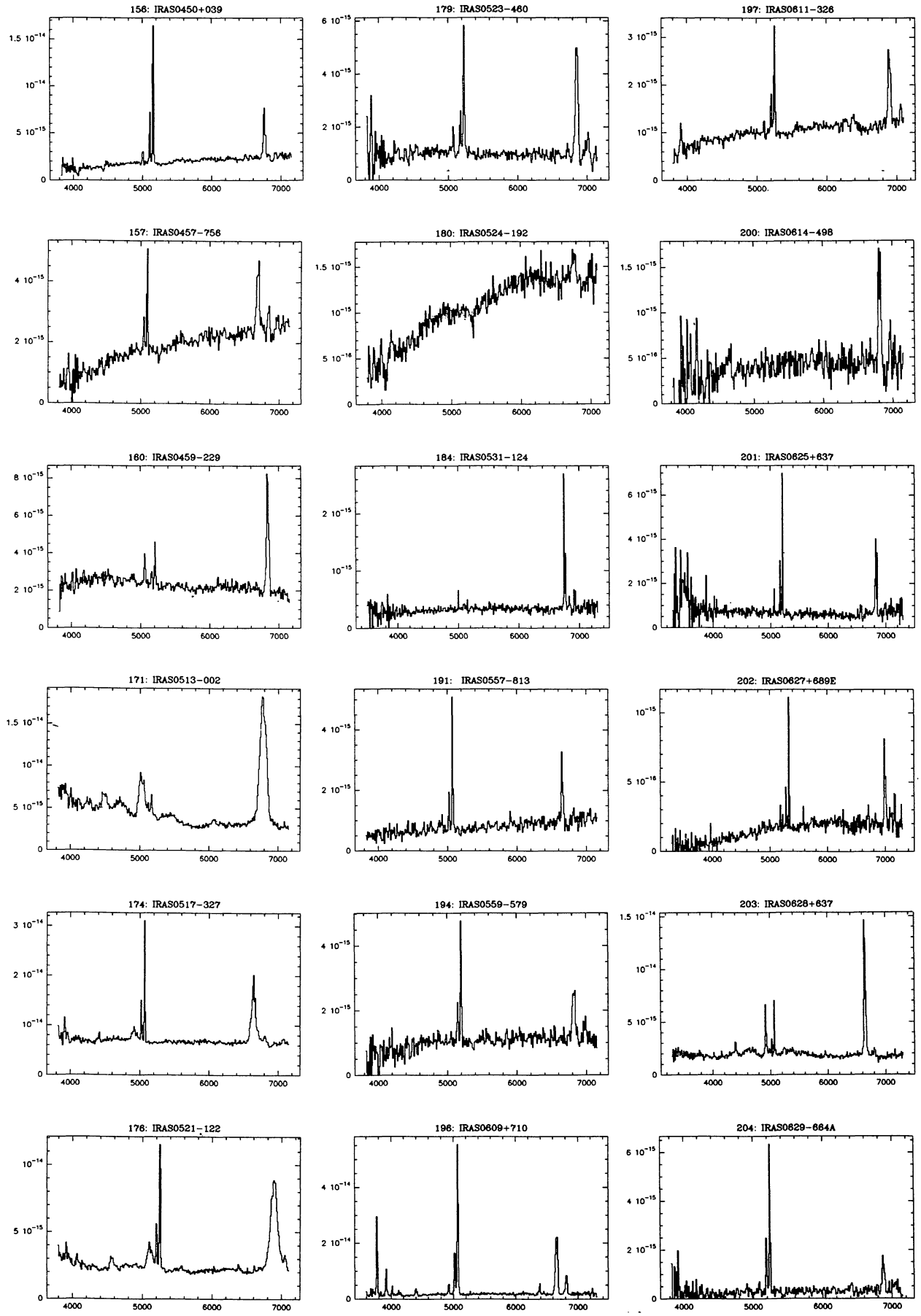

FIGURE 2. *(continued)*

© European Southern Observatory • Provided by the NASA Astrophysics Data System

1992A&AS...96..389D

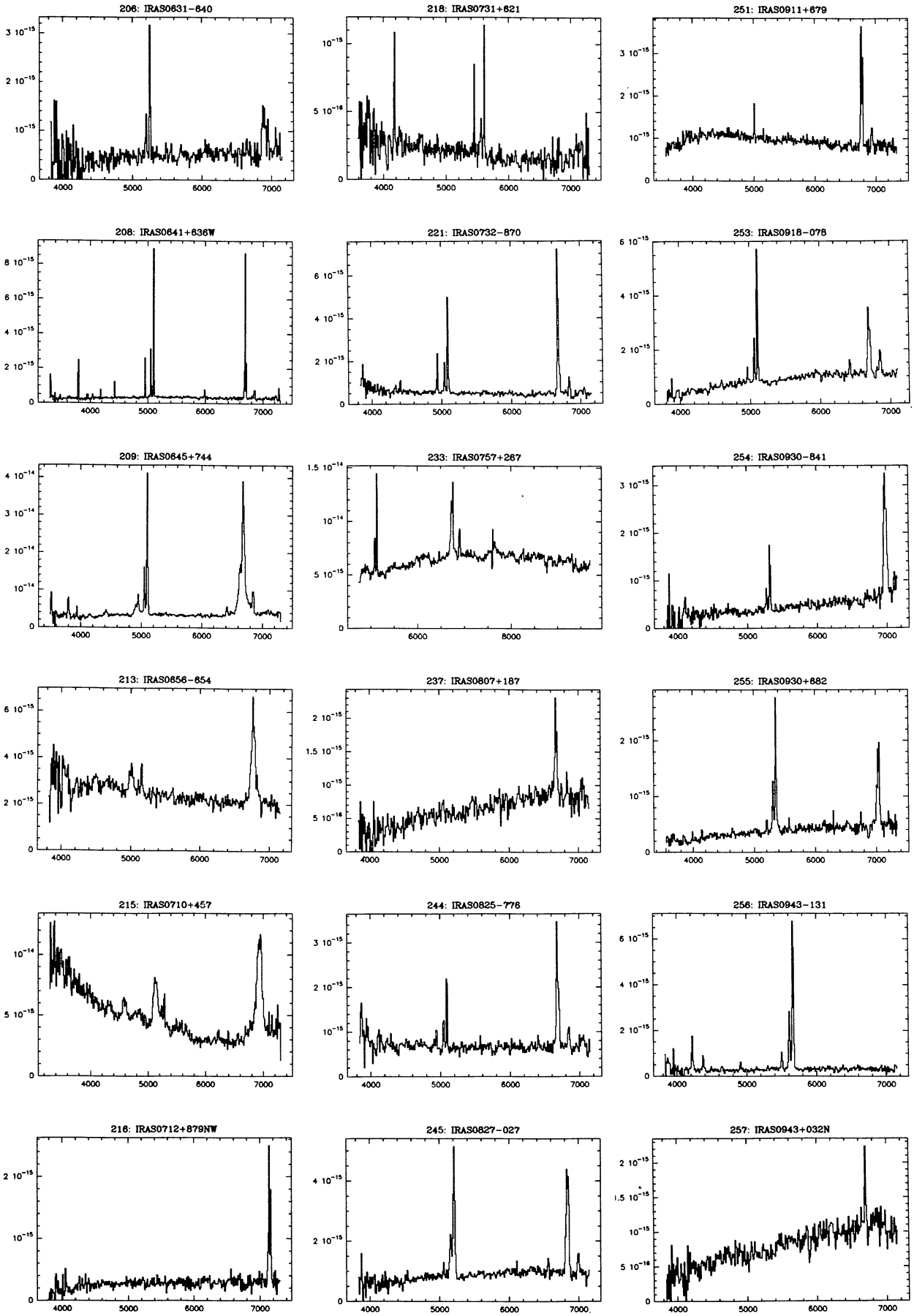

FIGURE 2. *(continued)*

© European Southern Observatory • Provided by the NASA Astrophysics Data System

1992A&AS...96..389D

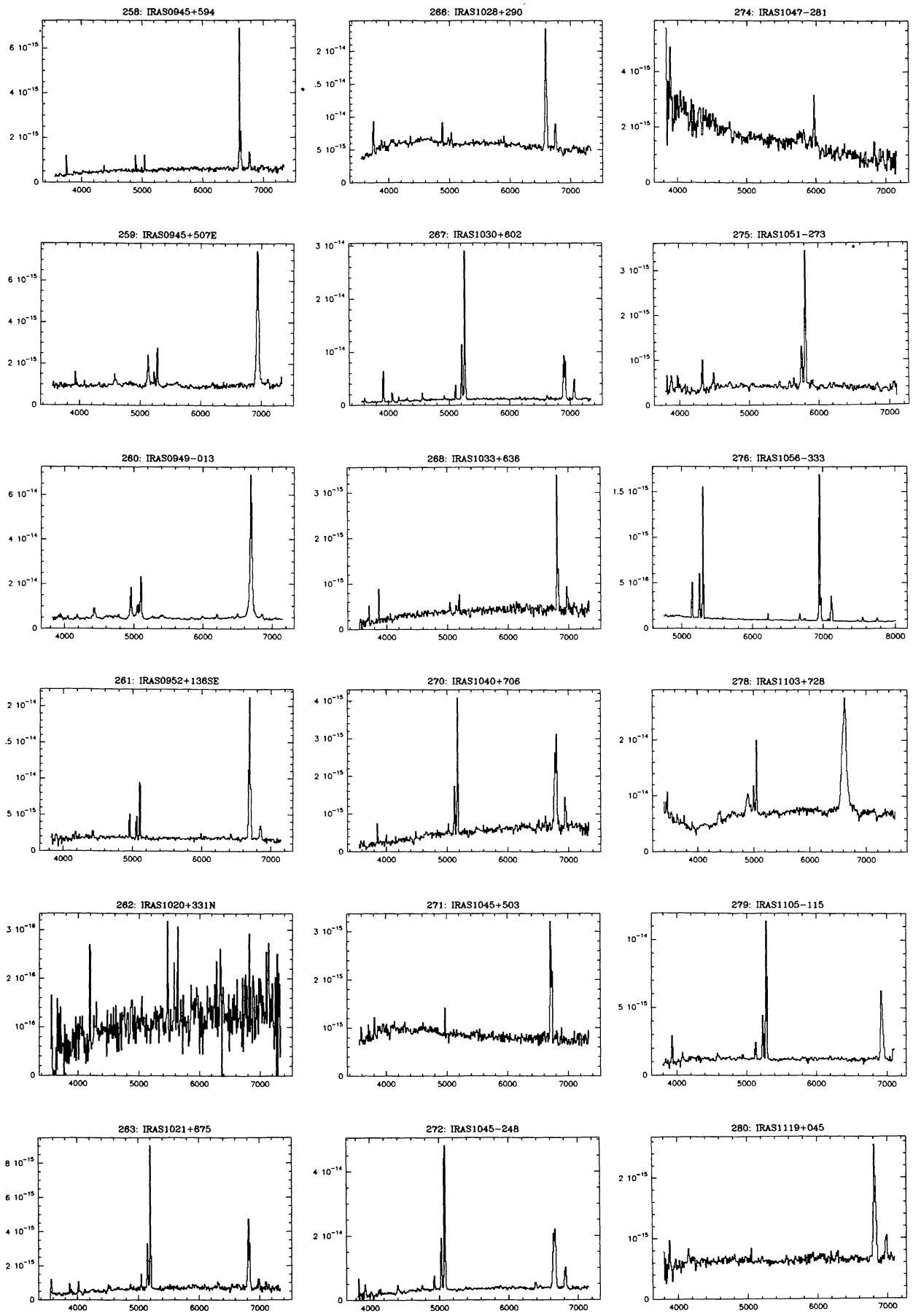

FIGURE 2. *(continued)*

© European Southern Observatory • Provided by the NASA Astrophysics Data System

1992A&AS...96..389D

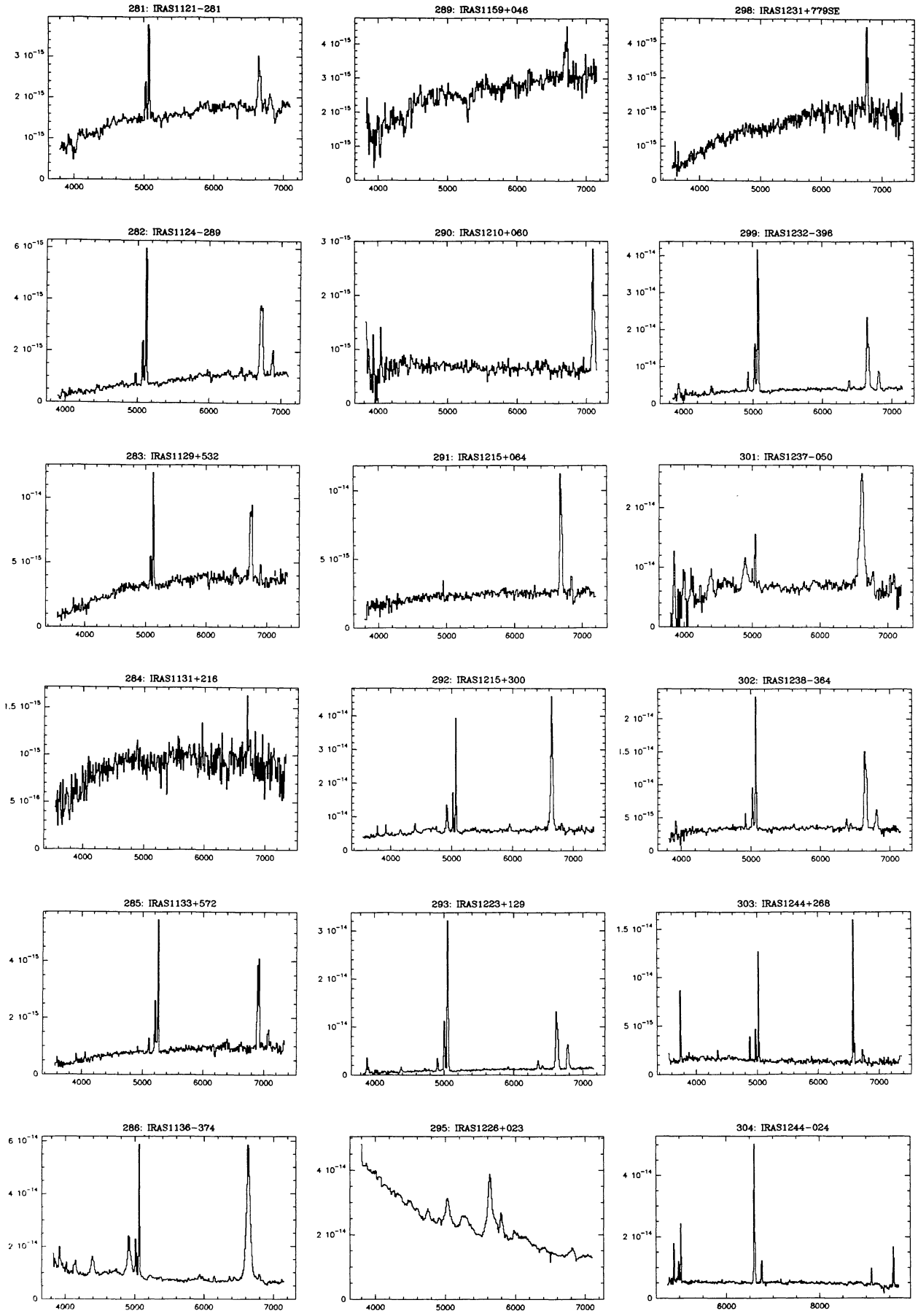

FIGURE 2. *(continued)*

© European Southern Observatory • Provided by the NASA Astrophysics Data System

1992A&AS...96..389D

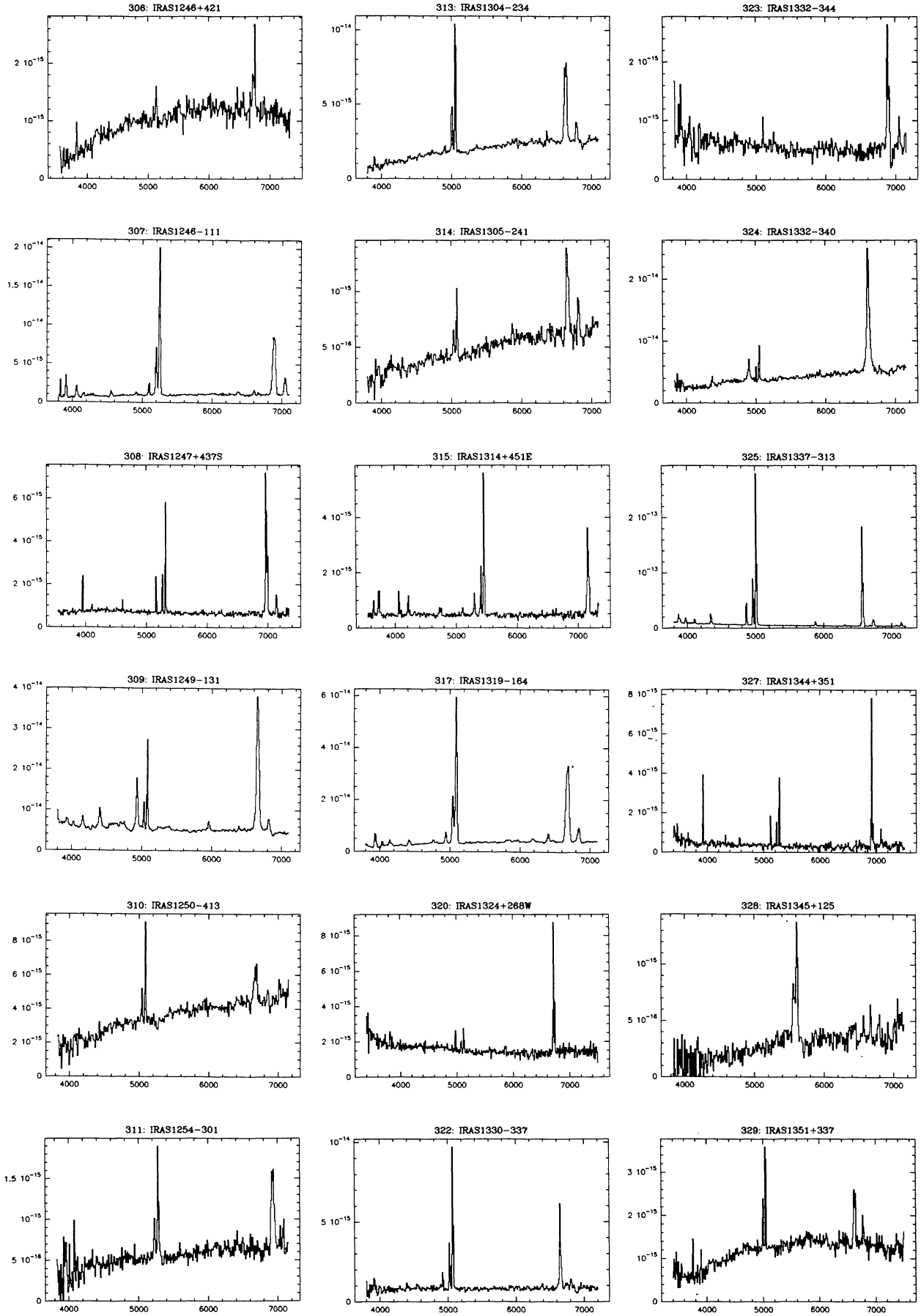

FIGURE 2. *(continued)*

© European Southern Observatory • Provided by the NASA Astrophysics Data System

1992A&AS...96..389D

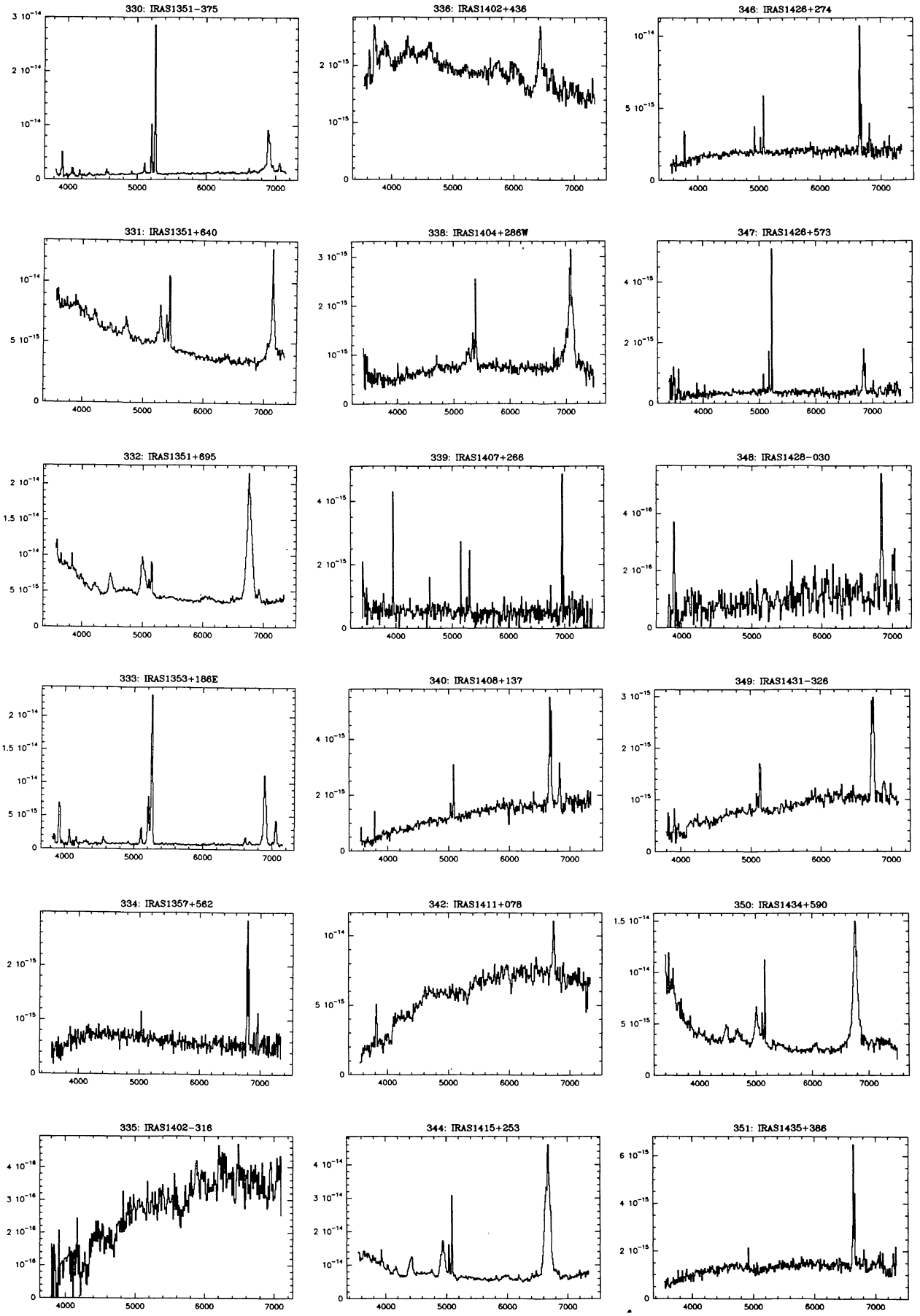

FIGURE 2. *(continued)*

© European Southern Observatory • Provided by the NASA Astrophysics Data System

1992A&AS...96..389D

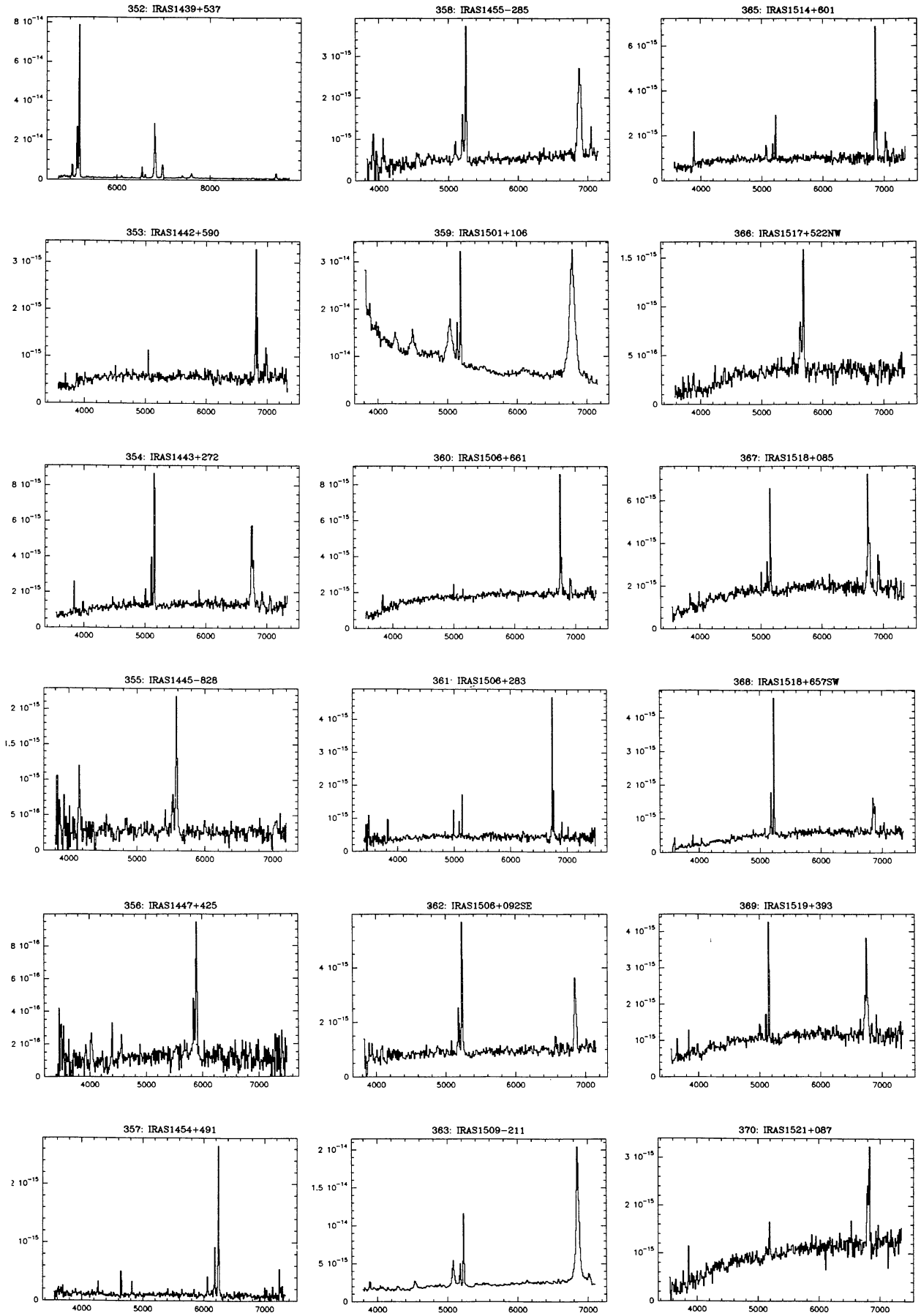

FIGURE 2. *(continued)*

© European Southern Observatory • Provided by the NASA Astrophysics Data System

1992A&AS...96..389D

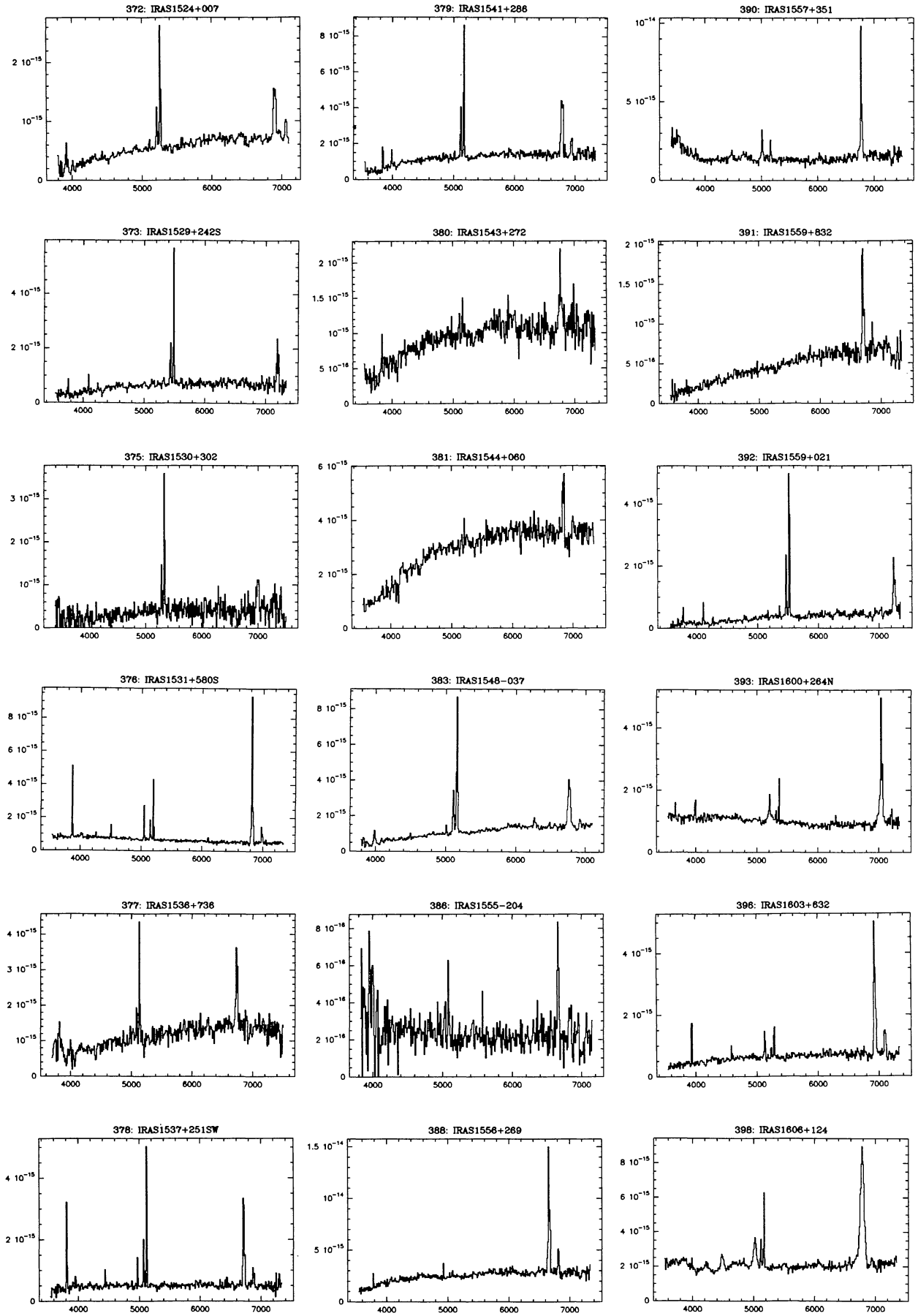

FIGURE 2. *(continued)*

© European Southern Observatory • Provided by the NASA Astrophysics Data System

1992A&AS...96..389D

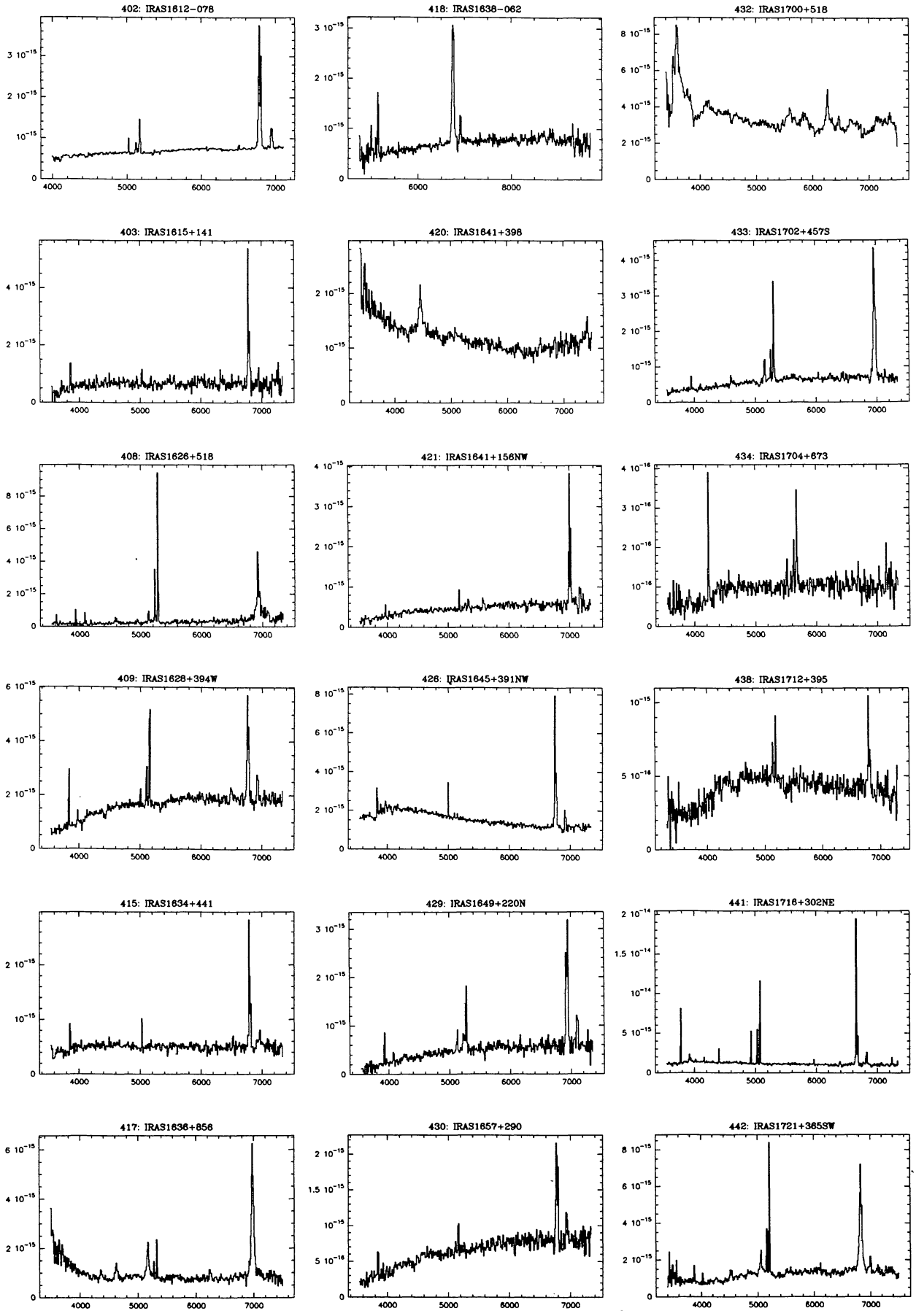

FIGURE 2. *(continued)*

© European Southern Observatory • Provided by the NASA Astrophysics Data System

1992A&AS...96..389D

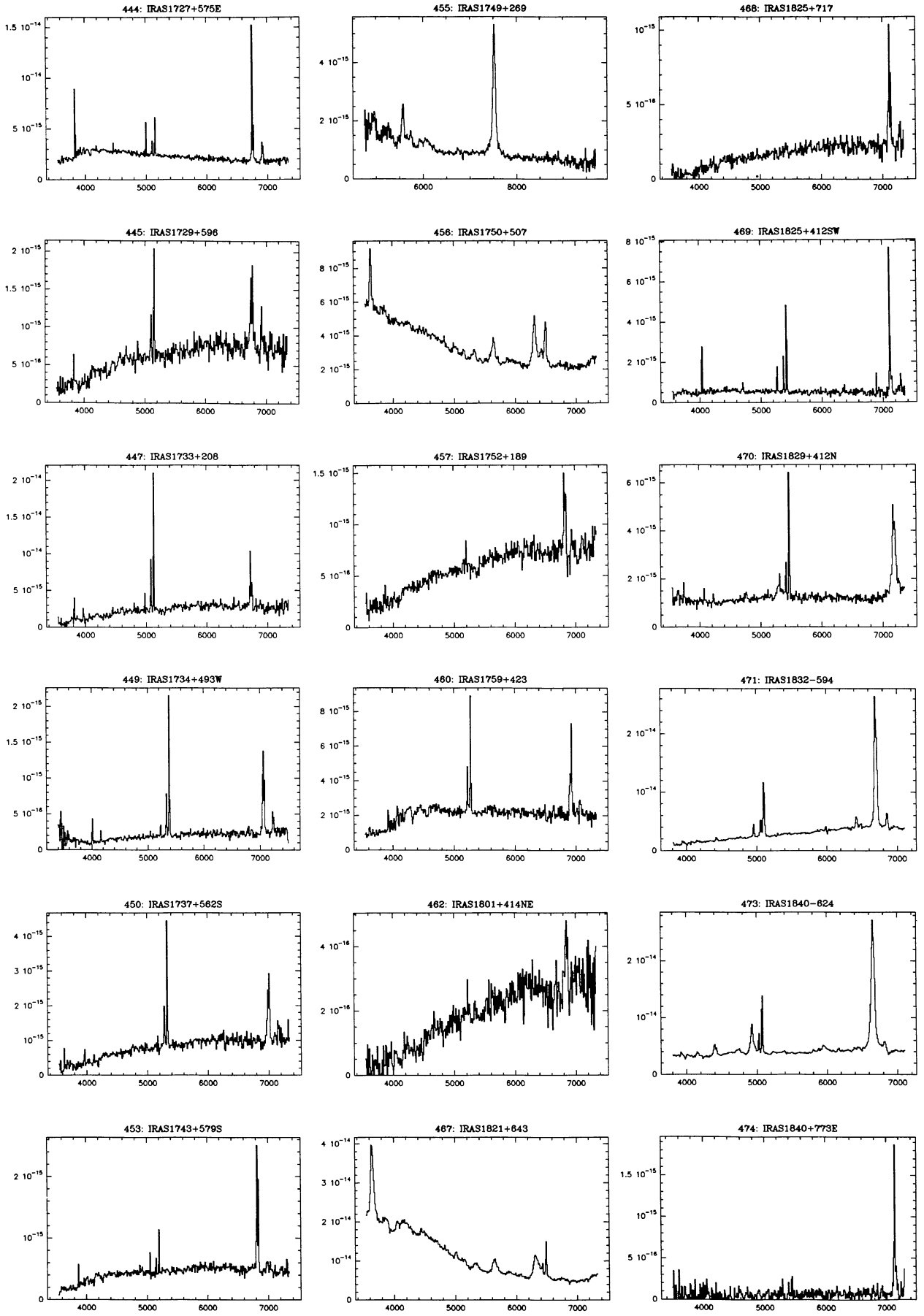

FIGURE 2. *(continued)*

© European Southern Observatory • Provided by the NASA Astrophysics Data System

1992A&AS...96..389D

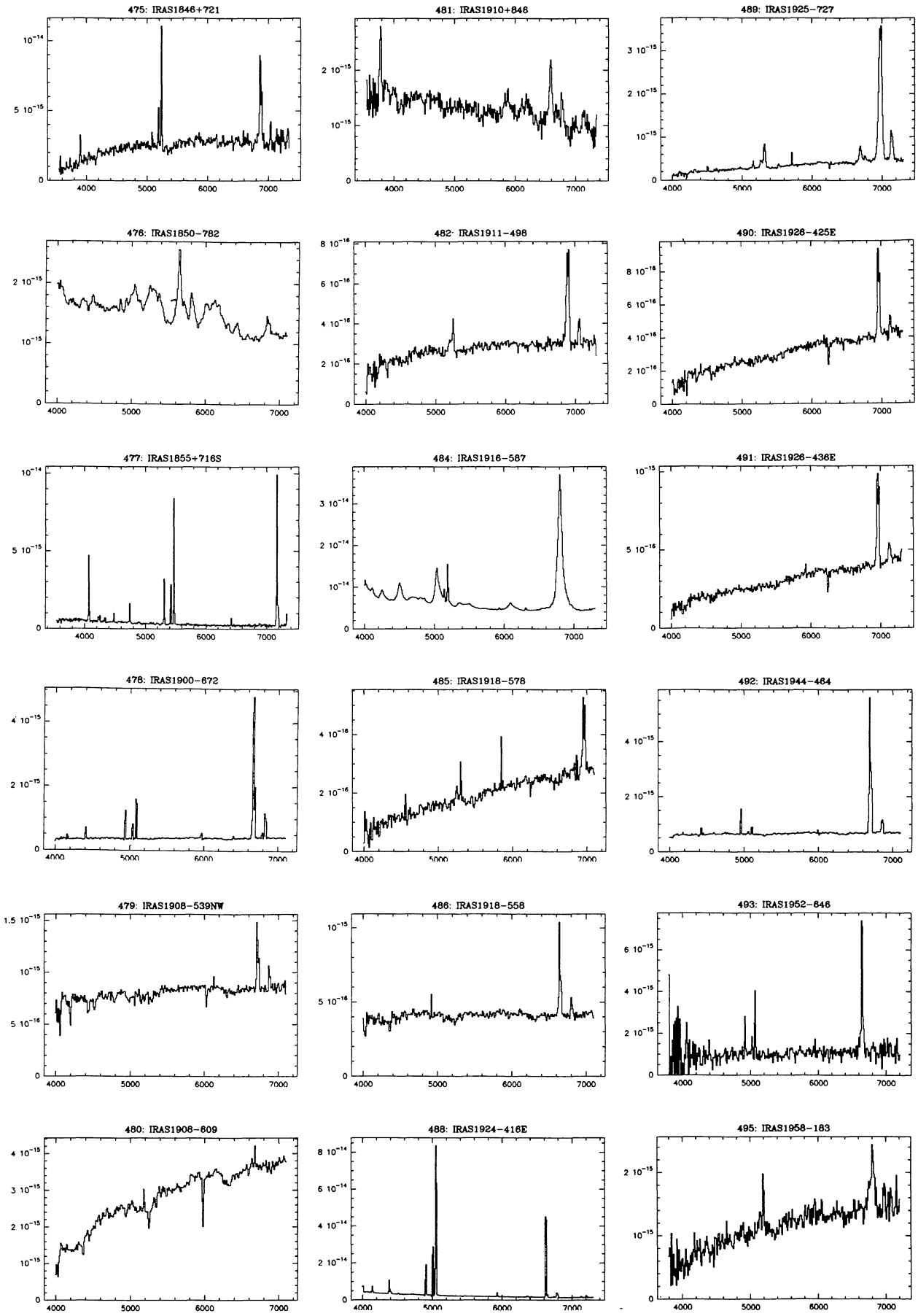

FIGURE 2. *(continued)*

© European Southern Observatory • Provided by the NASA Astrophysics Data System

1992A&AS...96..389D

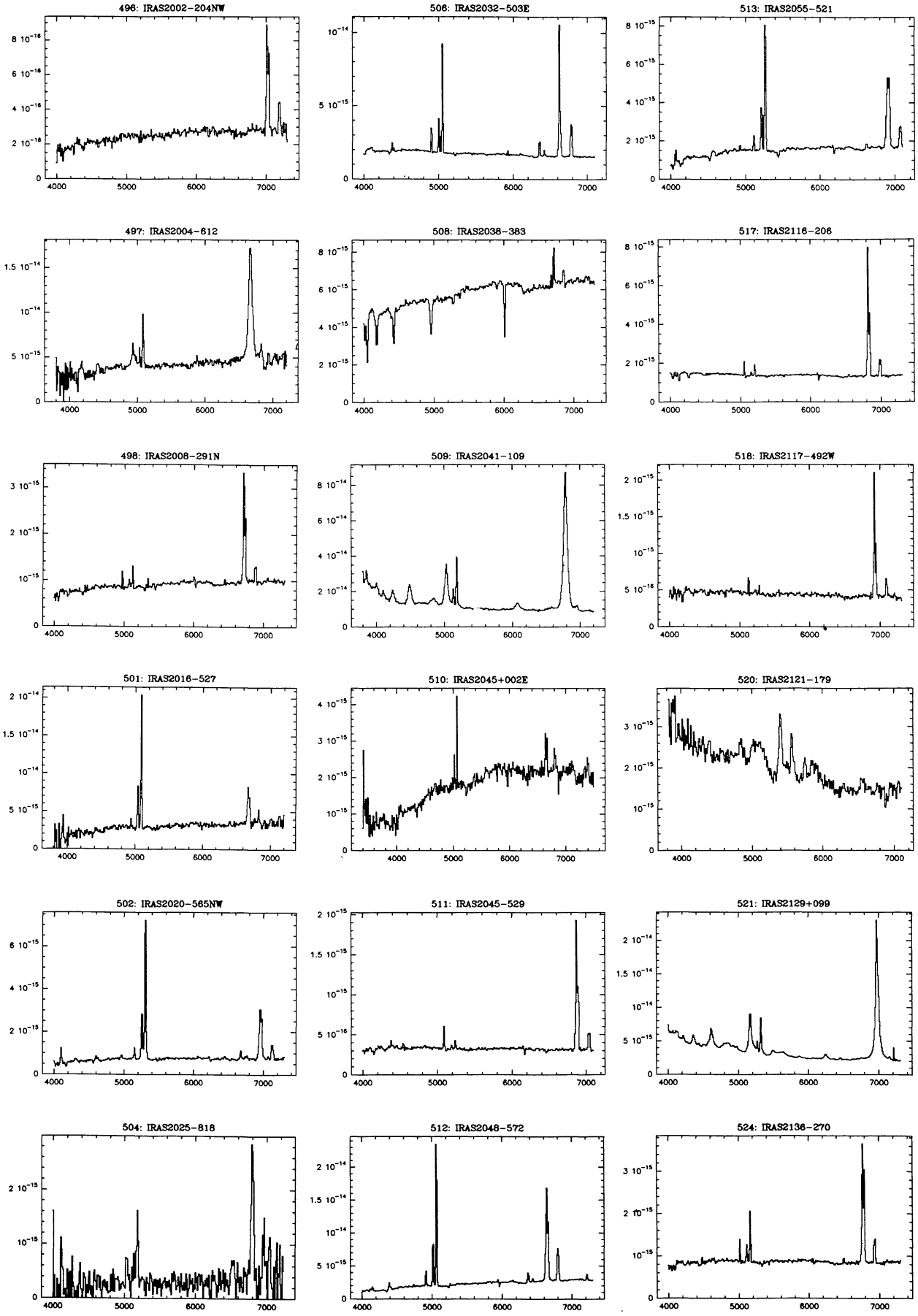

FIGURE 2. *(continued)*

© European Southern Observatory • Provided by the NASA Astrophysics Data System

1992A&AS...96..389D

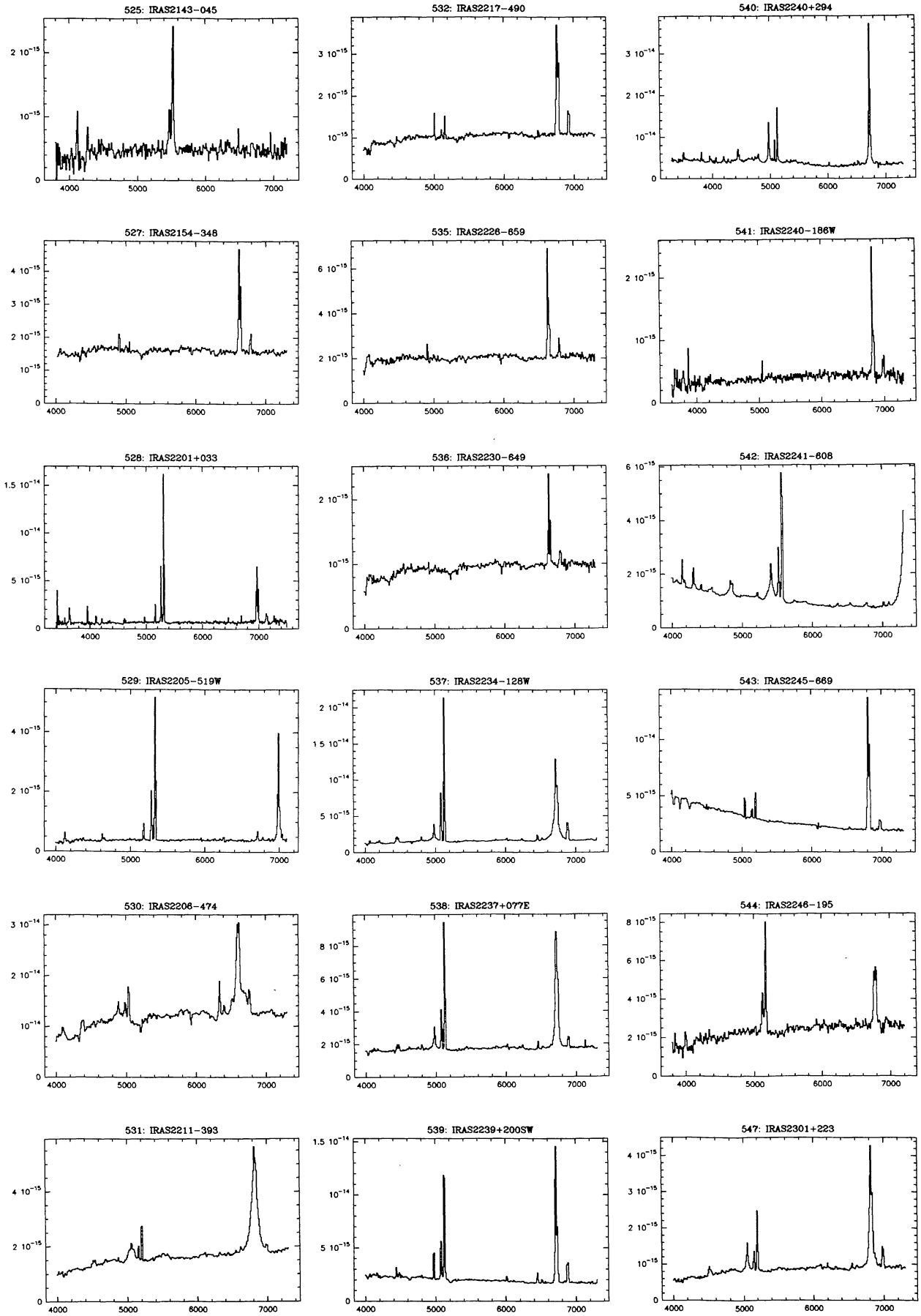

FIGURE 2. *(continued)*

© European Southern Observatory • Provided by the NASA Astrophysics Data System

1992A&AS...96..389D

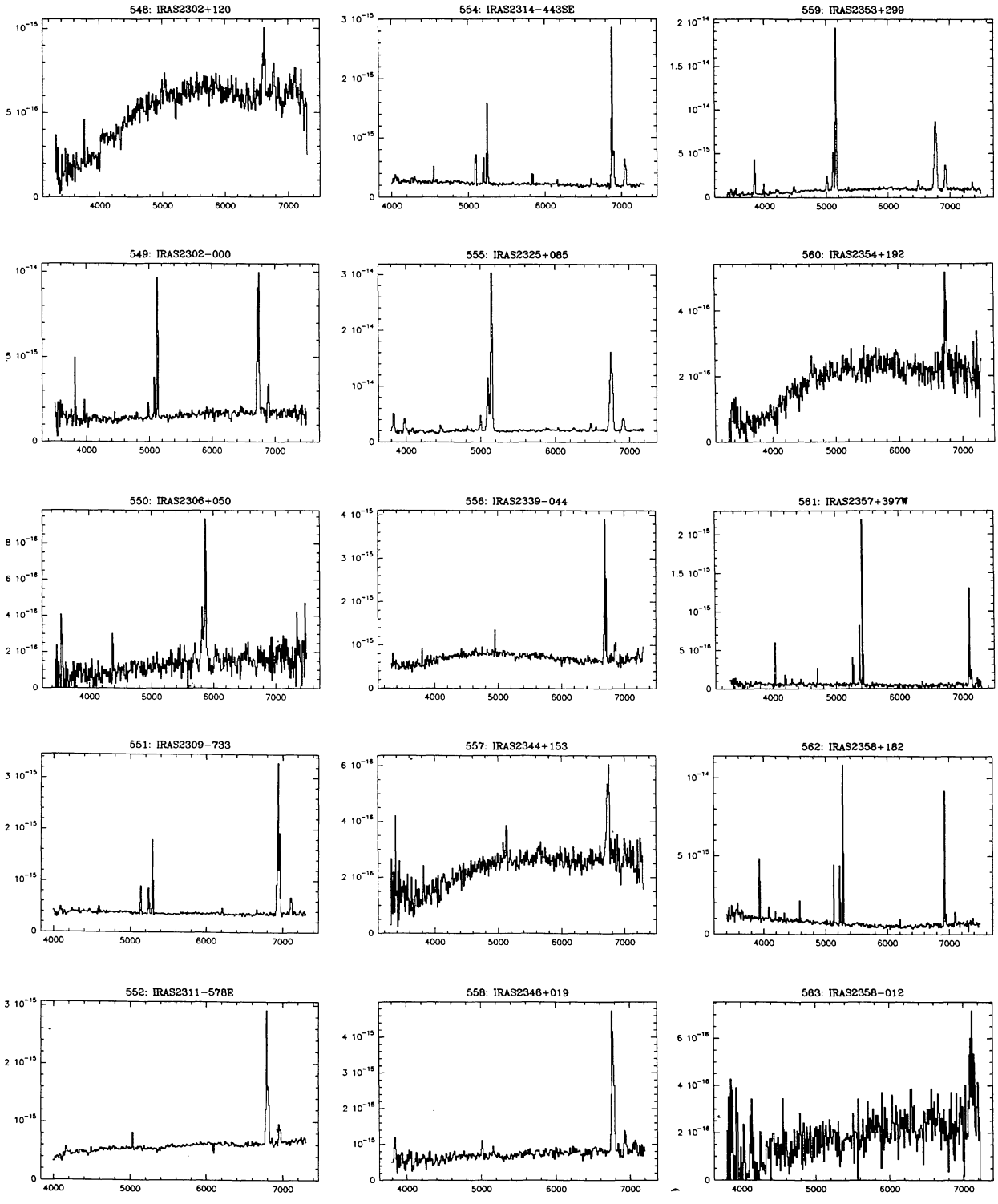

FIGURE 2. *(continued)*

© European Southern Observatory • Provided by the NASA Astrophysics Data System

1992A&AS...96..389D

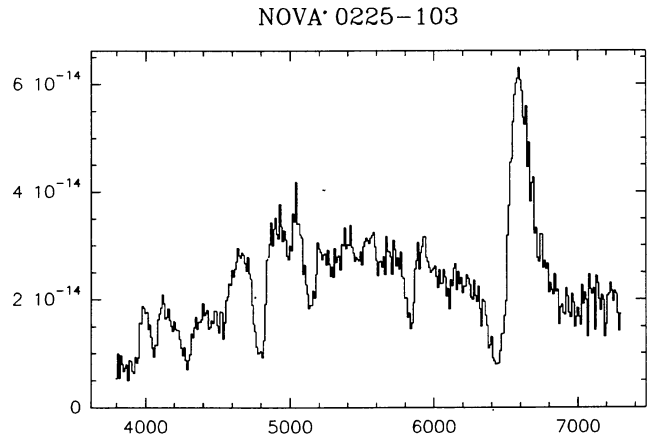

FIGURE 3. The supernova found in IRAS 0225-103, observed in 1985 September with the 2.5-m INT and IPCS. The flux scale is approximate, due to frequent clouds. Note the strong P Cygni profiles of the Balmer lines and strong Fe II features, especially in the blue.

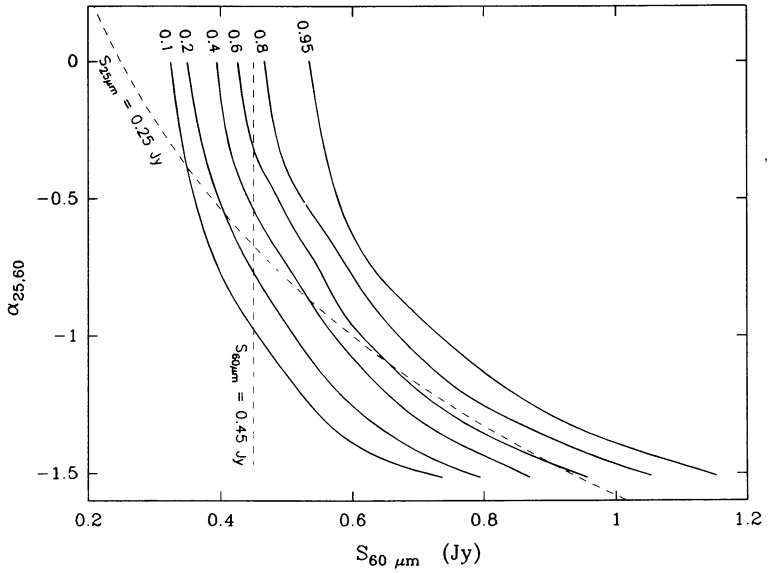

FIGURE 4. The completeness fraction of the sample is a function of flux densities at 60 and 25 microns, shown here as a contour map. The chosen flux density cutoffs are denoted by dashed lines.

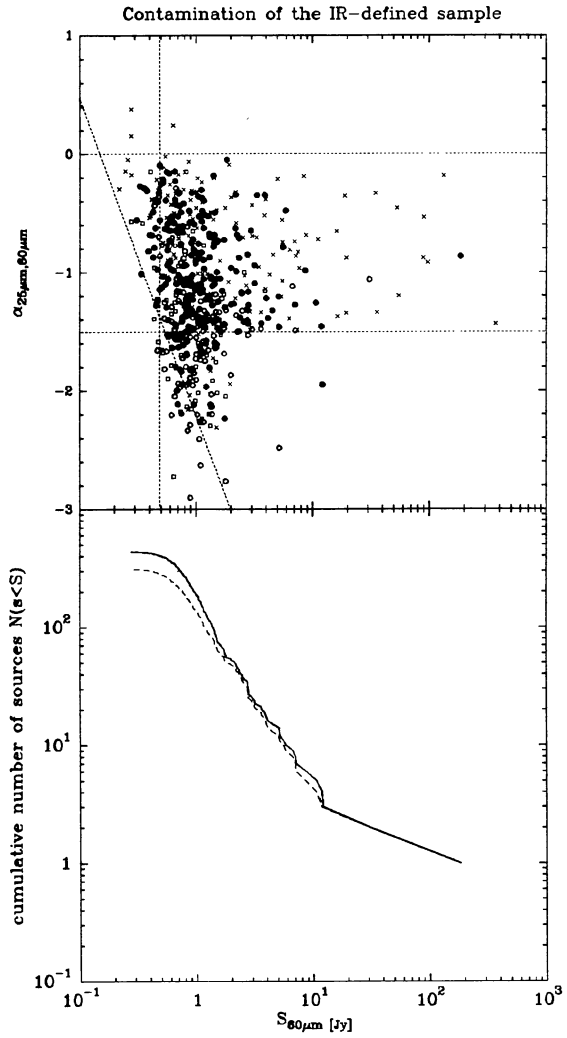

FIGURE 5. Sample revision caused by co-added fluxes. a (top): Infrared colour-magnitude distribution using co-added data. Colour and flux limits are denoted by dashed lines; crosses designate foreground objects, filled circles represent AGNs, open circles HII-type galaxies and the open squares are objects for which no spectroscopic data are available. Clearly a number of objects are not "warm" at all and should not be incorporated in a revised sample. b (bottom): cumulative source counts of all extragalactic sources. At high flux levels the source counts are dominated by a single object (NGC 1068). An excess between 0.5 and 2 Jy is produced by "cold" sources. If these are excluded (dashed line), the source counts are in excellent agreement with a line of slope −1.5 above 1 Jy. A detailed analysis of completeness below 1 Jy is shown in Fig. 4.

© European Southern Observatory • Provided by the NASA Astrophysics Data System

1992A&AS...96..389D

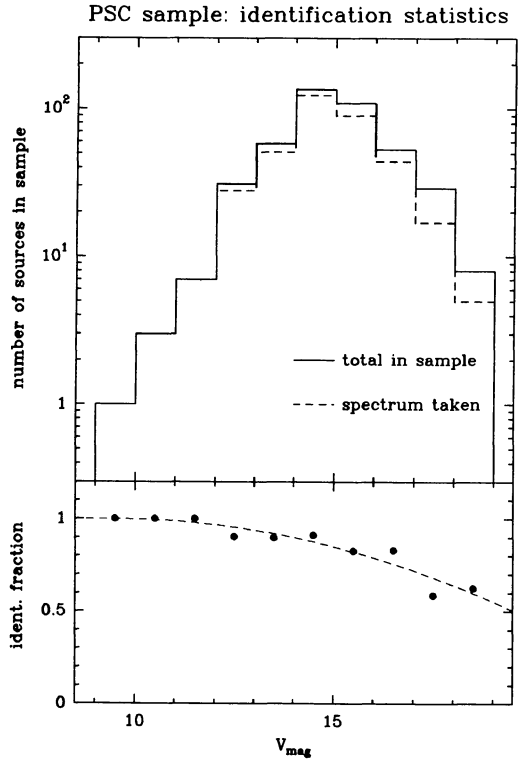

FIGURE 6. Availability of spectroscopic data. The brightest sources were classified most easily; of the 8 faintest sources only 5 were classified. This trend would influence space density estimates if no correction were applied. Comparison of IR/visual flux ratios and AGN fraction suggest that faint sources are not intrinsically different from bright ones. It therefore appears justified to correct this effect by applying a weighting factor $f(V)$.

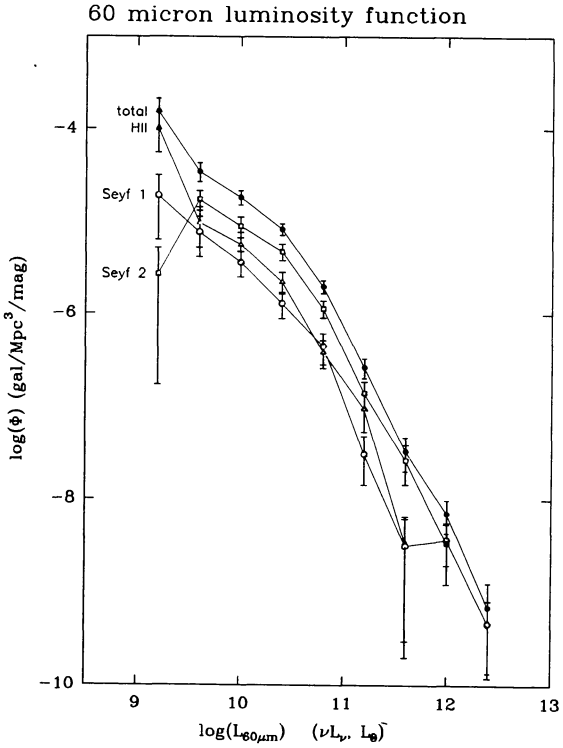

FIGURE 7. The 60-micron luminosity function of the revised sample.

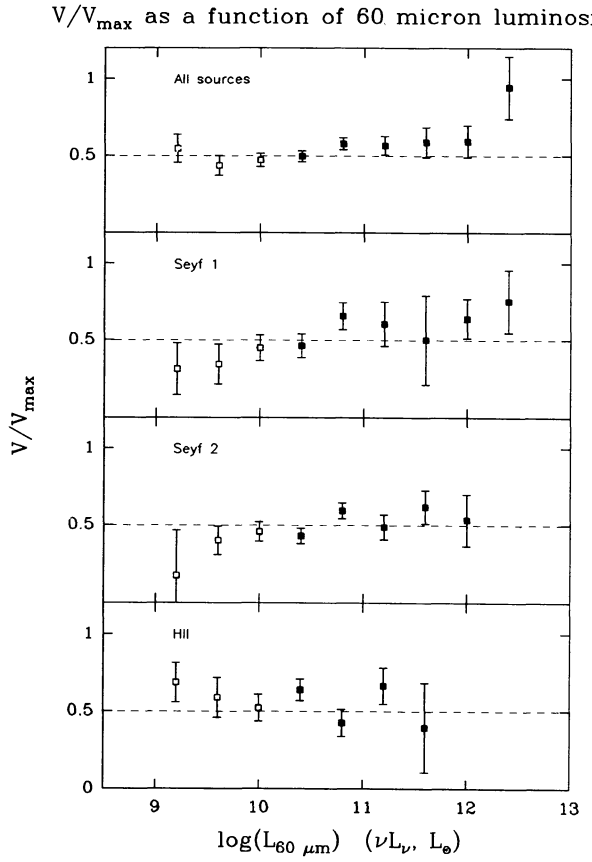

FIGURE 8. V/V_{max} distributions for the various spectroscopic classes. Open squares denote values that are influenced by the local supercluster.

© European Southern Observatory • Provided by the NASA Astrophysics Data System

1992A&AS...96..389D

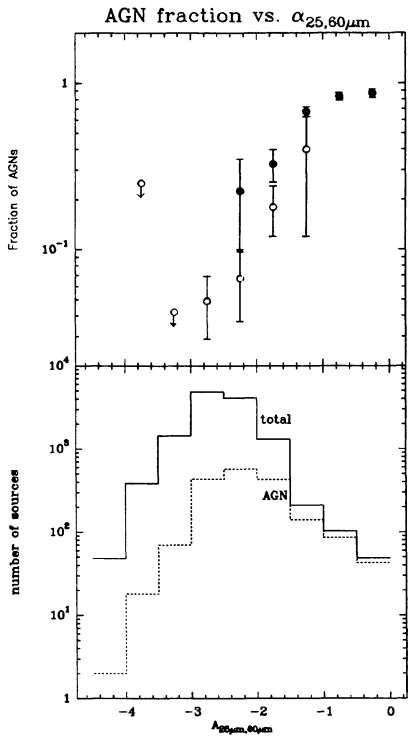

FIGURE 9.

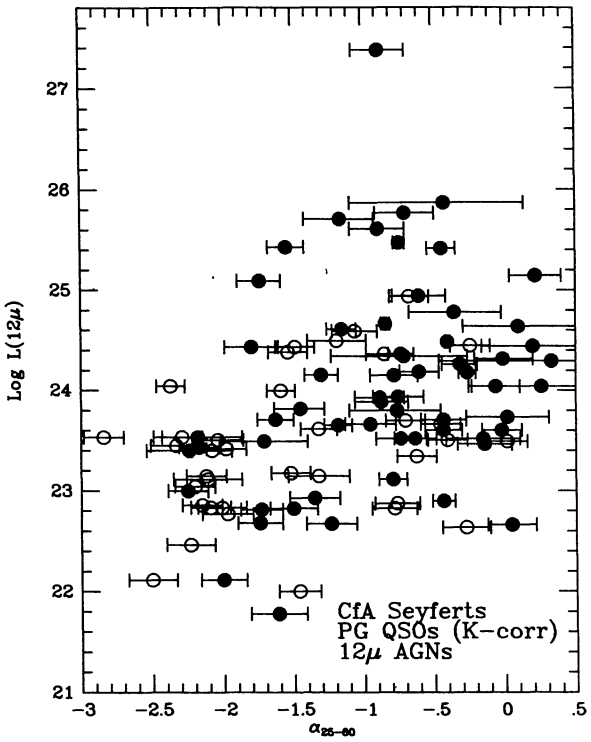

FIGURE 10.

FIGURE 9. Infrared colours of AGN. a (top): Estimates of the AGN fraction of IRAS sources have been made using 2 methods: fraction of sources from the sample discussed in this paper (provides good statistics in the range $\alpha_{25,60} = [-1.5, 0.0]$) : filled circles, and from fraction of AGNs in a 60 micron flux limited sample containing mostly bright NGC galaxies (open circles). Filled circles at $\alpha_{25,60} < -1.5$ were derived from the sources that were excluded from the revised sample. b (bottom): Using the fractions from fig. 8a, an estimate of the total number of AGNs in the PSC is made: despite the low frequency of steep spectrum AGNs, the overwhelming numbers of steep spectrum sources hide a lot of AGNs.

FIGURE 10. Infrared colours of various samples of AGN as a function of luminosity, evaluated at 12μ in the emitted frame. The CfA Seyferts galaxies, Seyfert galaxies from the 12μ sample of Spinoglio & Malkan (1989), and Palomar-Green quasars are included. Narrow line objects are shown by open symbols. Relatively cool (steep) IR spectra are much more common at low luminosities, consistent with a bias introduced by emission from the surrounding galaxies.

Commission paritaire N° 62.321

© Les Editions de Physique 1992

Directrice de la Publication : Jeanne BERGER

Saisie, composition MATHOR3-TEX
Impression JOUVE, 18, rue Saint-Denis, 75001 PARIS
N° 206494P. Dépôt légal : Décembre 1992

© European Southern Observatory • Provided by the NASA Astrophysics Data System